NUMERICAL INVESTIGATION OF NATURAL CONVECTION
FROM INCLINED PLATE FINNED HEAT SINKS

A THESIS SUBMITTED TO
THE GRADUATE SCHOOL OF NATURAL AND APPLIED SCIENCES
OF
MIDDLE EAST TECHNICAL UNIVERSITY

BY

MEHDI MEHRTASH

IN PARTIAL FULFILLMENT OF THE REQUIREMENTS
FOR
THE DEGREE OF MASTER OF SCIENCE
IN
MECHANICAL ENGINEERING

AUGUST 2011

Approval of the thesis:

NUMERICAL INVESTIGATION OF NATURAL CONVECTION FROM INCLINED PLATE FINNED HEAT SINKS

submitted by **MEHDI MEHRTASH** in partial fulfillment of the requirements for the degree of **Master of Science in Mechanical Engineering Department, Middle East Technical University** by,

Prof. Dr. Canan Özgen   _____
Dean, Graduate School of **Natural and Applied Sciences**

Prof. Dr. Süha Oral   _____
Head of Department, **Mechanical Engineering**

Assoc. Prof. Dr. İlker Tarı   _____
Supervisor, **Mechanical Engineering Dept., METU**

Examining Committee Members:

Asst. Prof. Dr. Cüneyt Sert   _____
Mechanical Engineering Dept., METU

Assoc. Prof. Dr. İlker Tarı   _____
Mechanical Engineering Dept., METU

Assoc. Prof. Dr. Almıla Güvenç Yazıcıoğlu   _____
Mechanical Engineering Dept., METU

Asst. Prof. Dr. Tuba Okutucu Özyurt   _____
Mechanical Engineering Dept., METU

Assoc. Prof. Dr. Ayhan Yılmazer   _____
Nuclear Engineering Dept., H.Ü.

Date: _____

I hereby declare that all information in this document has been obtained and presented in accordance with academic rules and ethical conduct. I also declare that, as required by these rules and conduct, I have fully cited and referenced all material and results that are not original to this work.

Name, Last name   :   MEHDI MEHRTASH

Signature   :

iii

ABSTRACT

NUMERICAL INVESTIGATION OF NATURAL CONVECTION
FROM INCLINED PLATE FINNED HEAT SINKS

Mehrtash, Mehdi

M.Sc., Department of Mechanical Engineering

Supervisor: Assoc. Prof. Dr. İlker Tarı

August 2011, 145 pages

Finned heat sink use for electronics cooling via natural convection is numerically investigated. An experimental study from the literature that is for vertical surfaces is taken as the base case and the experimental setup is numerically modeled using commercial CFD software. The flow and temperature fields are resolved. A scale analysis is applied to produce an order-of-magnitude estimate for maximum convection heat transfer corresponding to the optimum fin spacing. By showing a good agreement of the results with the experimental data, the model is verified. Then the model is used for heat transfer from inclined surfaces. After a large number of simulations for various forward and backward angles between 0-90 degrees, the dependence of heat transfer to the angle and Rayleigh number is investigated. It is observed that the contributions of radiation and natural convection changes with the angle considerably. Results are also verified by comparing them with experimental results available in literature.

Keywords: Natural convection, Finned heat sinks, Radiative Heat Transfer, Electronics cooling, Computational Fluid Mechanics.

ÖZ

EĞİMLİ PLAKA KANATCIKLI ISI ATICILARDAN DOĞAL
TAŞINIMIN SAYISAL İNCELENMESİ

Mehrtash, Mehdi

Yüksek Lisans, Makina Mühendisliği Bölümü

Tez Yöneticisi: Assoc. Prof. Dr. İlker Tarı

Ağustos 2011, 145 sayfa

Kanatçıklı ısı atıcıların elektronik aletlerin doğal taşınım ile soğutulmasında kullanımı sayısal olarak incelendi. Literatürde dikey kanatçıklı ısı atıcılar için yapılmış detaylı bir deneysel çalışma ele alınarak, deney düzeneği sayısal olarak modellendi ve ticari bir Hesaplamalı Akışkanlar Dinamiği programı ile akış ve sıcaklık dağılımları çözümlendi. Optimum kanatçık aralığına karşilik gelen maksimum taşınım ile ısı transferinin büyüklüğünü elde etmek için boyut analizi yapıldı. Sonuçların deneysel verilerle iyi uyum gösterdiği gösterilerek sayısal modelin geçerliliği ispatlandıktan sonra model eğimli yüzeylerden ısı atımının incelenmesi için kullanıldı. Öne ve arkaya doğru 0-90 derece arasında farklı açılar için yapılan simülasyonlar sonucunda ısı aktarımının açıya ve Rayleigh sayısına bağımlılığı incelendi. Açıyla ışınımın ve doğal taşınımın katkılarının çok değiştiği gözlemlendi. Sonuçlar literatürde bulunan mevcut deneysel sonuçlarla karşılaştırılarak doğrulandı.

Anahtar Kelimeler: Doğal taşınım, Kanatçıklı ısı atıcılar, Işınım, Elektronik aletlerin soğutulması, Hesaplamalı akışkanlar mekaniği.

To My Parents

Farideh Kalantari

Yadollah Mehrtash

ACKNOLEDGMENTS

TABLE OF CONTENTS

LIST OF TABLES

LIST OF FIGURES

FIGURES

xiv

LIST OF SYMBOLS

A	Area, m^2
Nu	Nusselt number
Gr	Grashof number
Pr	Prandtl number
h	Convection heat transfer coefficient, $W/(m^2K)$
S	Fin spacing, m
H	Fin height, m
N	Number of fins
L	Fin length, m
W	Fin width, m
t	Fin thickness, m
d	Base plate thickness, m
S_{opt}	Optimum fin spacing, m
Q_{in}	Power supplied to heater plate, W
Q_c	Total convection heat transfer rate from fin array, W
$(Q_0)_c$	Convection heat transfer rate from vertical plate, W
Q_{out}	Heat transfer rate from the bottom plate to upper plate, W
$Q_c^{(1)}$	Convection heat transfer rate from fins in small-S limit, W
$Q_c^{(2)}$	Convection heat transfer rate from fins in large-S limit, W
Q_r	Radiation heat transfer rate from fin array, W
Ra	Rayleigh number
T_w	Average base plate temperature, ºC

T_a	Ambient temperature, ºC
T	Temperature, ºC
T_1	Temperature of heated plate, ºC
T_2	Temperature of opposite plate, ºC
T_f	Film temperature, ºC
ΔT	Base-to-ambient temperature difference, ºC
θ	Angle of inclination with respect to vertical position, deg
$\dot{m}$	Mass flow rate, kg/s
k	Thermal conductivity, W/(m K)
g	Gravitational acceleration, m/s^2
μ	Dynamic viscosity, s/m^2
β	Volumetric thermal expansion coefficient, 1/K
σ	Stefan-Boltzman constant, W/m^{2}K^4
ν	Kinematic viscosity, m^2/s
α	Thermal diffusivity, m^2/s
ε	Emissivity

CHAPTER 1

INTRODUCTION

Heat transfer by natural convection occurs when there is a change in the density of the fluid, which can be a gas or a liquid. Fluids tend to expand as they are heated, which results in a reduced density. In a gravity field, the fluid, which has a lower density, is lighter and therefore rises, creating a movement in the fluid to pick up heat and carry it away. When the fluid movement is produced only by a difference in the fluid density, the process is called natural convection or free convection. The driving force for natural convection is not great because it depends upon the density change in the fluid. Therefore, any small obstacle or resistance in the flow path will sharply affect the fluid flow rate and therefore the cooling rate.

Natural convection is encountered in several technological applications. Dissipation of heat from electronic circuits where component performance is strongly dependent on operating temperature is a particular interest among researchers. Heat removal in an efficient way is necessary in order to maintain reliable operation of electronic devices. In order to increase the speed of the circuits, the circuit power has to be increased, which leads to a temperature augmentation. This has made the design of cooling systems more significant, and thermal management of electronic equipment has become an important issue. In these kind of systems, all modes of heat transfer exists; conduction through the materials, convection to an external cooling agent and radiation heat transfer which occurs naturally. Natural convection represents an inherently reliable cooling process.

Furthermore, this mode of heat transfer is often designed as a back-up in the event of the failure, due to fan breakdown, of a forced convection system.

In applications where the heat dissipation surface is smooth, it may be necessary to enhance the surface to achieve the desired temperature level or rate of heat transfer. The most common solution is to add fins. Finned surfaces are frequently used as an efficient method of rejecting waste heat from electronic equipment. These finned surfaces, commonly known as heat sinks, are economical and highly reliable when cooling is by natural convection and radiation. Fins are extensively used in air cooled automobile engines, air craft engines, generators, motors, transformers, refrigerators, computer processors and other electronic devices.

Previously, a great number of experimental and numerical works has been carried out to study the effect of fin parameters like fin height and fin spacing on the heat transfer rate from fin arrays by investigators. Several authors have developed thermal relationships for closed channels and parallel plates. However, many practical heat sink designs may consist of a series of relatively short fins attached to a heated base plate and cannot be accurately approximated by parallel flat plates.

Rectangular fin geometries and their thermal effectiveness in vertical orientation have been investigated in the literature. However most of the studies are done for limited range of fin configurations. Furthermore although many experimental studies exist in this area, the amount of numerical studies is lacking. Hence the present numerical study is performed to investigate the effects of fin spacing, fin height and magnitude of heat flux on natural convection from rectangular fin arrays by using commercial CFD software. The main objective of this work is to demonstrate a convenient CFD based solution to determine the performance of different fin configurations. Since it is not possible to perform experiments on every possible fin configuration, a CFD solution can be used to predict the effectiveness of different fin configurations.

Heat sinks are usually used in vertical and horizontal orientations. But in some situations, we need to use them for effective cooling by natural convection in inclined orientations. Likewise, electronic devices can be moved and oriented in any inclined orientation during their operation. Natural convection heat transfer over inclined fin array heat sinks has been gaining significant attention recently. Some mechanical designs such as modern telecommunication equipment show the necessity of exploring the natural convection from tilted heat sinks. Fundamental data for such heat transfer phenomena are required for the design of various kinds of devices.

The influence of important variables in general extended surface and heat sink applications are investigated for inclined orientations in the present study. There are almost no studies that discussed quantitatively the influences of flow structure on the heat transfer with an emphasis on the transition process of the natural convection over an inclined heat sink. This subject has not been explored before. The present work is designed to fill this gap by the numerical determination of convection heat transfer along heat sink surfaces. The purpose of this investigation is to numerically determine the magnitude of free convection heat transfer for rectangular fin arrays of various orientations dissipating heat to room air. The study concerns the instability, transition and separation of the natural convection flows induced by buoyancy forces over vertical, inclined and horizontal surfaces. The realization of these objectives was facilitated by the use of flow visualization in CFD.

An experimental study from the literature that is for vertical surfaces is taken as the base case and the experimental setup is numerically modeled using ANSYS Fluent. The numerical investigations are carried out for different heater power and with inclination angles varying from the horizontal facing upwards position, through the vertical position, to the horizontal facing downwards position. The flow and the wall temperature fields are visualized and the heat transfer coefficient is measured over an inclined heat sink under uniform heat flux.

The governing equations solved by the help of Fluent are given below.

The mass conservation equation:

$$\frac{\partial \rho}{\partial t} + \nabla.(\rho \vec{v}) = 0 \tag{1.1}$$

where ρ is fluid density and $\vec{v}$ is the velocity vector.

The conservation of momentum equations:

$$\frac{\partial}{\partial t}(\rho \vec{v}) + \nabla.(\rho \vec{v}\vec{v}) = -\nabla p + \nabla.(\tilde{\tau}) + \rho \vec{g} + \vec{F} \tag{1.2}$$

where $\vec{F}$ contains other source terms that may rise from resistances, sources, and etc. and $\tilde{\tau}$ is the stress tensor and can be defined as:

$$\tilde{\tau} = \mu \left[(\nabla \vec{v} + \nabla \vec{v}^T) - \frac{2}{3} \nabla.\vec{v}I \right] \tag{1.3}$$

The conservation of energy equation:

$$\frac{\partial}{\partial t}(\rho h) + \nabla.(\rho h \vec{v}) = \nabla.\left[(k + k_t)\nabla T \right] + S_h \tag{1.4}$$

where h is sensible enthalpy and S_h is the volumetric heat source.

The thesis organized in 5 chapters with 3 appendices covering relevant details. In Chapter 2, previous studies regarding the various fin configurations are examined. In Chapter 3, vertical case is modeled and verified by the experimental study. The results are correlated and compared with literature. In Chapter 4 vertical model is considered for investigating the inclined case by changing the gravity acceleration direction. Results are presented and compared with the experimental results. Finally conclusion is given in Chapter 5.

CHAPTER 2

PREVIOUS STUDIES

Several studies of free convection from multiple surfaces can be found in the literature. For extended surfaces many studies were performed in order to determine the optimum fin configuration which provides maximum heat transfer. Here a number of published results are gathered to provide a general image from the works done so far. The geometrical parameters of the fin configurations considered in previous studies are listed in Table 2.1 to increase the readability of this chapter.

2.1   Experimental Studies

Recent study corresponded to the steady state natural convection heat transfer from vertical rectangular fins on a vertically base was done by Yazıcıoğlu [1]. Thirty different fin configurations were used to investigate the effect of fin spacing, fin height, fin length on the performance of heat dissipation from the fin arrays. From the results it was concluded that the effects of these parameters are very much interconnected. Higher rate of heat dissipation was observed for longer fins compared to shorter fins. Larger fin heights resulted in higher rate of heat dissipation which is due to larger surface area for heat transfer. Furthermore for each fin configuration optimum fin spacing was suggested. These optimums were reported between 8.8 mm and 14.7 mm. Yazıcıoğlu employed the scale analysis suggested by Yildiz [15] in order to predict the order of

magnitude of optimum fin spacing at a given fin length and base-to-ambient temperature difference. From this scale analysis the following correlations were derived:

$$\frac{S_{opt}}{L} = 3.53 Ra_L^{-0.25} \qquad (2.1)$$

$$Q_{c\max} = (Q_0)_c + 0.125 Ra_L^{0.5} kH\Delta T\left(\frac{W}{L}\right) \qquad (2.2)$$

where $Q_{c\max}$ is total convection heat transfer rate and $(Q_0)_c$ is the convection heat transfer rate when there are no fins.

Güvenç [4] investigated natural convection heat transfer from vertically rectangular fin arrays with base vertically oriented. The same fin geometric parameters as the study done by Yüncü and Anbar [14] were used. Enhancement in heat dissipation has been viewed by obtaining the ratio of convection heat transfer from the plate-finned heat sink to convection heat transfer from the bare plate. Results revealed that the most important parameter which affects the quantity of natural heat transfer is the inter-fin spacing. Comparing the outcomes of these similar studies indicates higher steady heat dissipation rates in vertically oriented fin arrays in comparison to the horizontally oriented ones.

Another experimental study regarding the natural convection heat transfer from both vertically and horizontally oriented fin arrays was done by Leung and Probert [7]. Since the material which had been used in this study had a low surface emissivity, amount of radiation heat transfer contribution was low. Optimal inter-fin separations to obtain maximum heat transfer rates corresponding to vertical fins protruding outwards from the vertical base and upwards from the horizontal base were reported nearly between 9–10 mm. Referring to this study, since the radiation component is almost independent of the other modes of heat dissipation these values would also apply to the surfaces with higher emissivities.

Ko and Leung [8] investigated the effect of material on the amount of convective heat transfer from the heat exchangers with vertical rectangular fins. Duralumin and stainless steel were used as a fin material in this study. S_{opt} for vertically-based finned system and horizontally-based ones were found as 12±1 mm and 23±1 mm respectively for $\theta \leq 40$ K. Only small reduction ($\approx$ 13.5 %) in the maximum rates of heat loss has been seen when fins were made of stainless steel rather than duralumin.

In another experimental study by Leung et al. [9] steady state rates of heat transfer from rectangular fins on vertical and horizontal rectangular bases were investigated experimentally. For the vertical fins on a vertical base, the most important parameter influencing the heat transfer rate was observed as fin spacing. Moreover it was determined that unlike fin spacing the variation in fin height did not cause an effective change in dissipation of heat. It was concluded that among the all considered base positions, vertical fins on a vertical base was the best solution for better heat transfer performance. For this study the optimum inter-fin separation for maximum surface heat dissipation were reported as 10±1 mm.

Leung and Probert [11] performed a similar extensive study with polished duralumin extended plate heat exchanger while all parameters were altered for achieving maximum heat transfer rates. For a base of width 190 mm and 250 mm length, the optimal inter-fin separation was reported as 11.1 mm. Second stage of this study was dedicated to find the optimal fin thickness. Base width, Base length and fin height kept constant as 190 mm, 500 mm and 60 mm respectively while inter-fin spacing was increased from 15 mm to 55 mm. The optimal fin thickness has been viewed almost invariant to temperature changes.

In another experimental study done by Leung and Probert [12] the effect of gap width between consecutive vertical rectangular fin arrays were investigated. It was observed that a gap width of 18 mm slightly increases the rate of heat transfer by means of natural

7

convection. On the other hand, it was found that heat dissipation rate decreases if the gap width between two consecutive vertical fin arrays was less than 12 mm. It was also estimated that a slight improvement in heat dissipation can be achieved when short fins are used instead of long fins.

Natural convection heat transfer from vertical rectangular fin arrays with the base horizontally oriented was investigated by Yüncü and Anbar [13]. 15 sets of fin arrays with different fin spacing and fin heights were used. Electrical heater was used to make the temperature difference between fin surface and surroundings. It was found that effect of base-to-ambient temperature on the optimum fin spacing is negligible. Also it was observed that Optimum fin spacing decreases as the fin height increases. A correlation was suggested relating the enhancement of heat transfer rate from fin arrays with fin spacing, fin height and number of fins.

Experimental study related to natural convection performance from annular fins on a horizontal cylinder was conducted by Yildiz [15]. In this analysis fin thicknesses were fixed at 1 mm while the other parameters like fin diameter, fin spacing and the base-to-ambient temperature difference were varied. Radiation mode of heat transfer were evaluated and subtracted from the total heat transfer to obtain the pure convection heat transfer from the fin arrays. The optimum fin spacing equal to 8 mm was suggested for annular fin arrays on horizontal cylinder. A scale analysis is also performed in order to estimate order-of-magnitude of optimum fin spacing at a given fin diameter and base-to-ambient temperature difference. The equation which relates the Rayleigh number based on fin diameter and ratio of optimum spacing and maximum convection heat transfer rate were obtained.

Elenbaas [17] conducted the first comprehensive experimental work, which has served as a benchmark for most subsequent studies. Laminar natural convection heat transfer in parallel–plate vertical channels was investigated and a detailed study of the thermal

characteristics of cooling by natural convection was reported. He determined that in the limit of small gap width, Nusselt number varies proportional to the channel Rayleigh number. Also he has done extensive work with rotated plates on an experimental and semi-empirical basis. He believed that by turning the plates through an angle θ the only component which causes the flow of the air is $g \, cos \, \theta$ and therefore g should be replaced by $g \, cos \, \theta$ in calculating the Nu number.

Starner and McManus [18] were perhaps the first to investigate in detail the thermal performance of natural convection heat sinks as a function of the geometry (spacing and height) and angle of base plate orientation (vertical, horizontal, and 45°). Starner and McManus found that the measured heat transfer coefficients for the vertical orientation were generally lower than the values expected for parallel-plate channels reported by Elenbaas [17]. The correlation of Elenbaas would be expected to apply closely for the case of a completely vertical system if the fins projected perpendicularly a distance equal to a large percentage of the flow path and if the base and corner sections were a small part of the total surface area. The inclined orientation (45°) resulted in reduction in the heat transfer coefficient because of blocking effect. Results for the horizontal orientation showed more favorable results than the 45 degree positioning due to the ample flow from above down into the array.

Welling and Wooldridge [19] performed a study to compare actual rectangular fin experiments with those of vertical plate, enclosed duct and parallel plate data from previous studies. Their results revealed that in the range of fin spacing between 4.8 to 19 mm and fin heights from 6.3 to 19 mm, the heat transfer coefficients along the total wetted surface were lower than attained by an isolated flat plate but generally above those associated with parallel-plate flow. Closely spaced fins compared to wider fin spacing brought about lower heat transfer coefficient due to boundary layer interference. In this study it was observed for the first time that for any given inter fin spacing there is an optimum fin height beyond which thermal performance per unit surface area declines.

Table 2.1 Geometrical parameters

Ref.	Fin Length L (mm)	Fin Width W (mm)	Fin Height H (mm)	Fin Thickness t (mm)	Fin Spacing S (mm)	Base-to-Ambient Temperature Difference ΔT (°C)	Optimum Fin Spacing S_{opt} (mm)	Angle of Orientation θ (deg)
[1]	250,340	180	5-25	3	5.85-85.5	21-162	11.2	0
[4]	100	250	5-25	3	5-34	14-106	7	0
[5]	250,375	190	60	3	5-77	40	11	0
[6]	250	190	32-90	3	2.85-33.2	20-80	11.5	0
[7]	150	190	10,17	3	3-45	20-40	10	0,-90
[8]	500	190	60	3	5-77	20-40	12	0,-90
[9]	190	250	60	3	2.85-33.2	20-80	11	0
[10]	250	190	32-90	3	3-77	20-60	10.5	0
[11]	250,500	190	30-90	1.5-3.6	3-77	20-40	11.1	0
[12]	250,500	190	60	3	10	40	-	0
[13]	100	250	6-26	3	6.2-83	13-133	10.5-20	-90
[14]	100	-	5-35	-	5-20	36-96	-	-90
[18]	127	254	6.35-25.4	1.02	6.35-7.95	25-90	-	0,-45,-90
[19]	203	66.3	6.35-19.05	2.3	4.8-19	35-90	-	0
[22]	144,280	115	8.6-25.5	2	6-13.8	-	-	0,-30,-60,-90
[23]	127-381	-	6.3-50	-	4-38.1	33-100	-	-90
[24]	25-49	25-49	13.5	1	3-11	15-22	-	0
[25]	320	200	10-30	1.5	8-20	-	-	0,-90
[27]	127-381	-	26-47	-	4-38.1	20-70	-	-90
[28]	7-50	-	7-12	3-7	4-12	40-60	-	-90
[29]	250-340	180	5-25	3	5-85.5	16-180	11	0
[31]	130-390	130	10.5-34	1.1	7	16-76	6-11	90
[32]	200	130	21.5-34	1.1	7-17	16.4-55.6	-	60,70,80,90

A similar study of upward and downward facing fin arrays on a horizontal base was reported by Jonas and Smith [20]. An interferometer was used to measure local temperature gradients. The measured temperature gradients were used to determine the

corresponding heat transfer coefficients. One more time the significant effect of fin spacing on the heat transfer coefficients was reported. The following correlations were also obtained:

$$Nu_s = 6.7 \times 10^{-4} \times Gr_s \times \Pr \times \left[1 - \exp\left(\frac{7460}{Gr_s \times \Pr} \right)^{0.44} \right]^{1.7} \qquad S < 51 \text{ mm} \qquad (2.3)$$

$$Nu_s = 0.54 \times (Gr_s \times \Pr)^{0.25} \qquad S > 51 \text{ mm} \qquad (2.4)$$

Fitzroy [21] conducted a study for determining the optimum spacing of a set of parallel vertical fins dissipating heat by free convection in the laminar flow regime. A correlation which relates h_d (average heat transfer coefficient for inner surfaces at surface spacing, d) to h_∞ (average heat transfer coefficient for a single vertical plate remote from any other surface) was suggested.

"Bilitzky [22] completed a comprehensive investigation of natural convection heat transfer from multiple heat sink geometries that differed primarily in fin height and spacing. The heat sinks were operated at different heat dissipations as well as different angles of inclination and orientation. The base was first kept vertical, while the fins were rotated through four different positions. Then the base was tilted backward toward the horizontal orientation through four different positions. In all 12 heat sinks studied, the vertical–vertical orientation, that is, a vertically oriented base with vertical fins and channels, yielded the highest heat transfer coefficients most often. On the other hand, vertical–horizontal orientation, that is, the base plate vertical and the fins rotated 90° from the axis, led to the lowest heat dissipation rates. For the unrotated fins, the lowest heat transfer coefficients were almost always found to occur at a base plate angle of 30° from the horizontal. The use of smoke revealed a relatively complex three dimensional flow pattern around the heat sinks, with very substantial inflow from the direction of the fin tips when the base plate was strongly inclined and when the heat sinks were in the

vertical base–horizontal fins orientation. The influence of the spacing between the fins for short and long base plates was examined by comparing pairs of heat sinks that differed only in geometric parameters. Bilitzky observed that the highest heat transfer coefficients were attained with the larger fin spacing." [39]

Harahap et al. [24] investigated the effect of miniaturizing on steady state rate of natural convection heat transfer from miniaturized vertical rectangular fin arrays. It was found that reducing the base area of fin arrays increase the average heat dissipation coefficient and the steady state heat transfer rate. The optimum inter-fin separation distance was reported as 11 mm. It was observed that regardless of the fin spacing heat dissipation rate per unit area increases with decrease in base area of fin arrays. Effect of miniaturizing was more significant for square base plates than non-square base plates. Furthermore it was viewed that higher rate of heat can be dissipated from the fin arrays when the width of the base plate is larger than the length of the base plate.

Nada [25] performed an experimental study in order to investigate the free convection heat transfer and flow characteristics from fin arrays with different fin spacing and fin length in horizontal and vertical narrow enclosures. Effects of fin spacing, fin length and enclosure orientation were investigated for wide range of Rayleigh numbers. Insertion of fins always showed a higher heat transfer rate in compare with the bare plates. It has been found that for a high range of Rayleigh numbers, Nusselt number increases but fin effectiveness decreases and on the other hand for a small range of Rayleigh numbers and at large S/H, increasing Rayleigh number increases both Nusselt number and fin surface effectiveness. The maximum value of heat transfer coefficient and finned surface effectiveness occurs when the dimensions of S and H are the same.

An analytical model has been developed for four different types of fin array named as longitudinal trapezoidal fin array, longitudinal rectangular fin array, annular trapezoidal fin array and annular rectangular fin array by Kundu and Das [26] in order to investigate

12

the performance and optimum design analysis of these fin array types. From the temperature distributions, profound effect of conduction in supporting structures and convective cooling through inter-fin spacing was viewed. A method for optimizing the fin dimensions in case of known total fin volume and inter-fin spacing was suggested.

A combined analytical, numerical and experimental study was conducted by Dayan et al. [31] to investigate natural convection underneath a horizontal fin array. Like other studies, effects of various parameters on the heat transfer from the heat sink surface were examined. It was observed that between fin array geometrical parameters fin height has not significant affect on the heat transfer coefficient. They suggested that an optimal fin spacing exists which can be determined simply from the knowledge of the fin array length. Furthermore, a useful closed form correlation for the Nusselt number was developed for the first time as follows:

$$\overline{Nu_L} = \frac{\overline{Nu_L^s}}{1+\frac{2H}{S}}\left[\exp\left(-\frac{H}{S}\right)+0.65\left(\frac{2H}{S}\right)\left(\frac{4L}{S}\right)^{-\frac{4}{5}}Ra_L^{\frac{1}{5}}\right] \tag{2.5}$$

where $\overline{Nu_L}$ is the average Nusselt number for heat sink and $\overline{Nu_L^s}$ is the average Nusselt number for the horizontal infinite flat strip.

In order to investigate the natural convection underneath an inclined fin array, combined experimental, analytical and numerical study has been performed by Mittelman et al. [32]. They concentrated on the critical angles between 60º to 90º with respect to vertical position. Analytical expressions for heat transfer coefficient of slightly inclined fin arrays have been provided. However, they did not report any concrete correlation between the flow and the heat transfer. Higher rate of heat transfer has been observed when there is no flow separation along the fin array. Effects of different parameters on the heat transfer coefficient have been examined. According to this study optimum fin

spacing for horizontal fin arrays is applicable to inclined ones and this optimum value does not change by the inclination angle of the heat sink. Changes in fin height did not indicate any considerable influence on heat dissipation rate.

2.2   Numerical Studies

Yüncü and Mobedi [14] conducted a numerical study of three dimensional steady state natural convection from short rectangular fin arrays on a base horizontally oriented. They developed a finite difference code in Cartesian coordinate system based on vorticity-vector potential approach to solve the problem. Different geometric parameters of fin arrays were used to analyze the effects of each parameter on flow configurations occurring in the channels of fin array. From the analyses related to fin spacing it was observed that for narrow fin spacing, air can only enter into the channel from the end regions. On the other hand, if the fin spacing is large enough air can enter the channel from the middle part of the fin. Also from the examinations regarded to fin height and fin length revealed that an increase in these parameters leads to reduction in heat transfer from the surface which is due to boundary layer interference along the channel.

Baskaya et al. [23] carried out a numerical investigation on different parameters which affects the rate of heat dissipation from the horizontal rectangular fin arrays. It has been shown that it is not possible to achieve optimum performance in heat transfer by only concentrating on one or two parameters. In a general view, by increasing the height of the fin and decreasing the fin length the heat dissipation enhances. Additionally in this study optimum fin spacing values for maximum heat transfer were obtained.

Yalcin et al. [27] performed a numerical analysis using commercially available CFD package PHOENICS on natural convection heat transfer from horizontally placed rectangular shrouded fin arrays. Various experiments were done to investigate the effects of fin length, fin height, fin spacing and clearance parameter on the rate of heat

14

transfer from the fin array surfaces. Regarding to these analyses optimum configurations has been determined and related correlations for Nusselt number based on hydraulic diameter were proposed.

A numerical study was performed to investigate the natural convection from horizontally placed rectangular thick fin arrays with short length by Dialameh et al. [28]. Finite Volume method was used to solve the three dimensional elliptic governing equations. It was observed that the free convection heat transfer coefficient increases with increase in base to ambient temperature difference whereas decreases with increase in fin length. Furthermore it was found that effect of fin thickness and fin height on the heat transfer is negligible. Optimum fin spacing value was found to be 7 mm for maximum heat transfer from fin arrays with channel aspect ratio $H/L \leq 0.24$.

Çakar [29] conducted a numerical study on natural convection heat transfer from vertical rectangular fin arrays using ICEPAK. The main objective of this study was to show the advantages of CFD solutions to natural convection from finned heat sinks by simulating cases from literature. Various fin array configurations were modeled based on the experimental studies available in literature. The results obtained from the analyses follow a trend similar to the results of the experiments. An order-of-magnitude estimation of maximum heat transfer corresponding to the optimum fin spacing was provided.

CHAPTER 3

VERTICAL CASE

3.1   Vertical Heat Sink Model

Experimental study which was performed for vertical finned heat sinks in Ref. [1] is investigated numerically using commercial code ANSYS Fluent. In this study 30 different fin configurations are modeled. Modeling procedure inside this package and solution settings used in it are demonstrated. Finally, the effects of geometric parameters such as fin length, fin height and fin spacing on the heat transfer performance of fin arrays are examined.

3.1.1   Model Setup

According to the reference study [1] two similar experimental setups named as setup 1 and setup 2 were constructed to test vertically based rectangular fin arrays. The components and the dimensions related to each one through these setups are shown in Table 3.1. Air is selected as the working fluid. The problem is defined as three-dimensional natural convection in an air filled cube of 3 m sides. The 3D view of the model setup is shown in Figure 3.1. As can be seen in Figure 3.2 experimental assembly consists of an aerated concrete case and supporting frame on which the concrete is mounted, the heater and the fin array. The created numerical model has an aerated concrete, a heater plate for heat generation and a heat sink attached to the heater. Figure 3.3 shows different parts of the model assembly separately.

16

Table 3.1 Dimensions of the components

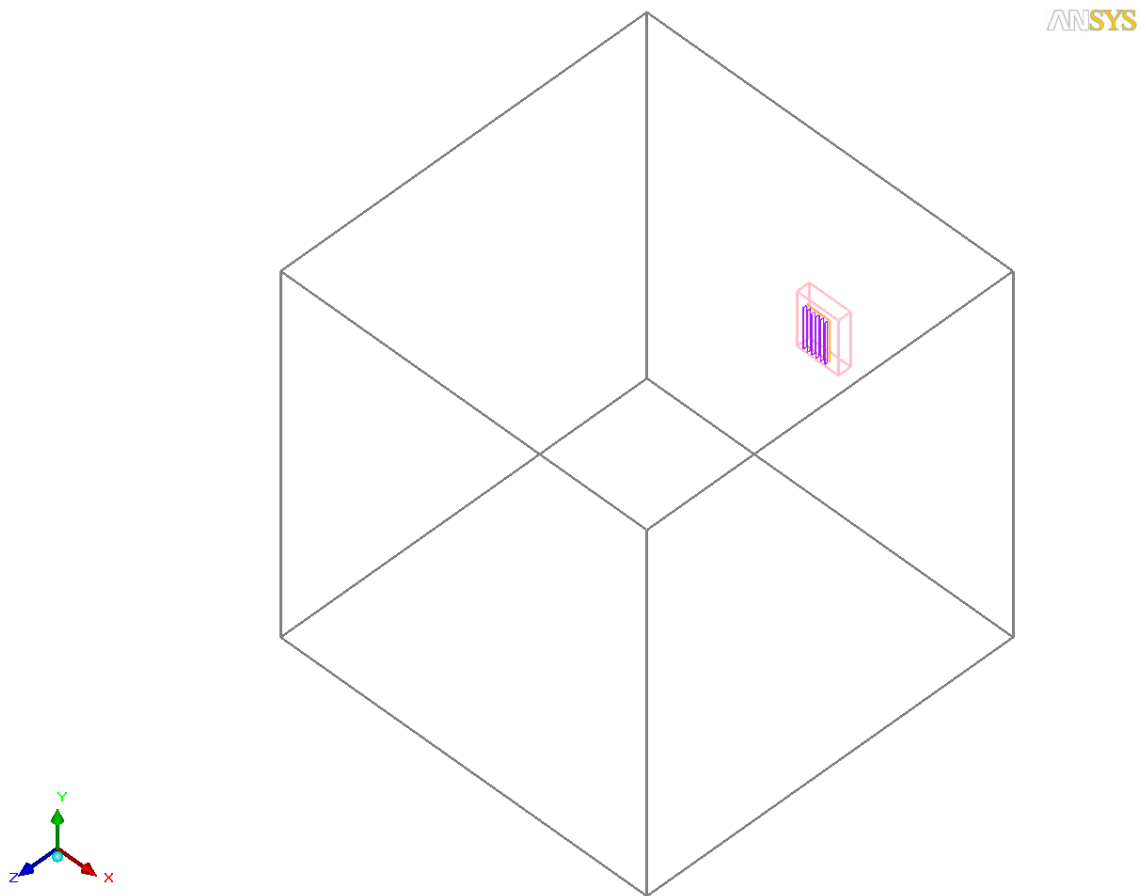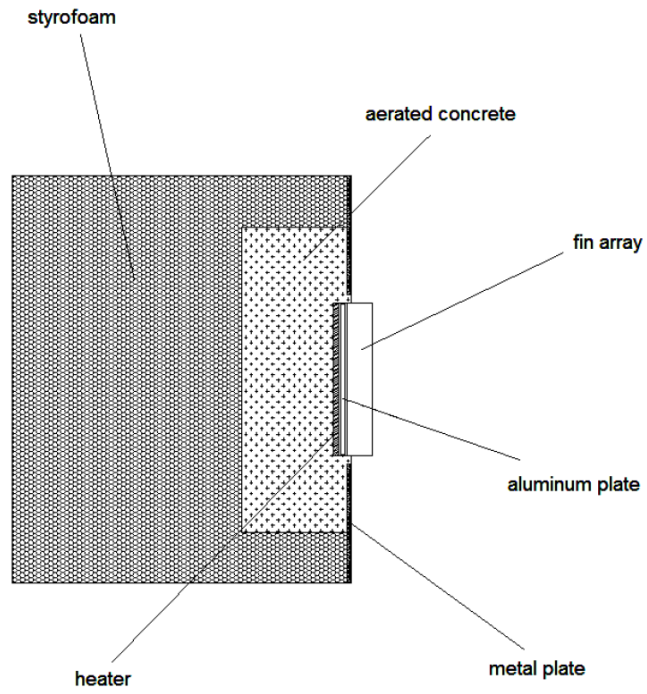| Dimensions (mm)		
Component	Model Setup 1	Model Setup 2
Heat sink	180×250×5	180×340×5
Heater base plate	180×250×5	180×340×5
Aerated concrete	340×450×100	340×450×100
Computational domain (cabinet)	3000×3000×3000	3000×3000×3000

Figure 3.1 The 3D view of model setup

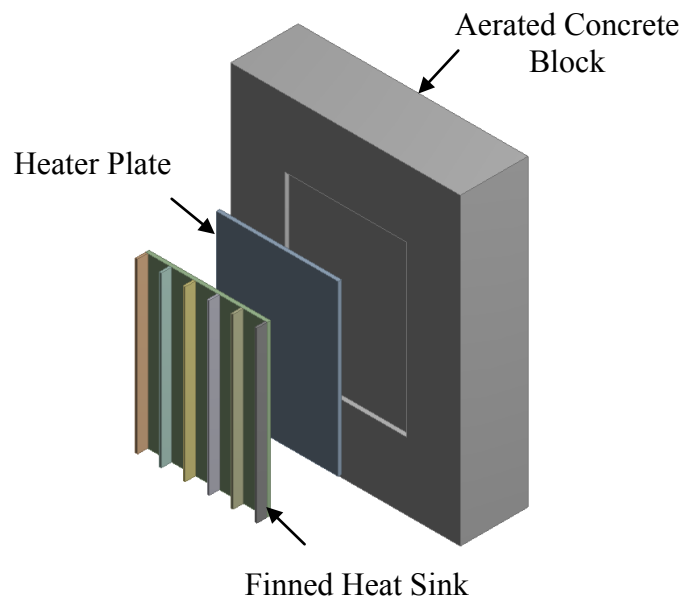Figure 3.2 Schematic view of experimental assembly

Figure 3.3 Schematic view of the model assembly

18

3.1.2 Material Properties

In this study the materials for each component of the model are taken as they are given in Ref. [1]. Table 3.2 demonstrates the material properties used in this analysis. Natural convection heat exchanger fins are usually manufactured from aluminum alloy because of its high thermal conductivity, structural strength and durability. As can be seen from this table, fin array material is aluminum. Aluminum has high conductivity which brings about almost the same surface temperature all over the fin array. However it has low emissivity. Therefore radiation contributes around 20% to the total surface heat transfer throughout this study.

Table 3.2 Material properties of the components

Component	Material Type	Specific Heat (J/kg C)	Conductivity (W/m K)	Emissivity	Roughness (mm)
Concrete Block	Aerated Concrete	1000	0.15	0.9	2
Heater Base Plate	Aluminum	900	130	0.2	0.02
Fin array	Aluminum	900	130	0.2	0.02

3.1.3 Dimensions of Fin Array Configurations

The test setups consisted of an array of vertical rectangular fins which are the same in dimensions of three parameters: fin thickness, base thickness and fin array width. The other parameters vary as shown in Table 3.3. Figure 3.4 shows fin array geometry with the symbols used to denote the dimensions.

Table 3.3 Dimensions of fin array configurations

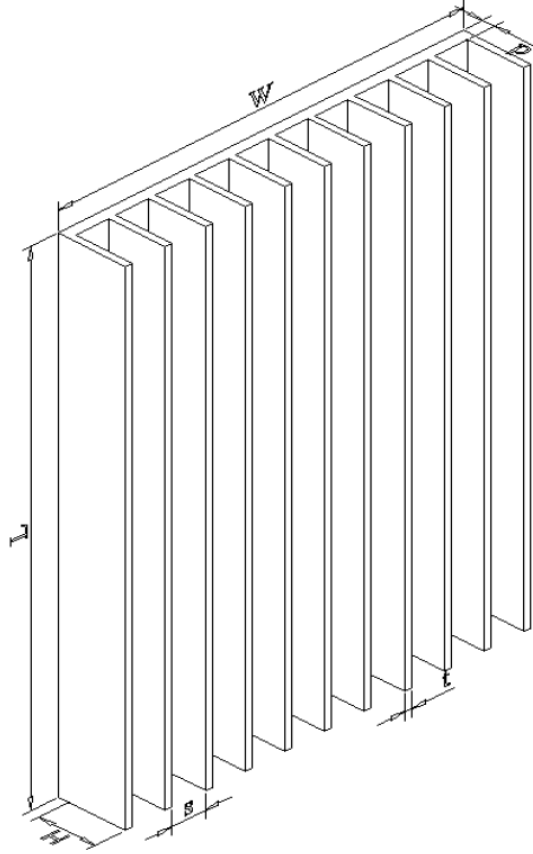| Fin Length L (mm)	Fin Width W (mm)	Fin Thickness t (mm)	Base Thickness d (mm)
250, 340	180	3	5
Set No.	Fin Height H (mm)	Fin Spacing S (mm)	Number of Fins (N)
1	25	85.5	3
2	25	32.4	6
3	25	14.7	11
4	25	8.8	16
5	25	5.85	21
6	15	85.5	3
7	15	32.4	6
8	15	14.7	11
9	15	8.8	16
10	15	5.85	21
11	5	85.5	3
12	5	32.4	6
13	5	14.7	11
14	5	8.8	16
15	5	5.85	21

Figure 3.4 The 3D view of fin array

In addition to the geometric parameters, five different input powers between 25 W and 125 W are used in this study.

Corresponding to the experimental work, six thermocouples are used in order to get the exact values of temperature on different parts of fin array surface. The exact places of these thermocouples are indicated in Figure 3.5. Similarly, these points are modeled inside Fluent and finally the average of these six values is presented as T_w. In the analysis, measurements at these six points should demonstrate a maximum difference of less than $1^{\circ}C$ during steady state, indicating that isothermal condition is achieved at the fin array base plate.
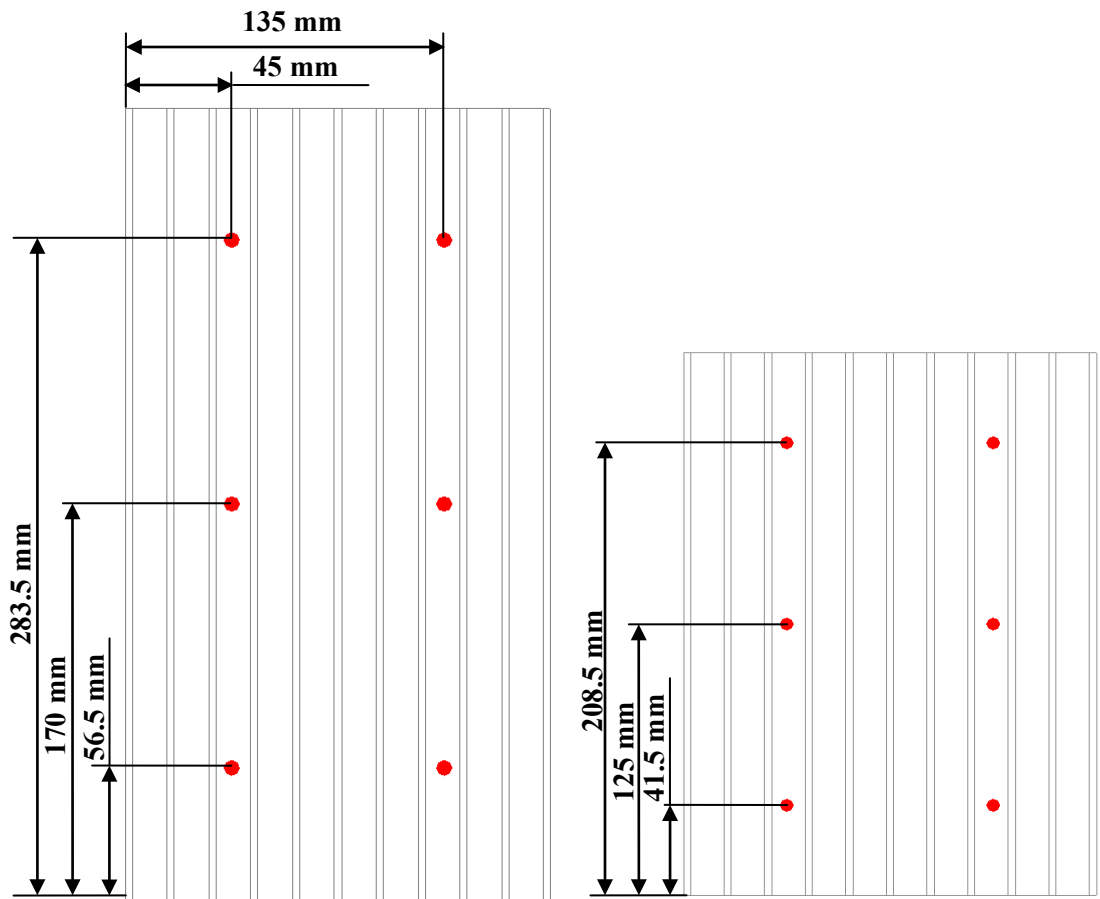
Figure 3.5 Locations of the six temperature reading points (Thermocouples)

3.1.4 Setup Operating Conditions and Assumptions

- Flow regime is assumed as turbulent and zero equation is chosen as a turbulence model. [44]

- Gravitational acceleration is taken as -9.80665 m/s^2 in y direction.

- Radiation is on. The surface to surface radiation model which uses view factors is chosen for calculating the radiation heat transfer from the heat sink surface.

- Cabinet wall temperature is taken as 20$^\text{o}$ C.

22

- The fluid is taken as air and the temperature of the ambient is 20° C.

- Ideal gas law is selected and the operating pressure is taken as 101325 N/m^2.

- Steady state solution is selected.

- No slip boundary condition for surfaces.

- No contact resistances.

3.1.5 Solution Settings

- Number of iterations is 250.

- The convergence criterion of flow is taken as 10^{-3}.

- The convergence criterion of energy is taken as 10^{-7}.

- Second order discretization scheme is used for pressure, momentum and temperature in order to increase accuracy of the results. In addition, double precision is selected.

- Underrelaxation factors are taken as follows:
  o Pressure : 0.3
  o Momentum : 0.7
  o Temperature : 1.0
  o Viscosity : 1.0
  o Body Forces : 1.0

3.1.6 Meshing

A good computational mesh is an essential ingredient for a successful and accurate solution. If the overall mesh is too coarse, the resulting solution may be inaccurate. If the overall mesh is too fine, the computational cost may become prohibitive. Cabinet, which represents a room, is large compared to the other parts in this study. It is not possible to model the entire room with a fine mesh due to computational costs.

Since we have higher temperature and velocity gradient near the plate fin we should have finer mesh near it and coarse mesh away from it. Due to these facts, the block, heater plate and fin array were separated from the computational domain as an assembly. By the help of this separate assembly definition, it is possible to create finer mesh sizes inside and coarser ones outside of it which leads to lower total number of cells. The unstructured hexahedral grid is used to generate mesh in this model. The non-conformal mesh structure of the model is shown on an *x-z* cross section in Figure 3.6.
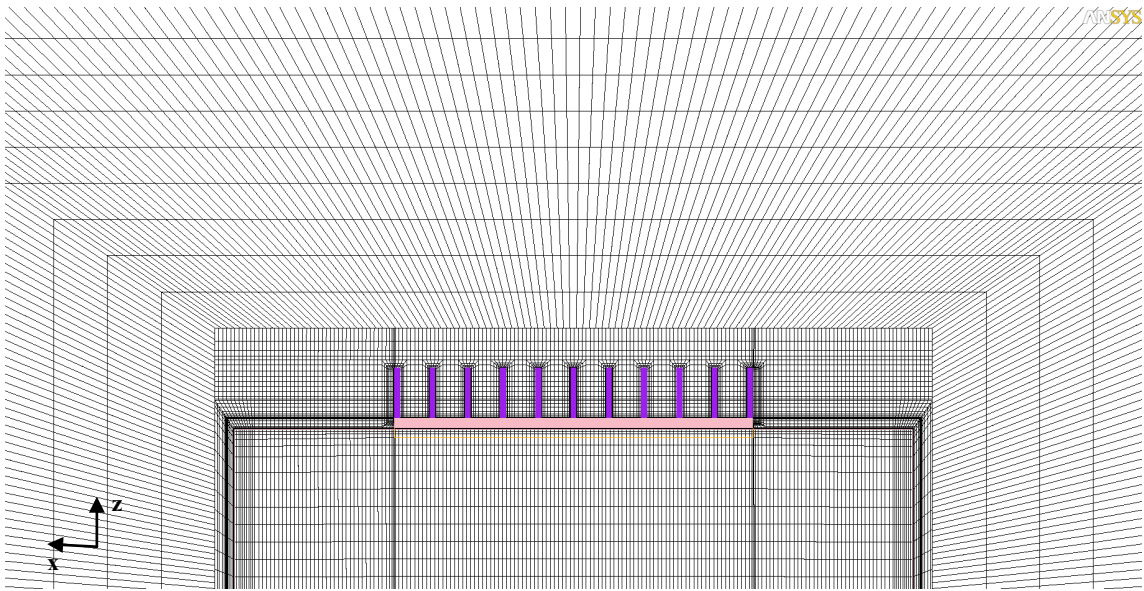

Figure 3.6 Top view of non-conformal mesh

The finer mesh around the fins can be seen in Figure 3.7. The average number of the cells for each analysis was estimated as 3 million. Effects of different mesh sizes on the results and the reason behind the selection of mesh size are given in Appendix A.
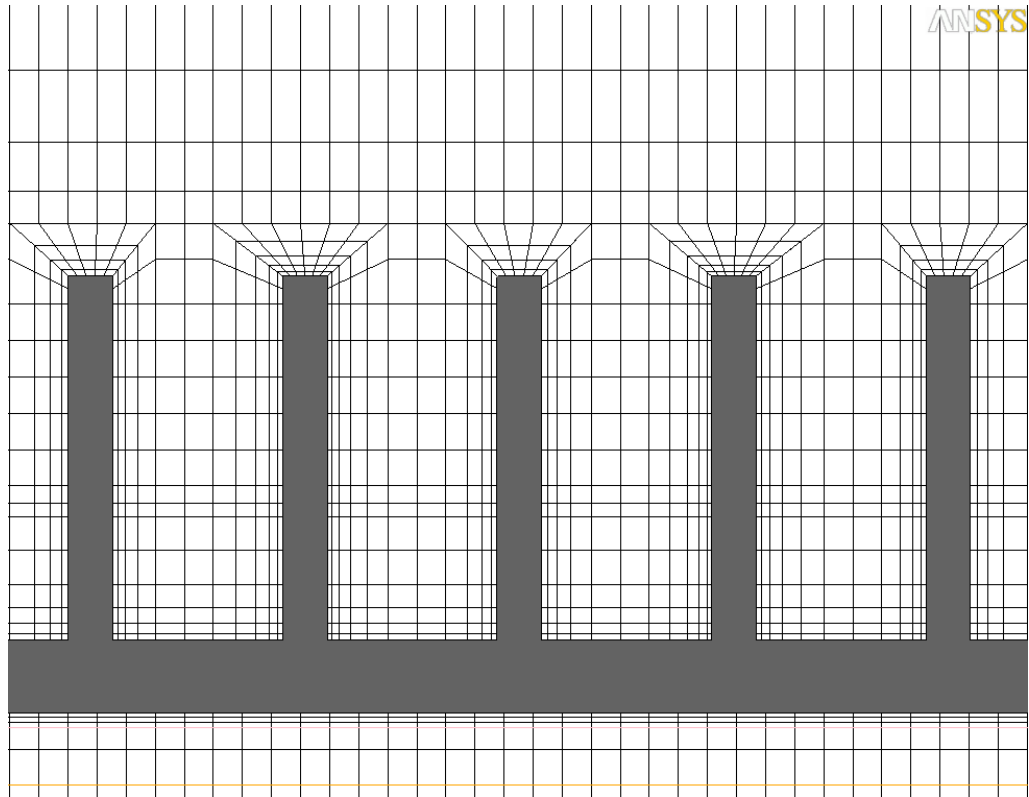
Figure 3.7 Fine meshes near the fins

3.2   Model Verification

The initial step in verification of the data is to adjust the main heater for heat losses. In order to obtain the fin array exact performance, the setup and the procedure had to be adjusted to determine the convection and radiation heat transfer rates. This was accomplished by two different methods. In the first method, natural convection over a vertical heated plate is investigated and the results are compared with the results of correlations that are available in literature. In the second method, two close parallel plates are used as explained in Ref. [1].

3.2.1 Vertical Flat Plate

In this method, heater base plate is used as the vertical flat plate. The dimensions are the same as the ones that are mentioned in Table 3.1. Various power inputs ranging from 20 W to 140 W are generated inside this plate. For each input power, the average temperature of the flat plate and also values for radiation and convection heat transfer from it are obtained. Steady state reached when the power input to the heater is equal to the total output heat transfer, which occurs by natural convection, radiation and by conduction to the remaining parts of the setup. The view of vertical flat plate method is presented in Figure 3.8.
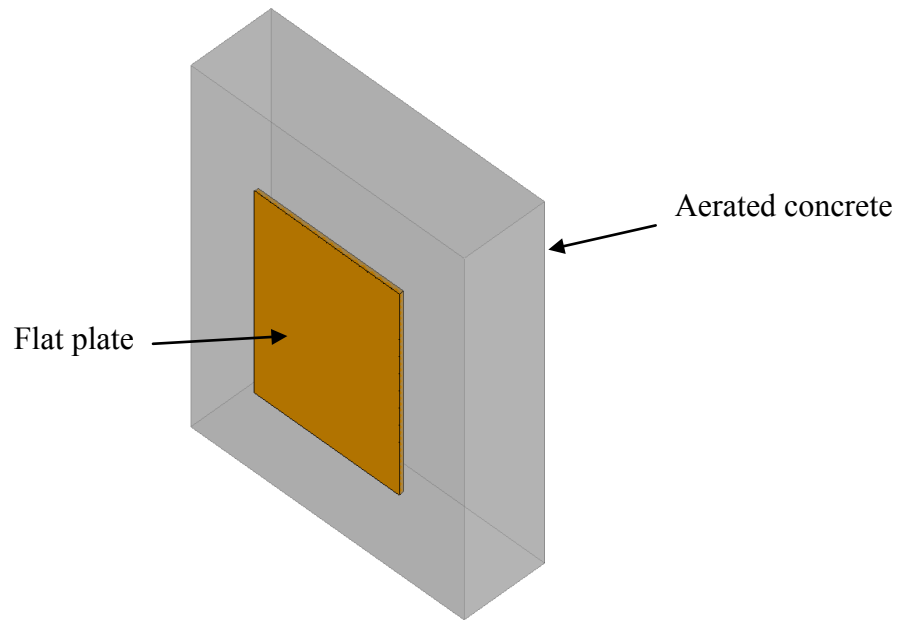

Figure 3.8 Schematic view of vertical flat plate model

Table 3.4 presents the convection heat transfer and surface average temperature values for the flat plate with different power inputs. In addition, Figure 3.9 shows the comparison between the values obtained for convection heat transfer rate in Ref. [1] and present study.

Table 3.4 Convection heat transfer and surface average temperature values
for flat vertical plate

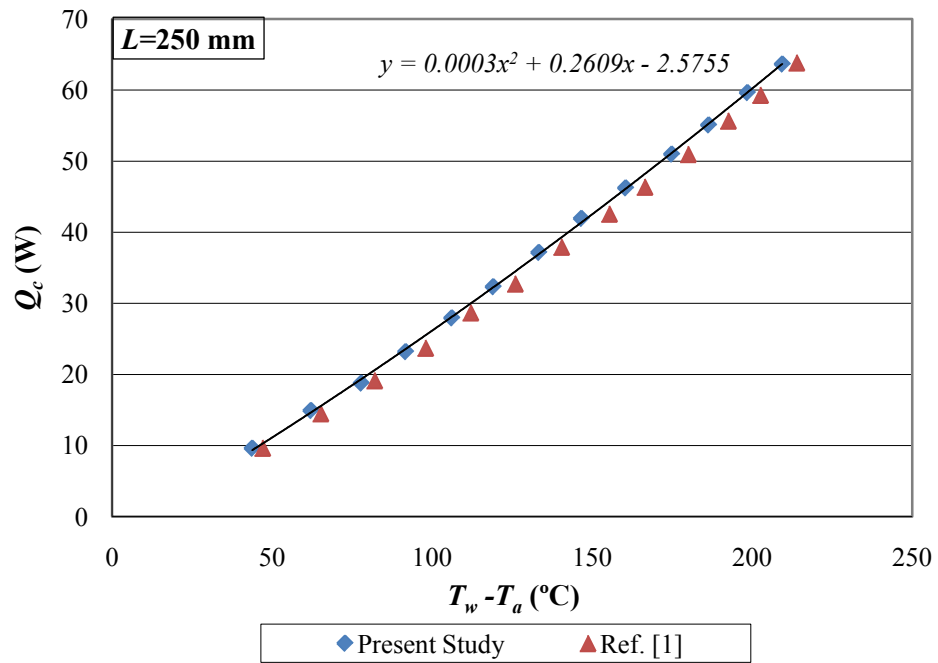| Q_{in} (W)	Q_c (W)	T_w (ºC)
20	9.61	62.77
30	14.92	81.12
40	19.77	96.83
50	24.19	110.71
60	28.94	125.12
70	33.33	138.07
80	38.15	152.32
90	42.94	165.62
100	47.63	179.44
110	52.98	193.82
120	57.08	205.37
130	61.63	217.48
140	65.65	228.39

Figure 3.9 Comparison of convection heat transfer rates between present study and
Ref. [1] for flat vertical plate

In order to compare the results with the experimental studies, Nusselt numbers related to surface heat transfer should be calculated. Also Nusselt numbers for each simulation were determined by using different correlations exist in the literature. The procedure for achieving the quantities is presented in Appendix B. The tabulated results and the comparison of the Nusselt numbers are given in Table 3.5. It can be inferred from the Table 3.5 that the results obtained from analyses are consistent with the results obtained from theoretical correlations.

Table 3.5 Comparison of Nusselt numbers

Q_{in} (W)	Ra	Nu				
		Present Study	McAdam's relation [43]	Churchill and Usagi's relation [43]	Churchill and Chu's first relation [43]	Churchill and Chu's second relation [43]
20	48576725	45.59	49.26	42.90	49.26	43.58
30	60842614	48.33	52.11	45.37	52.63	46.05
40	68545985	49.92	53.68	46.74	54.51	47.42
50	73641262	50.83	54.66	47.57	55.67	48.25
60	77812433	51.53	55.41	48.23	56.57	48.91
70	80123273	51.99	55.82	48.57	57.06	49.25
80	81679041	52.16	56.09	48.80	57.37	49.48
90	82662917	52.48	56.26	48.93	57.55	49.61
100	82894394	52.29	56.30	48.95	57.59	49.63
110	82847484	52.45	56.29	48.94	57.57	49.62
120	82500621	52.28	56.23	48.88	57.48	49.56
130	82029315	52.25	56.15	48.80	57.37	49.48
140	81434240	52.09	56.05	48.70	57.23	49.38

3.2.2 Vertical Two Parallel Flat Plates

As a second method for adjusting the setup, another plate is placed very close to the heater plate. The plates were of the same size and of the same material as the base-plate of the fin arrays. For setup 1 plate dimensions are 250 mm×180 mm and for setup 2 they are 340 mm×180 mm. According to Ref. [4] " In order to have pure conduction through the air between the plates, either the Rayleigh number based on plate width had to be less than 1000, or the aspect ratio (ratio of the plate width to the distance between the plates) had to be greater than or equal to 100." Since the Rayleigh number based on plate width in this study is on the order of 10^8 the first criteria could not be satisfied. But the second criterion can be satisfied depend on the ratio which is about 100. So that the dissipation modes between these plates are by conduction and radiation.

Like the first method, 13 different power inputs are used. Since the power input to the heater plate is known, the heat loss to the environment by means of conduction can be calculated by subtracting the radiative heat transfer between these two plates from the total power. The heated plate temperature is represented by T_1 and the opposite plate temperature is represented by T_2. The heat flow from the heated plate to the opposite plate is Q_{out}. The temperature of both plates and heat flow from the heated plate to the other one are obtained for various power input. The 3D view of the modeled two parallel plates mounted on the concrete block is shown in Figure 3.10.
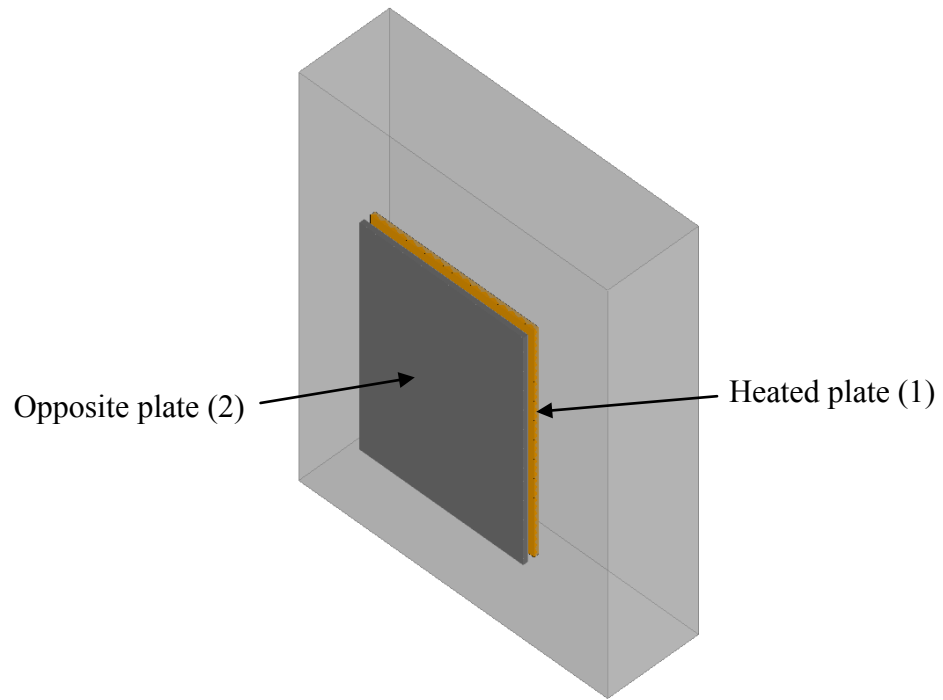
Figure 3.10 Schematic view of two parallel plates model

The variation of temperature in both plates and the output heat transfer rate from the heated plate to the opposite one (L=340 mm) for each of the power input are plotted in Figure 3.11 to Figure 3.13.
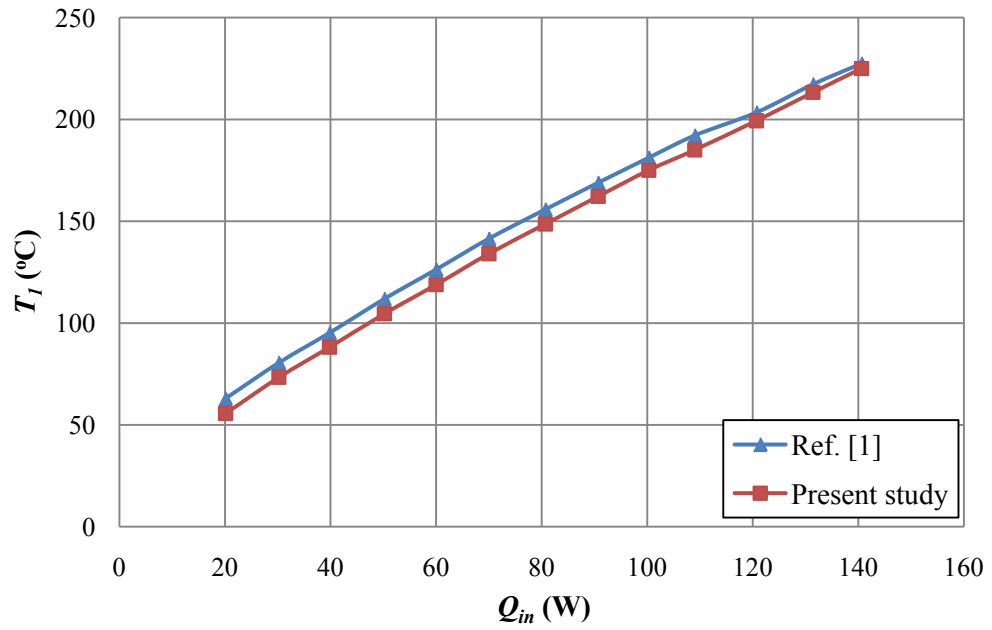
Figure 3.11 Variation of heated plate temperature with input power for *L*=340 mm
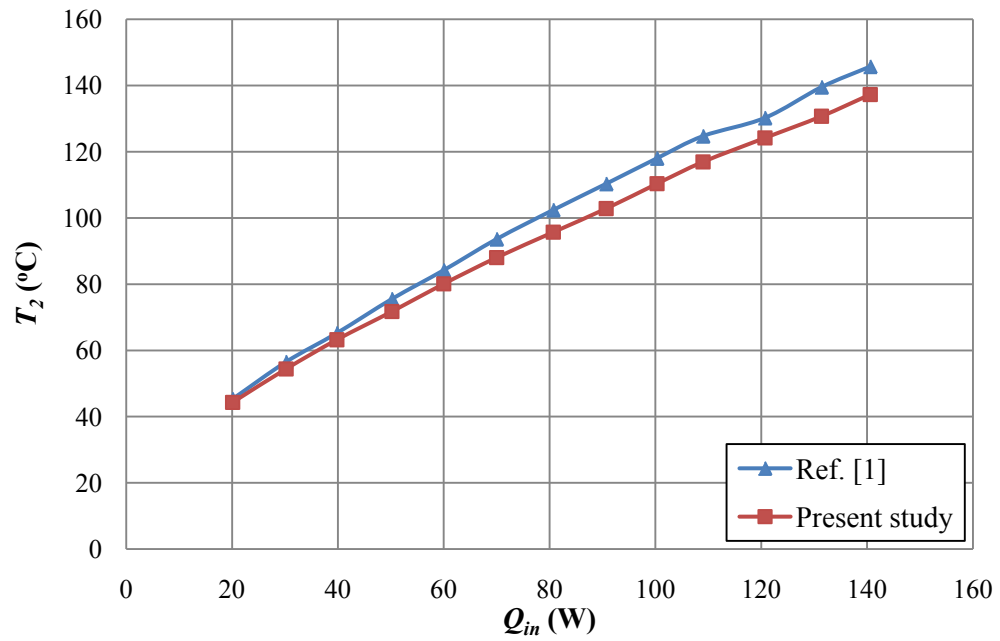

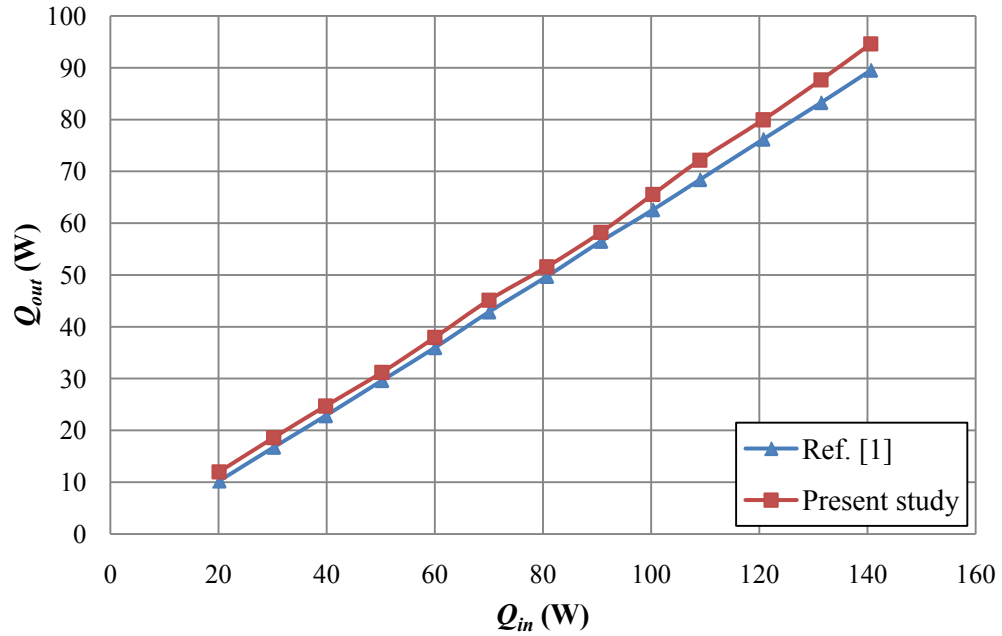Figure 3.12 Variation of opposite plate temperature with input power for *L*=340 mm

Figure 3.13 Variation of Q_{out} with input power for L=340 mm

These plots reveal that except T_2 which deviates around 5% in higher input powers, the numerical data are in good agreement with the experimental results. This agreement confirms the validity of this setup and numerical procedure. However, since the fin arrays are mounted on the plate by mechanical means, it is not possible to obtain an exactly similar model. It is possible that there was an imperfect contact between the bottom plate and the fin array. Accordingly, the contact resistance between the bottom plate and fin array may cause different output heat results. Since it is not possible to model this contact resistance precisely, in present study model it is assumed that the fin array mounted on the bottom plate with no contact resistance at all.

3.3   Results and Discussions

In this section the results that were obtained from the numerical analysis are presented. For the sake of comparison, these numerical results are being validated with the experimental results that are existed in Ref. [1]. The same number of fin configurations and power inputs which were used in the experiment are investigated in this study. The effects of different parameters such as fin spacing and fin height on the rate of heat dissipation are shown. Figures of only a few selected fin configurations are presented in each section in order to increase the readability of the chapter. The rest of the plots are given in Appendix D.

3.3.1   Effect of Fin Spacing

The basic equation describing heat loss from the fin array is:

$$Q=hA\Delta T \tag{3.1}$$

From Equation 3.1 it can be seen that, for a constant ΔT, if the heat transfer coefficient, h, is invariant, an increase of heat transfer rate could be obtained by an increase in the extended surface area. It implies that the fins should be placed as close together as possible. However, the heat transfer coefficient is, in fact, not a constant and decreases as the fin spacing is reduced because the local air temperature rises the closer the fins are together. The closer the fins are to one another:

- The greater the mean local air temperature.
- The more suppressed convective currents which cause to decelerate the air flow.
- The larger geometry view factor of one fin by an adjacent fin, and so a lower rate of thermal radiation loss per unit area of the fin's surface will ensue.

The surface area in contact with coolant increases as the number of fins per unit width increases due to decreasing fin separation. But, simultaneously, the local heat transfer coefficient for heat losses from the fins decreases. Because of these conflicting trends,

an optimal fin separation corresponding to a maximum steady state rate of heat dissipation exists.

In this stage, average temperature variations of fin arrays with respect to fin spacing are demonstrated. Besides that, variations of convection heat transfer with respect to fin spacing are presented as well.

Figure 3.14 and Figure 3.15 illustrate the variation of average fin temperature with fin spacing for 5 different power inputs Q_{in} = 25W, 50W, 75W, 100W, 125W. These figures represent special case of fin configuration with H=25 mm for fin length L=250 mm and L=340 mm respectively. The obtained results from Fluent are plotted along with the experimental data of Ref. [1].
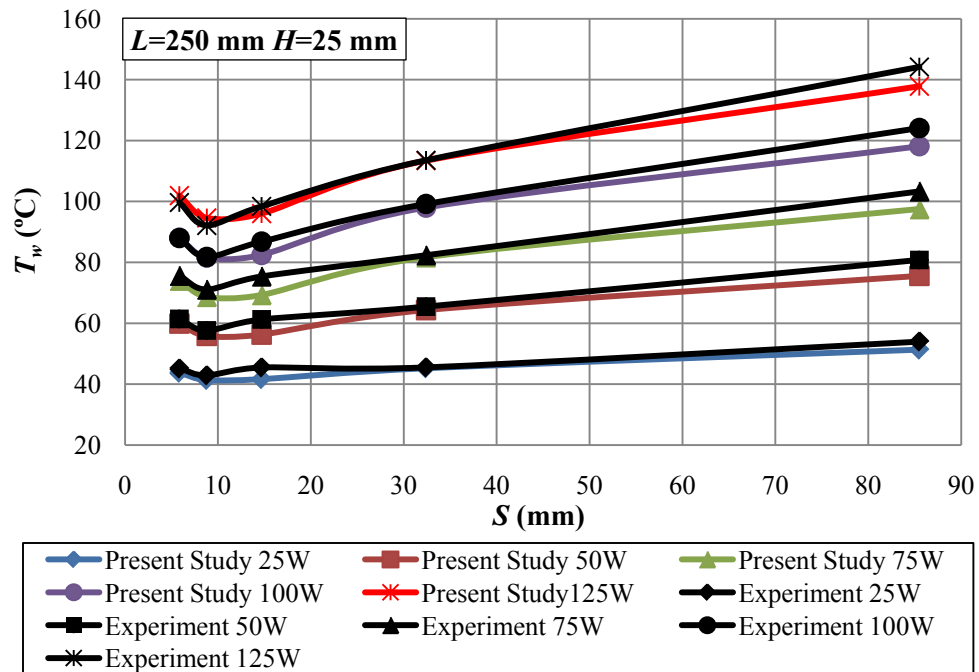
Figure 3.14 Variation of fin array average temperature with fin spacing for
L= 250 mm, H=25 mm
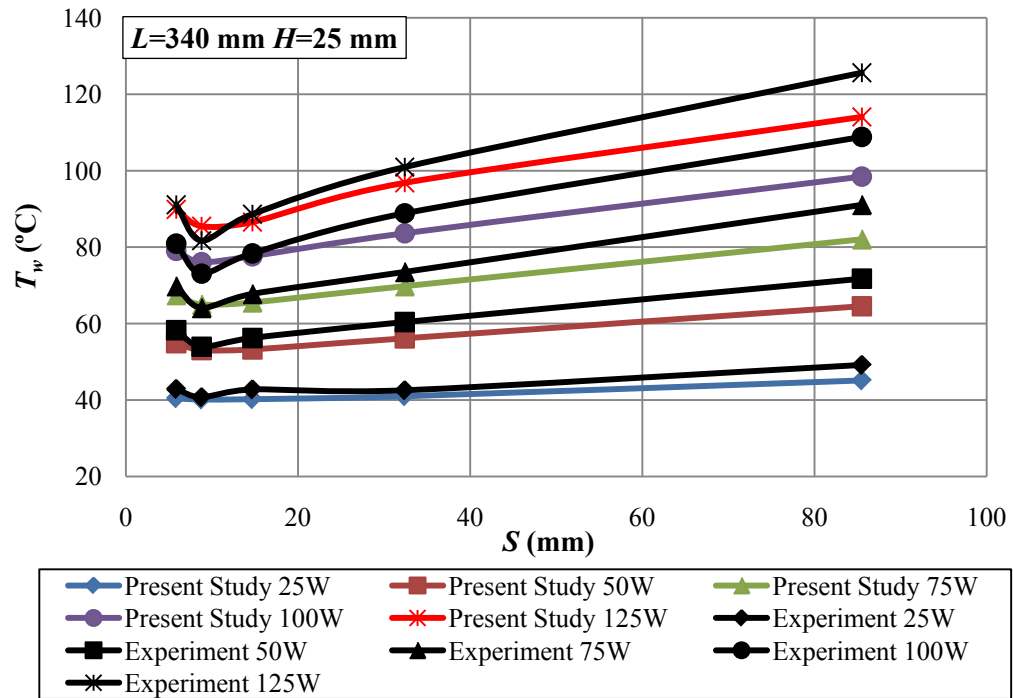
Figure 3.15 Variation of fin array average temperature with fin spacing for
L=340 mm, *H*=25 mm

A good agreement is observed between the numerical results and the experimental results. Although there are some differences between the numerical and experimental results, but both follow the same trend as can be seen in the figures.

Subsequently, change of the convection heat transfer which is decoupled from the radiation heat transfer, with respect to fin spacing is illustrated in Figure 3.16 and Figure 3.17. They present the special case of fin height *H*=25 mm for fin lengths *L*=250 mm and *L*=340 mm respectively. Each figure includes the results for 5 different input powers as mentioned before. The experimental results given in Ref. [1] are also plotted in the same figures in order to compare the results.

35
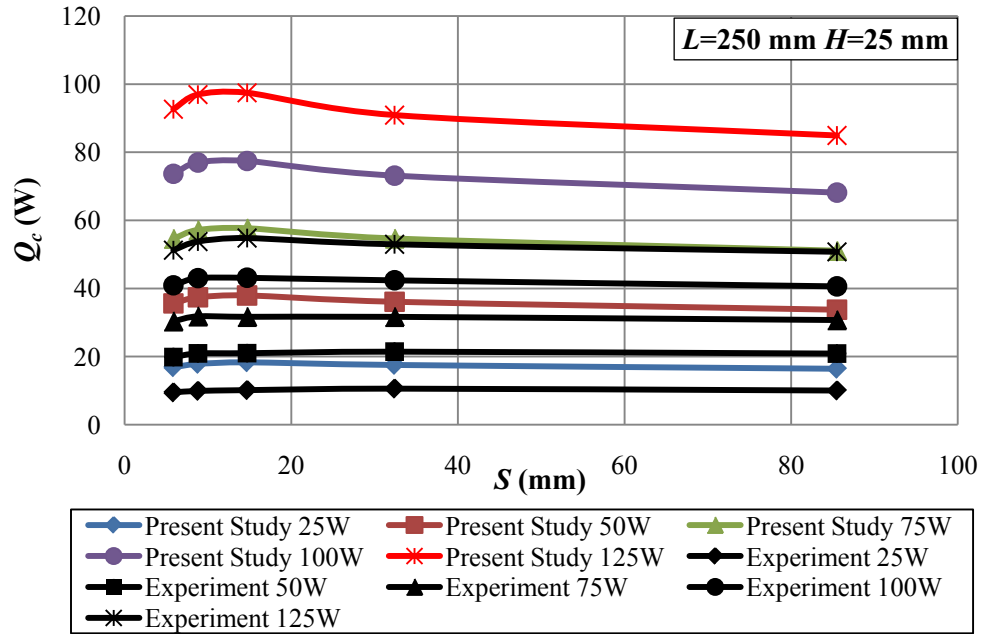
Figure 3.16 Variation of convection heat transfer with fin spacing for
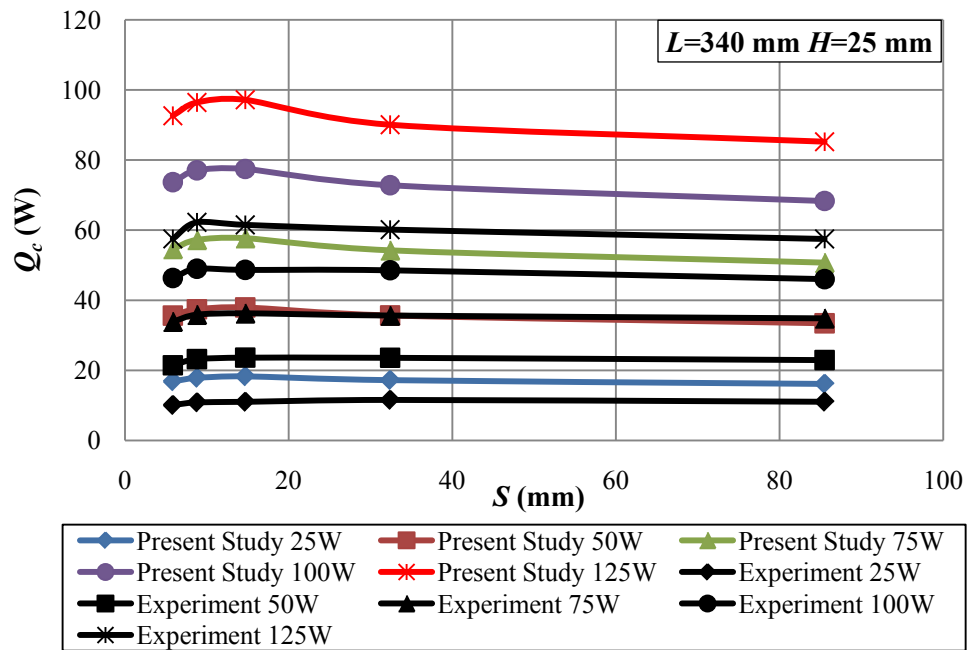*L*=250 mm, *H*=25 mm

Figure 3.17 Variation of convection heat transfer with fin spacing for
L=340 mm, *H*=25 mm

Fluent only gives the total heat transfer rate and the radiation heat transfer rate. In order to find the convection heat transfer rate from fins, radiation heat transfer rate is subtracted from the total value of heat transfer.

In this study the radiation heat transfer from the fin array to the surrounding is relatively small due to the use of low emissivity (≈ 0.2) material. In practice, high emissivity surfaces should be used in order to maximize the rate of heat dissipated by radiation. Although the contribution of radiation heat transfer from the fin array increases with decreasing fin spacing, the effect of this variation on the optimal determined fin spacing in this study will usually be negligible for higher emissivity surfaces.

In the plots related to convection heat transfer the difference between the experimental and numerical results is more significant. Despite the fact that the model used in present study is verified as explained in Section 3.3.1, it is still not possible to obtain the same results with the experimental ones. Although total heat transfer rates obtained in this study match with the results provided in Ref. [1] but convection heat transfer rates which are calculated by subtracting the radiation heat transfer rate from the total heat dissipation does not match well with the experimental results. The unknown experimental radiative conditions, the mounting of the fin arrays on the heater base plate, the neglected contact resistance and the lack of details of the experimental setup may be the reasons behind the difference in the results. However similar to the average temperature plots, although there are significant differences between the experimental and numerical analysis results, both follow the same trends.

It can be easily distinguished from the plots that in certain fin spacing, maximum rate of convection heat transfer is achieved. Close inspection of figures presented in Section 3.3.1 reveals that optimum fin spacing does not vary significantly with input power. According to the obtained results, for a given input power, with an increase in fin spacing, temperature first decreases to a minimum value and then increases continuously. Along with that increase in fin spacing the heat transfer first increase to a maximum value and then it decreases continuously. Furthermore when the fin spacing is

37

very low, convection heat transfer rate decreases due to the change in the interactions of the boundary layers along the fin channel. Under this condition, cold air enters from the bottom ends of the channel and leaves the channel without reaching the middle part of the channel since a greater part of the channel is occupied by stationary heated air. On the other hand in the wider fin spacing air can also enter the fin spacing from the above which accelerate the rate of heat transfer from the fin array.

3.3.2   Optimum Fin Spacing

The value of fin spacing at which the maximum convection heat transfer occurs is called the optimum fin spacing. It is clear from the figures presented in Section 3.3.1 that there is an optimum fin spacing at which maximum power can be dissipated and as a result the fin average temperature reaches the minimum value. It can be seen that these peaks are between $S = 8.8$ mm and $S = 14.7$ mm. For this reason and for the sake of finding this point precisely, more fin configurations which have fin spacing values of $S=9.64$ mm, $S=10.62$ mm, $S=11.75$ mm, $S=13.09$ mm are modeled with number of fins $N=15$, $N=14$, $N=13$ and $N=12$ respectively.

The average temperatures of fin arrays and also heat transfer rate from the fin arrays in the range of $S=8.8$ mm to 14.7 mm are plotted as a function of fin spacing for power inputs 25 W, 75 W and 125 W. As an example Figure 3.18 and Figure 3.19 show the results obtained for 3 fin heights $H=25$ mm, $H=15$ mm and $H=5$ mm. Figure 3.18 illustrates temperature changes and Figure 3.19 illustrates convection heat transfer changes of plate finned heat sink with respect to fin spacing for $L=250$ mm and $Q_{in}=125$ W
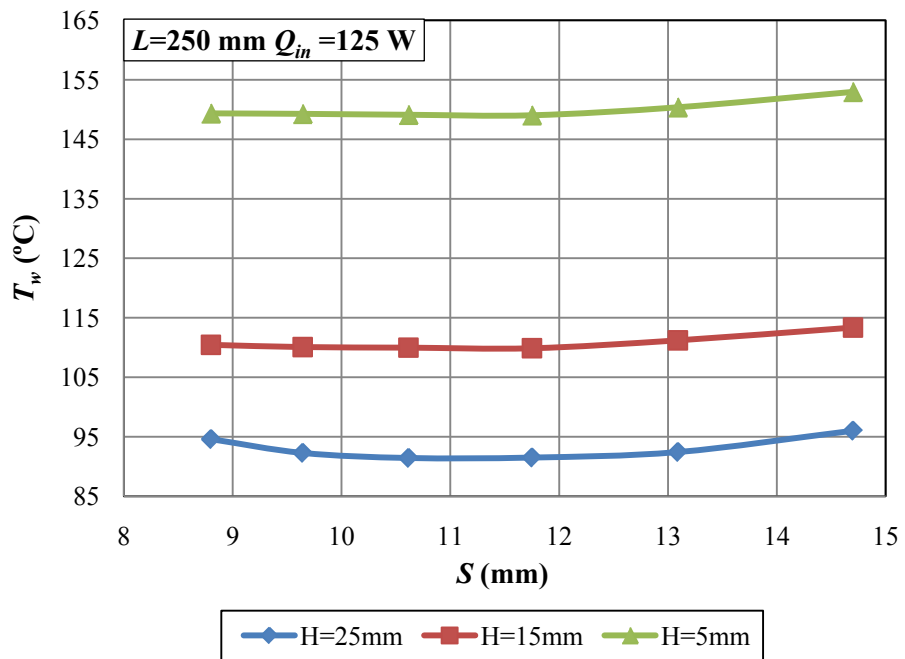
Figure 3.18 Variation of fin array average temperature with fin spacing for
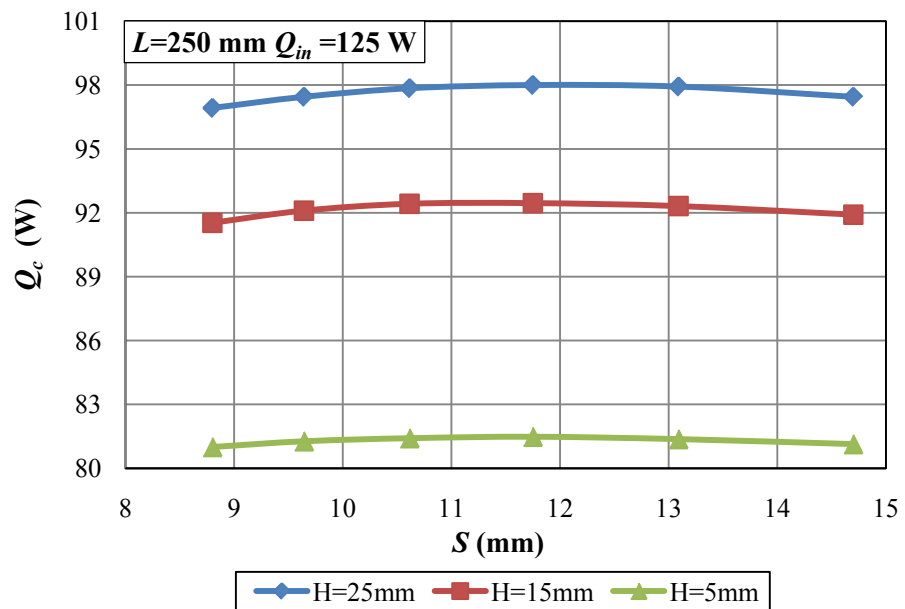*L*=250 mm, Q_{in}=125 W

Figure 3.19 Variation of convection heat transfer with fin spacing for
L=250 mm, Q_{in}=125 W

In order to find these optimum fin spacing values, a polynomial curve is fitted to each data. By taking the derivative of these polynomials, specific fin spacing in which the convection heat transfer is in the highest value can be found. Table 3.6 shows the optimum fin spacing for reaching maximum convection heat transfer rate and Table 3.7 shows the optimum fin spacing for getting lowest wall temperature in different cases. The differences between these two tables are due to changing view factors with fin spacing and related changes in radiation heat losses. For comparison, the optimum fin spacing values obtained in Ref. [1] are tabulated in Table 3.8.

Table 3.6 Optimum fin spacing values for maximizing convection heat transfer rate

Q_{in} (W)	Optimum Fin Spacing, S_{opt} (mm)					
	L=250 mm			L=340 mm		
	H=25 mm	H=15 mm	H=5 mm	H=25 mm	H=15 mm	H=5 mm
25	12.6	12.5	12.2	12.7	12.6	12.5
75	12.5	12.3	11.8	12.4	12.3	12.1
125	12.1	11.9	11.7	12	12.1	11.9

Table 3.7 Optimum fin spacing values for minimizing average temperature

Q_{in} (W)	Optimum Fin Spacing, S_{opt} (mm)					
	L=250 mm			L=340 mm		
	H=25 mm	H=15 mm	H=5 mm	H=25 mm	H=15 mm	H=5 mm
25	11.6	11.5	11.1	11.7	11.6	11.4
75	11.3	10.8	10.8	11.4	11.5	11
125	11.4	10.6	10.5	11.3	11.4	11

Table 3.8 Optimum fin spacing values from Ref. [1]

ΔT (K)	Optimum Fin Spacing, S_{opt} (mm)					
	L=250 mm			L=340 mm		
	H=25 mm	H=15 mm	H=5 mm	H=25 mm	H=15 mm	H=5 mm
50	11	10.9	-	11.9	11.8	-
75	10.9	10.8	10.7	11.8	11.7	11.6
100	10.8	10.7	10.6	11.7	11.6	11.5
125	10.7	10.6	10.5	11.6	11.4	11.4

3.3.3 Effect of Fin Length

Figure 3.20 presents the variation of heat dissipation according to different fin length and fin spacing for Q_{in}=75 W. Depend on the selection of two fin lengths, which are close in values, the effect of length is not meaningful. Close inspection of Figure 3.20 reveals that higher values of heat transfer obtained for L=250 mm compared to L=340 mm. The reason for these differences is the decrease of magnitude of fluid velocities with fin length, which causes also a decrease in the heat transfer. The increase of the fin length for a fixed value of the fin spacing causes an increase in the boundary layer interactions near the central part of the fin arrays. The interactions affect the heat transfer negatively. In addition, by carefully examining Figure 3.20 it is seen that in small fin spacings, the influence of fin length is more significant. Heat transfer reduction here is especially because of an inadequate space for air to move along the channel.
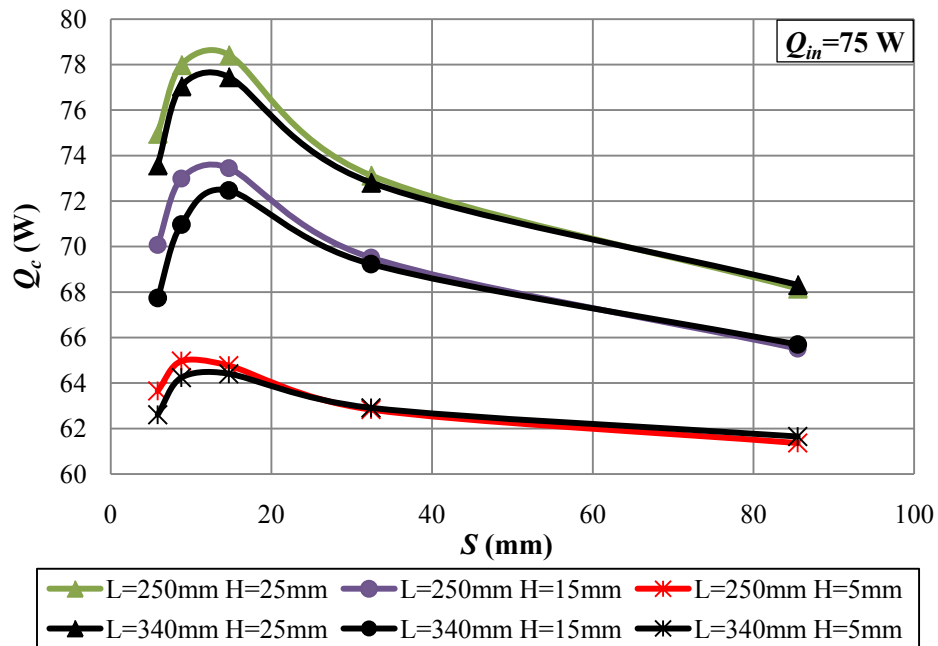
Figure 3.20 Variation of convection heat transfer with fin spacing for different fin lengths

3.3.4 Effect of Fin Height

The effect of fin height on convective heat transfer at selected average fin spacing using different power input values is shown in Figure 3.21 and Figure 3.22 for L =250 mm and L =340 mm respectively. They show that the performance of the heat sink depends on the fin height. These figures depict the fact that while the fin height increasing, the convective heat transfer rate increases from the fin arrays. Due to this reason in the case of larger fin heights, the available area of surface from which the heat transfers increases. Also due to the effect of the buoyancy force, increasing the height of the fin causes an increase in the pressure gradient along the fin length. This causes an increase in the flow rate of air entering the channel, therefore the average heat transfer increases. The plots related to different values of fin spacing are in Appendix D.
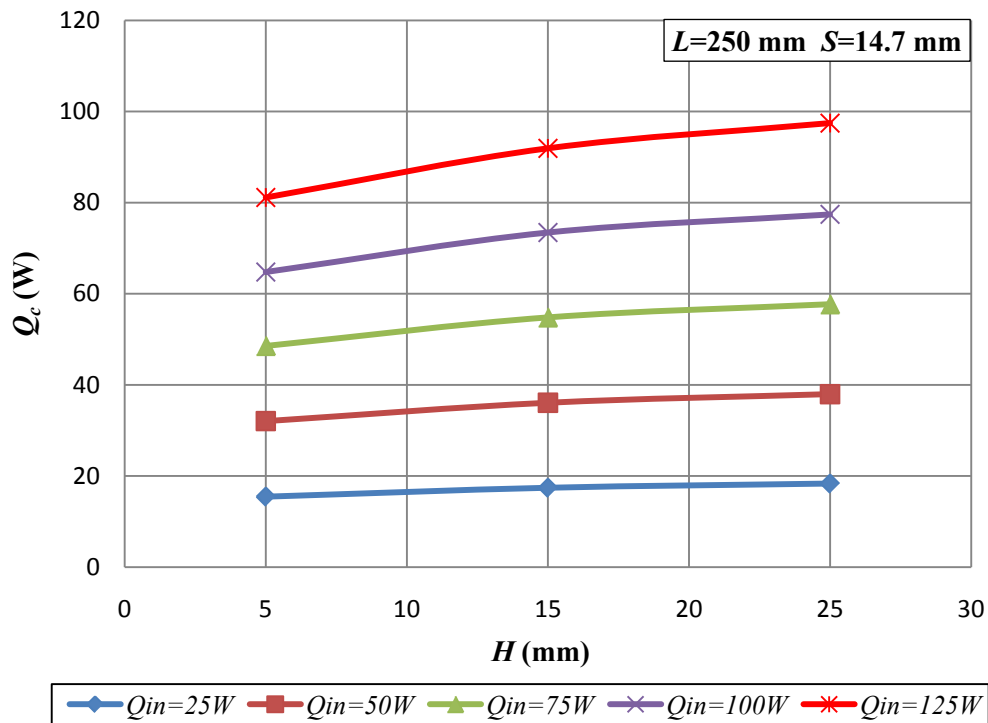
Figure 3.21 Variation of convection heat transfer with fin height for
L =250 mm, S =14.7 mm
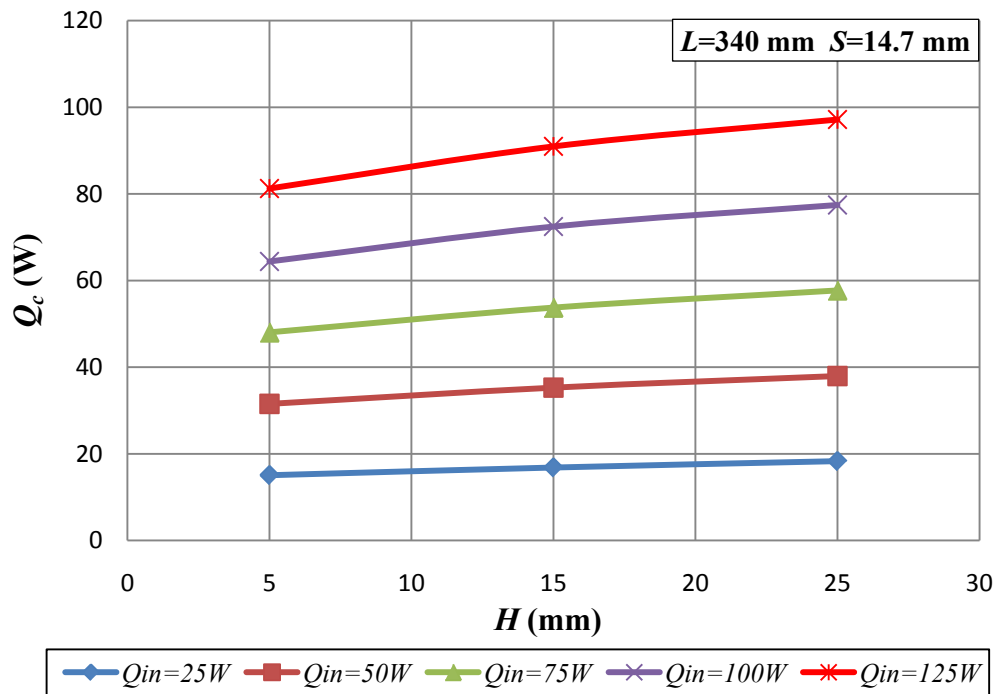
Figure 3.22 Variation of convection heat transfer with fin height for
L =340 mm, S =14.7 mm

3.4   Flow Visualization

An important advantage of CFD is its ability to visualize the flow. ANSYS Fluent contains a full suite of qualitative and quantitative post processing tools to generate meaningful graphics, animations and reports can readily convey simulation results. Visualization of velocity vectors, temperature contours, fluid particle traces, cut planes and x-y plots of results are all available for interpreting the results of a simulation. In this section the variation of temperature and velocity of the flow with different parameters are presented through visual images. The CFD simulations were performed over a wide range of fin array configurations. For each parameter effect, one of the mean fin array configurations is selected for comparison since there are many different fin array configurations to be investigated in this study and it is not possible to show them all.

43

3.4.1 Variation of Flow Speed with Input Power

In order to show the variation of flow speed with input power to the heater base plate, the following fin configuration is selected.

- Fin length, L=340 mm
- Fin height, H=25 mm
- Fin spacing, S=14.7 mm

Speed contours of the flow for three different input power, Q_{in}=25 W, Q_{in}=50 W and Q_{in}=75 W are shown on an x-y cross section in Figure 3.23 to Figure 3.25 respectively. The speed scale is same for all the figures.
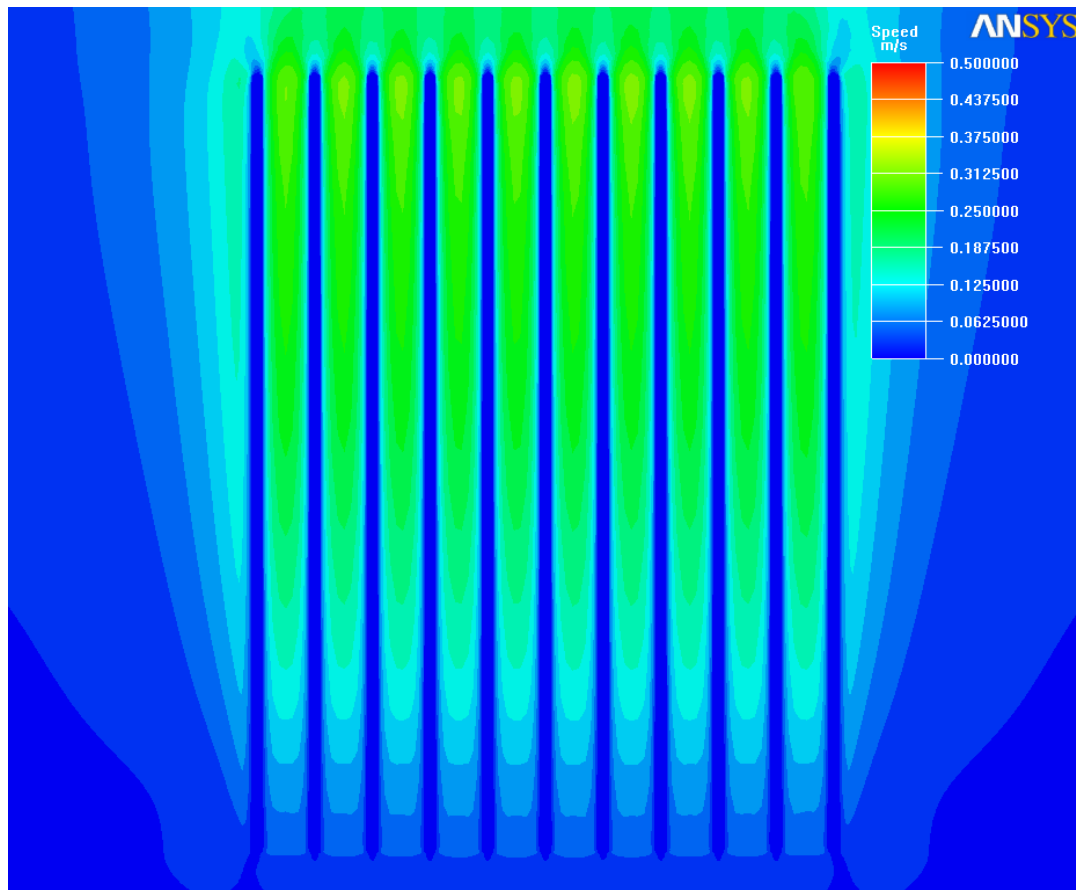
Figure 3.23 Speed contours for Q_{in}=25 W
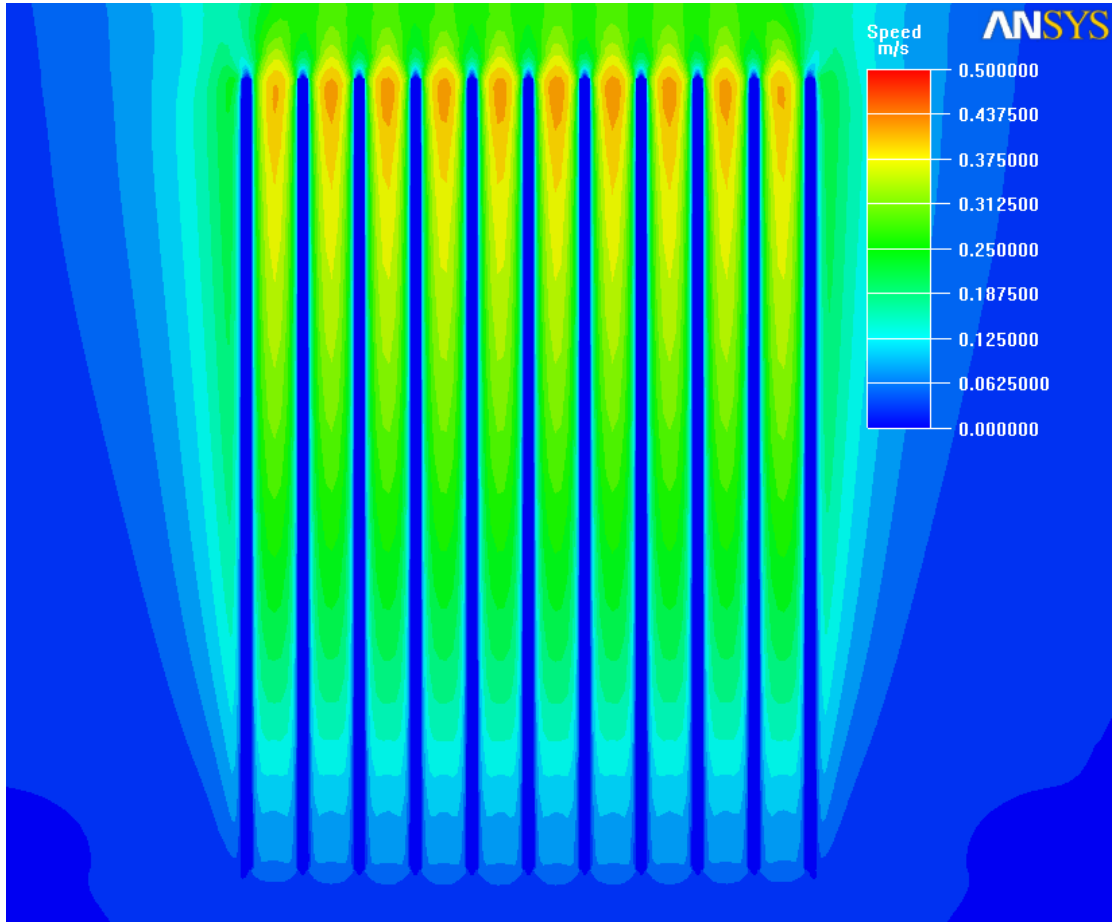
Figure 3.24 Speed contours for Q_{in}=50 W
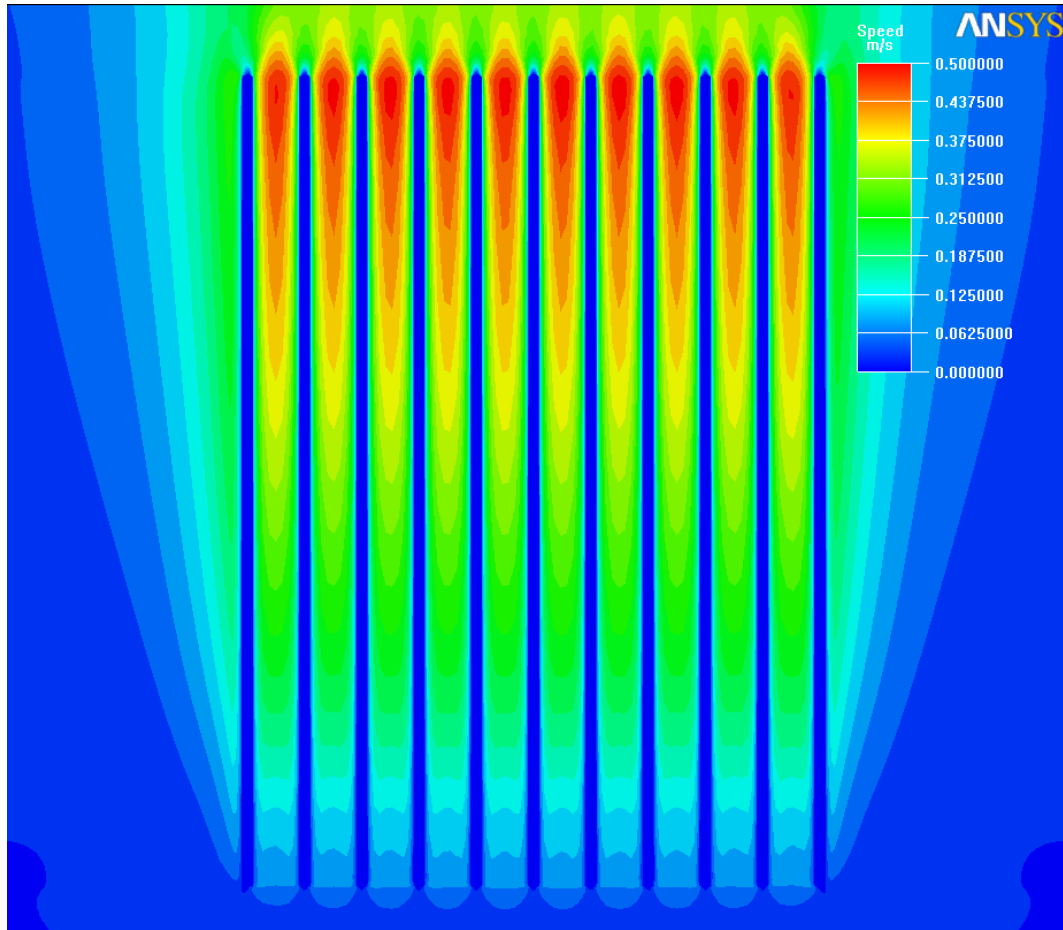
Figure 3.25 Speed contours for Q_{in}=75 W

As can be expected, speed of the flow increases by using higher input power. From the speed scale maximum speed for each case can be read which occurs near upper end of each channel. It is approximately 0.35 m/s, 0.43 m/s and 0.5 m/s for Q_{in}=25 W, Q_{in}=50 W and Q_{in}=75 W respectively.

3.4.2 Variation of Flow Temperature with Fin Height

For this aspect, the following fin configuration is used:

- Fin Length, L= 250 mm
- Fin Spacing, S = 14.7 mm
- Input power, Q_{in}= 50 W

Temperature contours of the flow for three different fin heights H=5 mm, H=15 mm and H=25 mm are shown on an x-z cross section in Figure 3.26 to Figure 3.28 respectively.
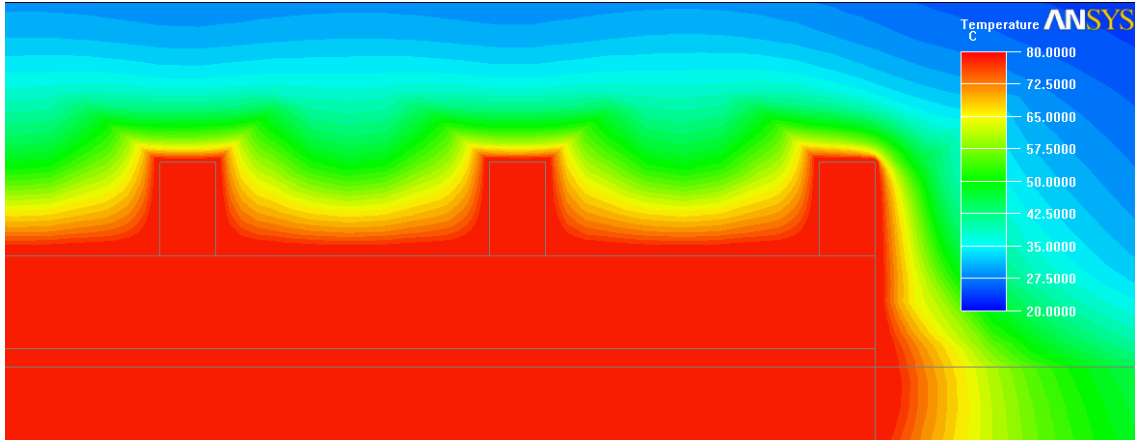
Figure 3.26 Temperature contours for H=5 mm
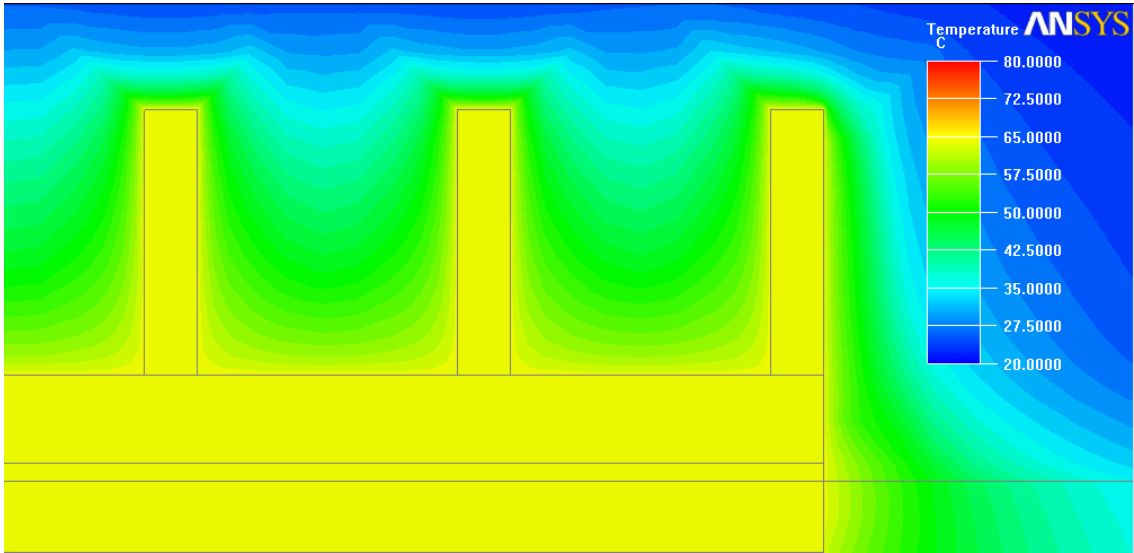
Figure 3.27 Temperature contours for *H*=15 mm
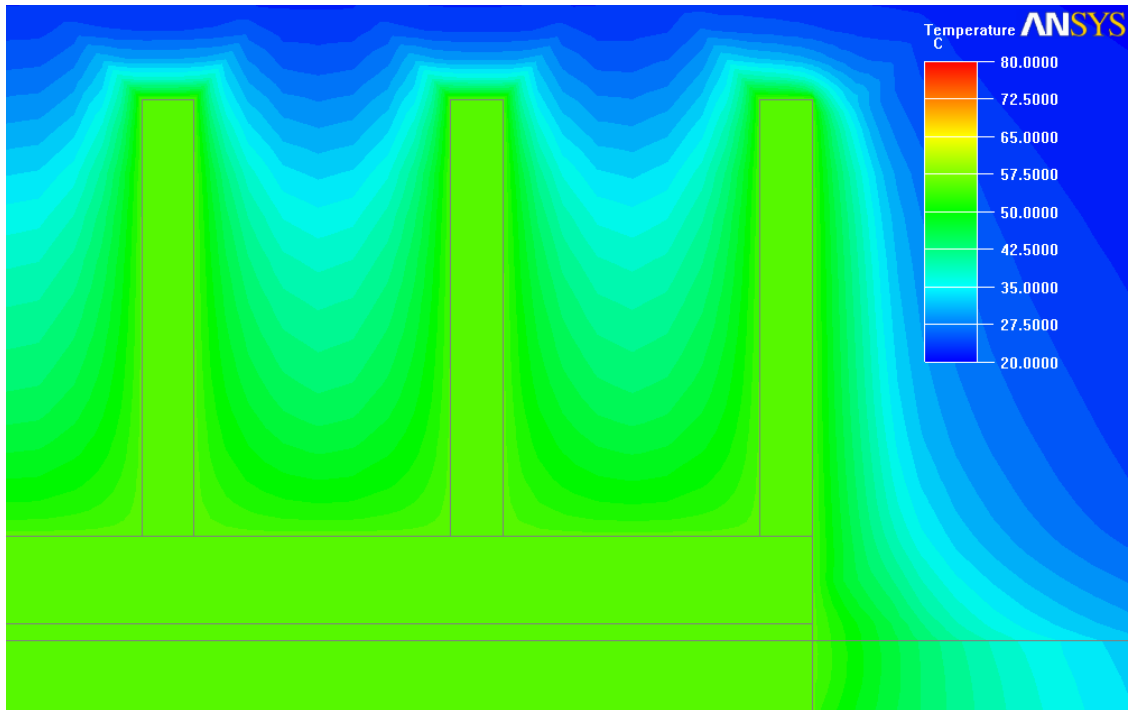

Figure 3.28 Temperature contours for *H*=25 mm

It can be seen that the fin configuration with a higher fin height dissipates higher amount of heat to the air which leads to a lower surface temperature in comparison to the other configurations. A taller fin height increases the surface area which dissipates heat to surroundings.

3.4.3 Variation of Flow Speed with Fin Spacing

Air speed is an important factor in heat sink performance. Generally a heat sink will perform better as the airflow is increased, since the higher speed generates greater heat transfer coefficients along the heat sink fins. In order to show the variation of flow speed with fin spacing following fin configuration has been selected:

- Fin Length, L=340 mm
- Fin Height, H=25 mm
- Power input, Q_{in}=75 W

Speed contours of the flow for different fin spacing values S =14.7 mm, S =8.8 mm and S =5.85 mm are shown on an x-z cross section in Figure 3.29 to Figure 3.31 respectively. Speed scale is kept fixed for all contours.
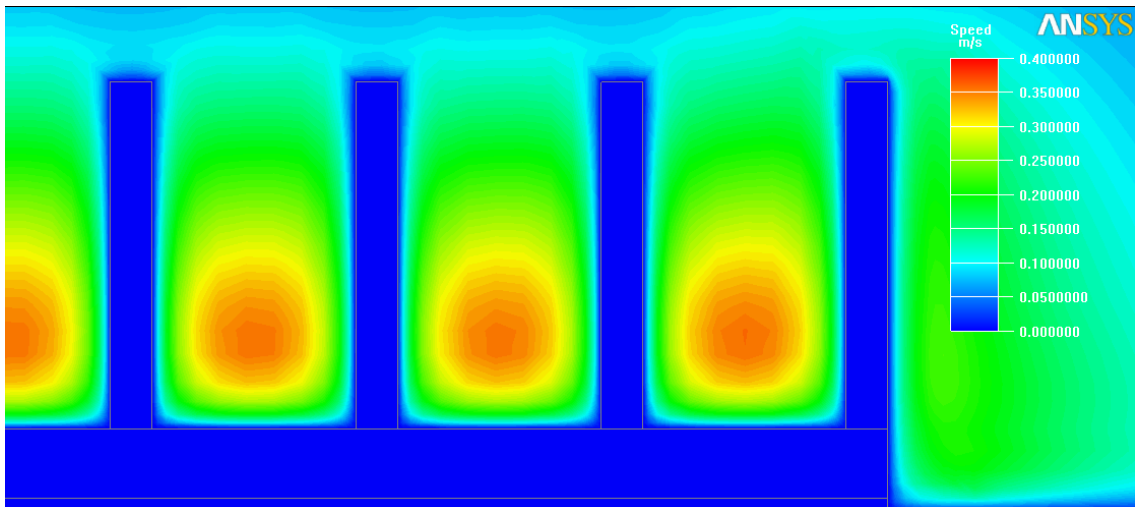
Figure 3.29 speed contours for S=14.7 mm
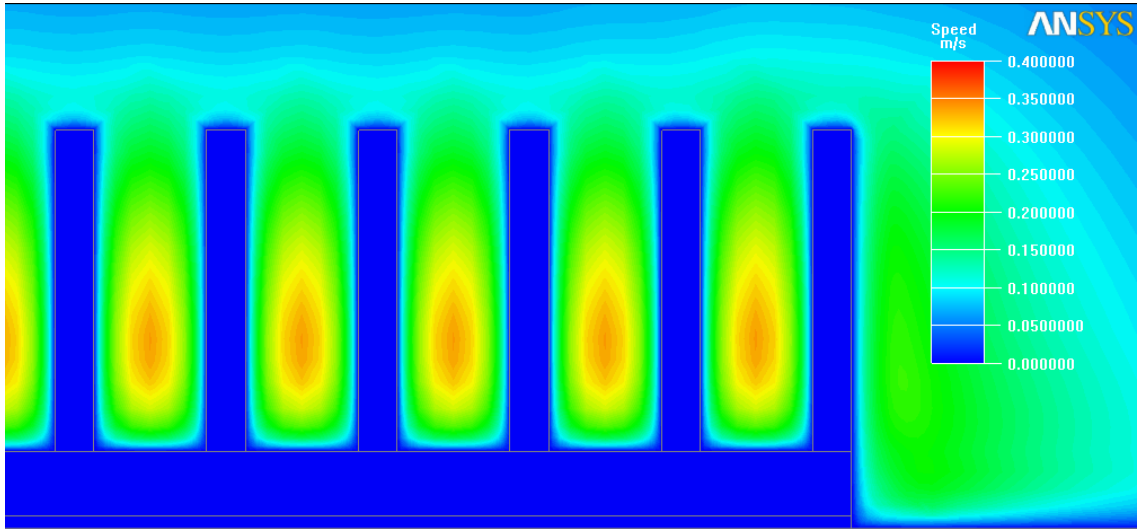
Figure 3.30 speed contours for *S*=8.8 mm
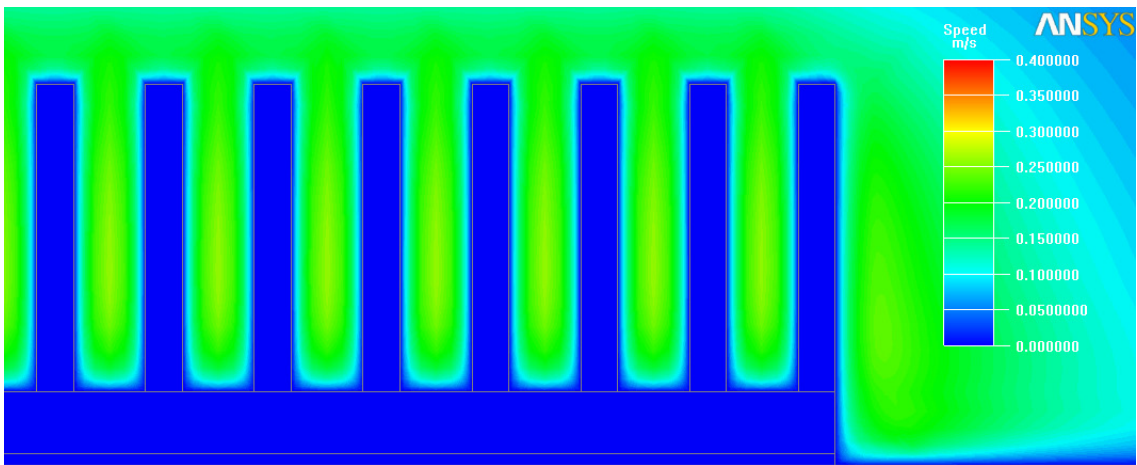
Figure 3.31 speed contours for *S*=5.85 mm

Flow speed through channels diminishes by decreasing the inter-fin spacing. The reduction in air velocity is caused by an increase in the resistance to flow between fins with a decrease in the fin spacing. The reason for this is the boundary layers which are formed between the two concecutive fins. In lower fin spacing (lower than S_{opt}) these boundary layers overlap with each other which makes a resistance to airflow and cauases a reduction in heat trasnfer.

3.4.4 Variation of Flow Speed with Fin Height

In order to show this aspect the following fin configuration is selected for visualization:

- Fin Length, *L*=100 mm
- Fin Spacing, *S*=14.7 mm
- Power input, *Q*$_{in}$=25 W

Velocity vectors of the flow for three different fin heights *H*=5 mm, *H*=15 mm and *H*=25 mm are shown on a *y-z* cross section in Figure 3.32 to Figure 3.34 respectively.
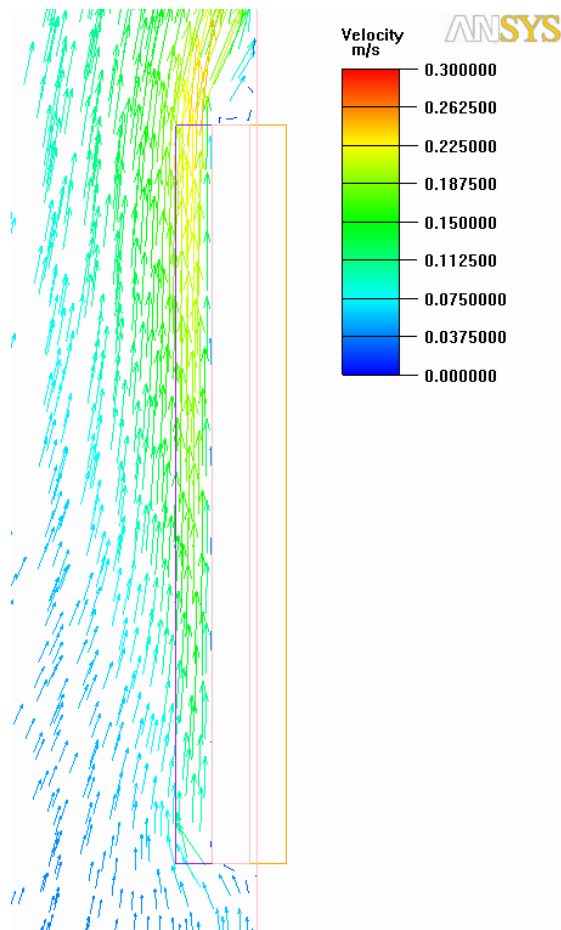
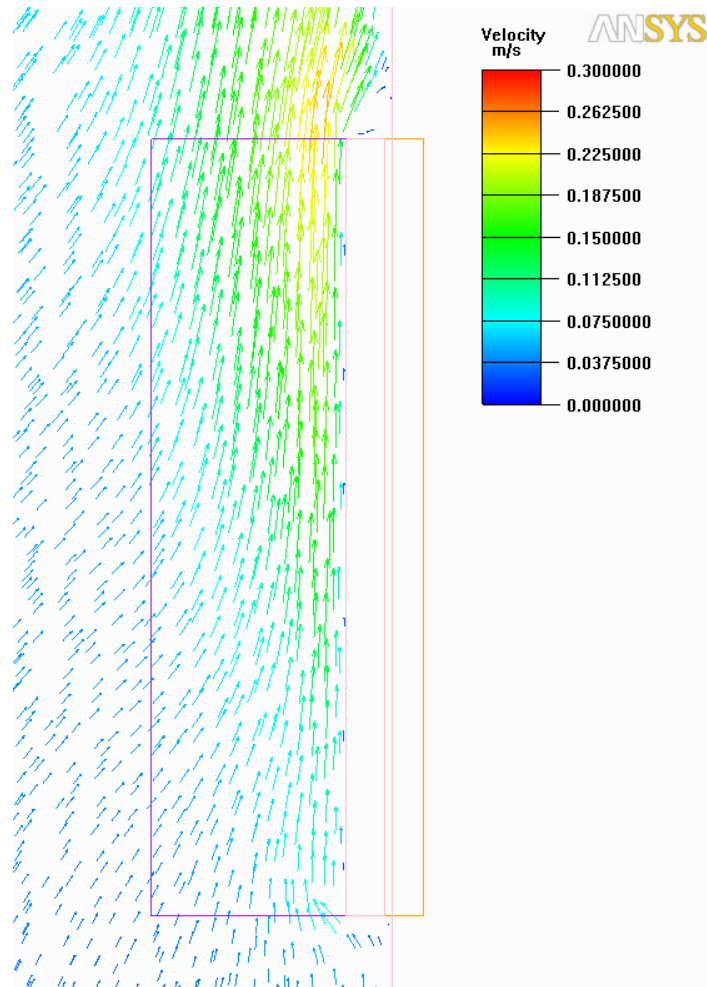Figure 3.32 Speed vectors for *H*=5 mm
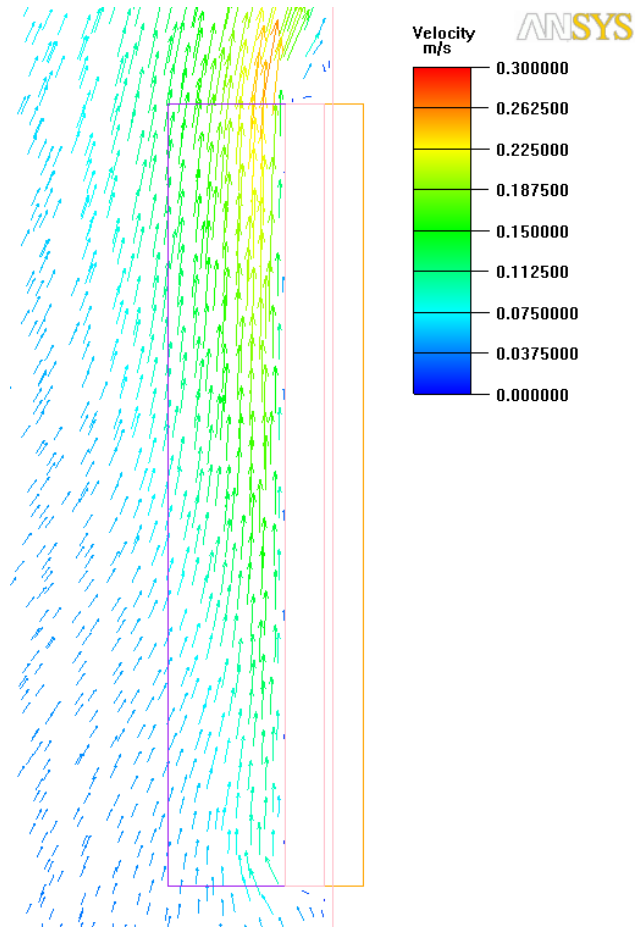
Figure 3.33 Speed vectors for *H*=15 mm

Figure 3.34 Speed vectors for *H*=25 mm

It is easily distinguishable that for the fin height of *H*=25 mm, more air enters the fin channels along the fin length. But in *H*=5 mm air enters the fin channels from the end of the fin. Accrodingly higher rate of heat transfer can be seen in taller fin height values comparing with the shorter ones.

3.5 Comparison and Verification

The objective of this study is to maximize the total heat transfer rate that can be removed by coolant from the fin array surface. It can be seen from the results, that were obtained for vertical case, by using an optimum number of fins this goal can be achieved. In this section the relation between optimum fin spacing and the maximum heat transfer are correlated.

3.5.1 Correlation of Optimum Fin Spacing with Rayleigh Number

The values of optimum fin spacing for a given power input and fin length were listed in Table 3.6 and Table 3.7. In order to find the correlation between the optimum fin spacing and Rayleigh number, average temperature of the fin array is calculated for each optimum fin spacing value. For calculating Rayleigh number we should know the flow properties. All these properties are found using the film temperature which is the average of the fin array temperature and ambient temperature. Then the corresponding Rayleigh number can be easily calculated.
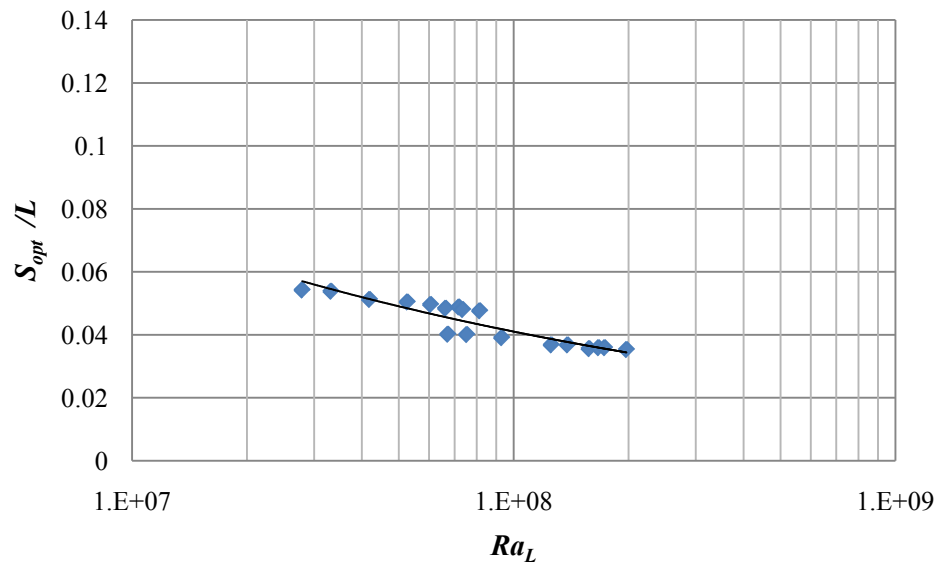
Figure 3.35 Variation of optimum fin spacing with Rayleigh number

According to all calculated numerical results, certain correlation can be obtained for fin spacing. Variation of S_{opt}/L versus Ra_L number is plotted in Figure 3.35.

A curve is fitted to all data and the obtained correlation is provided in Equation (3.2).

$$\frac{S_{opt}}{L} = 4.032 \times Ra_L^{-0.25} \qquad (3.2)$$

Yazıcıoğlu in Ref. [1] suggested three different correlations between the optimum fin spacing and Rayleigh number. These correlations are as follows:

$$\frac{S_{opt}}{L} = 4.064 \times Ra_L^{-0.25} \qquad (3.3)$$

$$\frac{S_{opt}}{L} = 3.0899 \times Ra_L^{-0.25} \qquad (3.4)$$

$$\frac{S_{opt}}{L} = 4.037 \times Ra_L^{-0.25} \qquad (3.5)$$

It is seen that the correlation suggested in this study for optimum fin spacing is similar to the equations provided by Yazıcıoğlu [1].

In this area related experimental studies can be found for comparison with the data obtained in this analysis. In Figure 3.36 results of various studies are illustrated in plot of S_{opt}/L versus Ra_L.
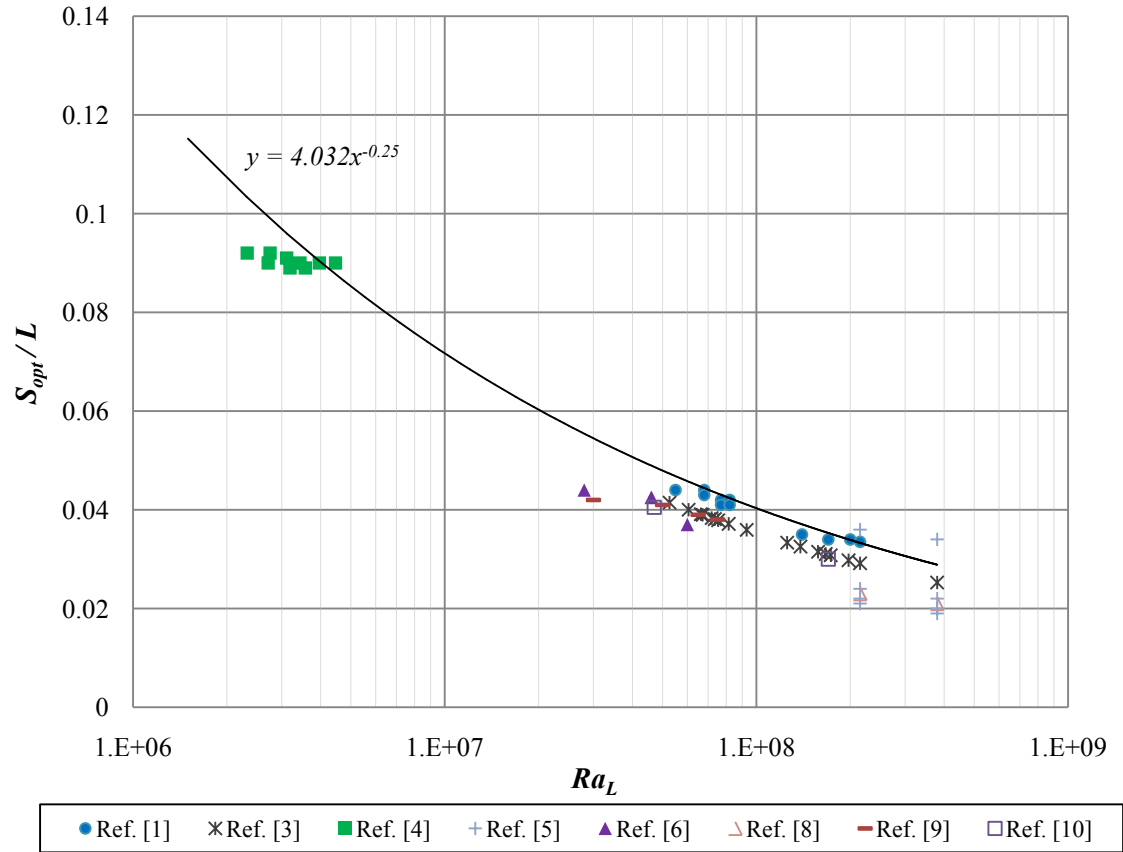
Figure 3.36 Comparison of correlations for optimum fin spacing

Figure 3.36 indicates that the suggested correlation from the present numerical analysis gives close results to the data from experimental analysis. Correspondingly the best fit with Ref. [1] can be easily seen.

3.5.2 Correlation of Maximum Convection Heat Transfer Rate with Rayleigh Number

According to the plots that were presented in previous chapters heat transfer reaches to the maximum value when optimum number of fins is used on vertical surface. Yazıcıoğlu and Yüncü [2][3] were made scale analysis in their experimental study for a vertical plate fin arrays. To find optimum fin spacing, which leads to maximum

convection heat transfer rate, they considered two extreme cases in which the cooling process may function:

1. Small-S limit that leads to a fully developed channel flow.
2. Large-S limit that leads to a boundary layer flow.

Aformentioned scale analysis is shown in Figure 3.37. The results from the scale analysis, according to their experimental study, heat transfer rate from fins in the case of small-S limit directly proportion with S^2 and in the case of large-S limit, it is inversely proportion with S.
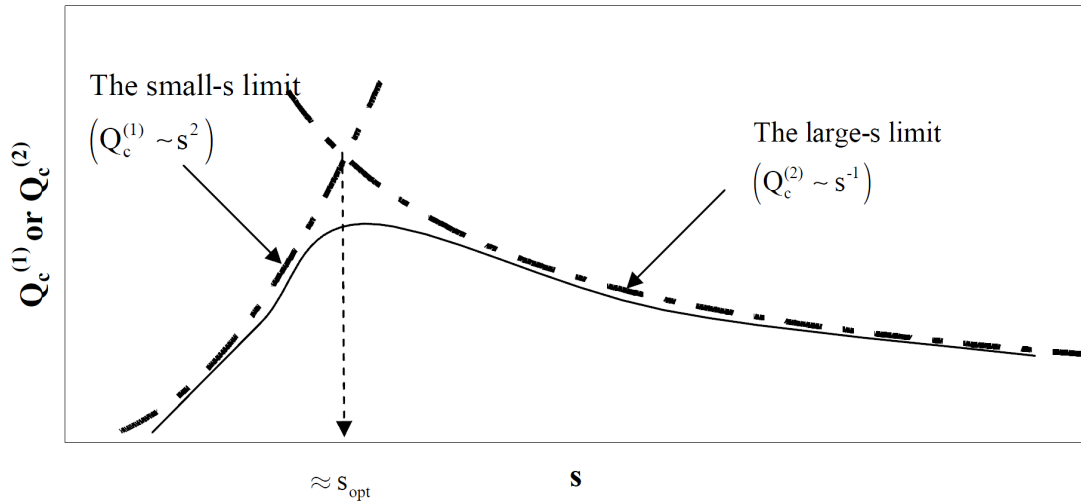
Figure 3.37 Asymptotic plot for extreme limits

Considering $Q_c^{(1)}$ which is the difference between total convection heat transfer rate and the convection heat transfer from the base-plate for small-S limit. In this extreme regime, we can use the Equation (3.6) as below for a single channel [41]:

$$Q_{\substack{single \\ channel}}^{(1)} = \dot{m}\,C_P\Delta T \qquad\qquad (3.6)$$

Where $\dot{m}$ is the mass flow rate through a single channel and C_p is the specific heat of air at constant pressure.

Knowing that $\dot{m} \approx \dfrac{\rho g \beta S^3 \Delta T}{v} H$, heat transfer from the fins can be expressed as:

$$Q_c^{(1)} \approx \frac{\rho g \beta S^3 \Delta T}{v} H C_P \Delta T \frac{W}{S} \qquad (3.7)$$

Equation 3.7 shows that in $S \rightarrow 0$ limit the total heat transfer rate decreases as S^2. This trend is indicated by the small-S asymptote plotted in Figure 3.37.

Finally by using non-dimensional number, $Q_c^{(1)}$ is written as follows:

$$Q_c^{(1)} \approx Ra_s k H \Delta T \frac{W}{S} \qquad (3.8)$$

In the opposite limit, S is large enough so that it exceeds the thickness of the thermal boundary layer that forms on each vertical surface. In this limit the boundary layers are distinct (thin compared to S), and the center region of the fin spacing is occupied by the fluid of temperature T_∞. In this condition the number of distinct boundary layers is 2N, because there are two for each inter-fin spacing. Here $Q_c^{(2)}$ is the difference between total convection heat transfer rate and the convection heat transfer from the base-plate for Large-S limit. The total convection heat transfer rate from a single fin can be expressed as:

$$Q_{\substack{\text{single} \\ \text{fin}}}^{(2)} = 2h\Delta T \qquad (3.9)$$

where h is the heat transfer coefficient over single fin and A is the area of single fin.

Applying the scale analysis to Navier-Stokes equation and energy equation [1] and substituting the values, the total heat transfer rate from the fins can be expressed as:

58

$$Q_c^{(2)} \approx 2\left(\frac{\rho g \beta s^3 \Delta T}{\nu}\right)^{0.25} kH\Delta T \frac{W}{S} \tag{3.10}$$

Equation (3.10) shows that in the large-S limit the total heat transfer rate decreases as the fin spacing increases. This second asymptote is also plotted in Figure 3.37.

Again by using non-dimensional number (Ra) it is demonstrated as:

$$Q_c^{(2)} \approx 2(Ra_L)^{0.25} kH\Delta T \frac{W}{S} \tag{3.11}$$

The trends of two curves reveal that the intersection of curves must give the maximum rate of total convection heat transfer which indicates the optimum fin spacing. As shown in Figure 3.37 the maximum occurs in the vicinity of the intersection where:

$$Q_c^{(1)} = Q_c^{(2)} \tag{3.12}$$

Finally an order of magnitude estimate for the maximum heat transfer rate from fins can be obtained by substituting S_{opt} in Equation (3.8) or Equation (3.11):

$$Q_{c\max} - (Q_0)_c \leq 0.289(Ra_L)^{0.5} kH\Delta T \frac{W}{L} \tag{3.13}$$

Corresponding to Ref. [2] and Ref. [3] the correlations that were suggested by Yazıcıoğlu and Yüncü are as follows:

$$Q_{c\max} - (Q_0)_c \leq 0.125(Ra_L)^{0.5} kH\Delta T \frac{W}{L} \tag{3.14}$$

$$Q_{c\max} - (Q_0)_c \leq 0.2116(Ra_L)^{0.5} kH\Delta T \frac{W}{L} \tag{3.15}$$

In Ref. [11] Bejan investigated the similar study. The procedure of finding maximum convection heat transfer that was used in this reference is similar and the suggested correlation can be used for comparison. Equation (3.16) demonstrates the suggested

correlation which is the same as the one obtained in this study but just with a different coefficient:

$$Q_{c\max} - (Q_0)_c \leq 0.45(Ra_L)^{0.5} kH\Delta T \frac{W}{L} \tag{3.16}$$

According to all calculated numerical results the variation of $Q_{c\max} - (Q_0)_c / kH\Delta T (W/L)$ is plotted as a function of Ra_L in Figure 3.38. A curve is provided to fit all data and shows the trend of the data points. As can be seen this power curve is approximately pass through all data points in Figure 3.38.
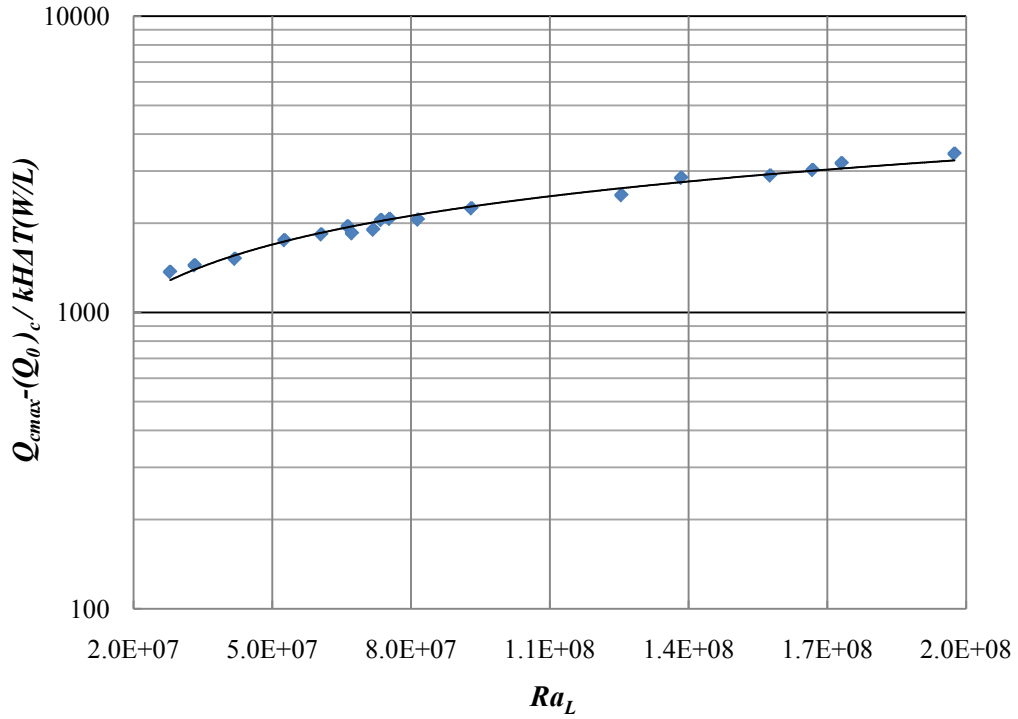
Figure 3.38 Variation of maximum heat transfer with Rayleigh number

The power curve fitted to the obtained results is presented in Equation (3.17) that is similar to the correlations suggested in the literature:

$$Q_{c\max} - (Q_0)_c \leq 0.2363(Ra_L)^{0.5} kH\Delta T \frac{W}{L} \tag{3.17}$$

The variation of $Q_{c\max} - (Q_0)_c / kH\Delta T(W/L)$ is plotted as a function of Ra_L for all experimental results in Figure 3.39 .
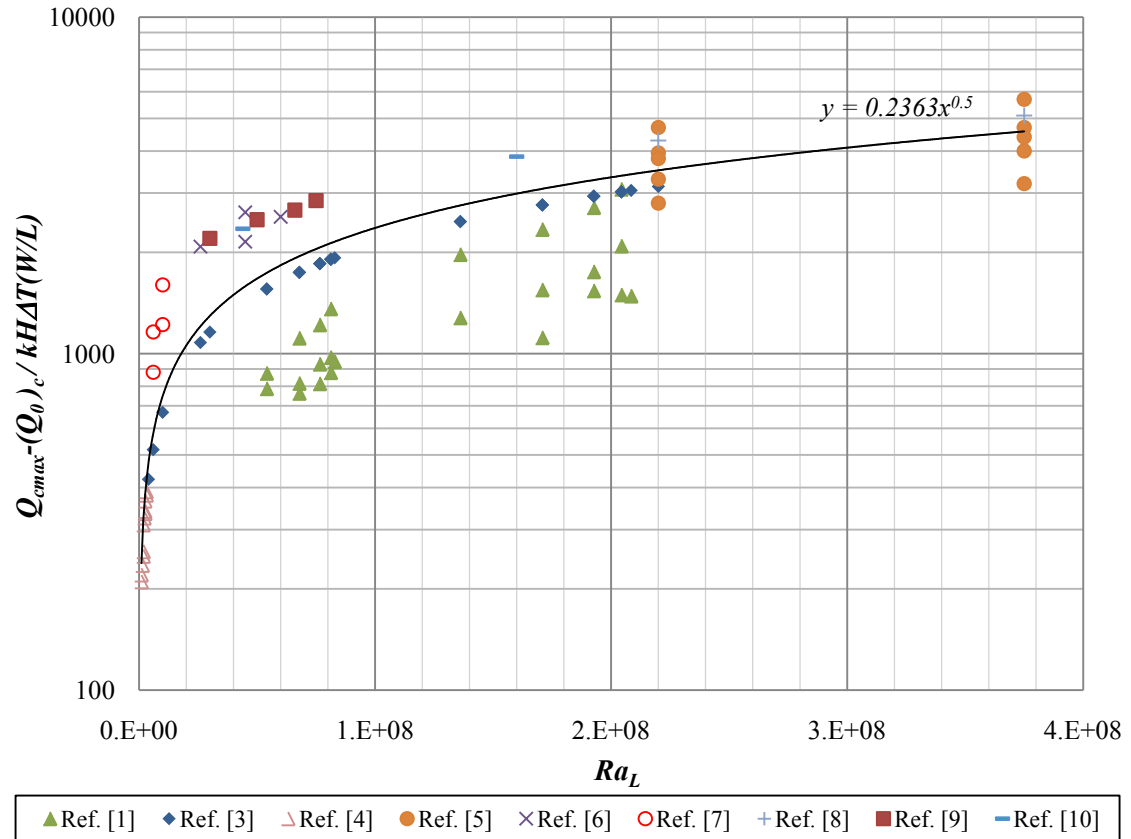
Figure 3.39 Comparison between numerical and experimental results

It can be easily seen from Figure 3.39 that the correlation obtained in this study is following the same trend as the Ref. [3]. Both show a stable trend with similar correlations.

CHAPTER 4

INCLINED CASE

4.1   Inclined Heat Sink Model

As mentioned in Chapter 2, the literature survey was not revealed any work on the natural convection heat transfer from the inclined heat sinks in upward directions aside from the one which was done for 45 degree of inclination with respect to vertical orientation by Starner and McManus [18]. On the other hand in downward direction the study conducted by Mittelman et al. [32] exists in which the investigated inclination angles are limited to the angles between 60 to 90 degrees from the vertical position.

The present study is designed to fill this gap by the numerical determination of convection heat transfer along inclined heat sink surfaces. The present investigation is aimed at establishing the relationship between the inclination angle and the magnitude of natural convection and determining quantitative information on the angular dependence of the instability in the course of heat sink inclination.

In case of inclined flat plates, boundary layer approximations, similar to those for a vertical surface, may be made. One of the ideas to make this procedure simple is to omit the certain terms, particularly by assuming that the velocity component normal to the plate is negligible compared to the tangential component. In this case the problem becomes identical to that for flow over a vertical surface except that g is replaced by $g\,cos\theta$ in the buoyancy term. Therefore, this replacement in all the expressions derived

for a vertical surface would yield the corresponding results for an inclined surface. This implied by using $Ra\,cos\theta$ in place of Rayleigh number and assuming equal rates of heat transfer on two sides of the surface. In reality, this is not the case since the buoyancy force is directed away from the surface at the top and toward the surface at the bottom resulting in differences in boundary layer thickness and heat transfer rates. However, this difference can be neglected in this approximation. Additional experiments have confirmed that the replacement of g by $g\,cos\theta$ in the Ra number is appropriate for inclination angles up to around 45°. Detailed experimental results on this problem were obtained by Fujii and Imura [31].

However, in spite of the fact that this approximation is appropriate for some angles of inclination in flat plates, the present study shows that it is not applicable for inclined heat sinks.

4.1.1   Model Setup

In order to model the heat transfer from tilted heat sink, vertical oriented setup which was tested in first stage (see Chapter 3) is directly used and only the direction of the acceleration of gravity is changed in both backward and forward inclined directions in the range of 0-90 degrees. Figure 4.1 and Figure 4.2 show the assembly in downward and upward inclined positions for a selected degree of inclination. Gravity vector is separated in two components which are used as gravity components in Y and Z directions. The difference between these two is the gravity vector in Z direction which is directed away from the surface in downward direction and toward the surface in upward direction.
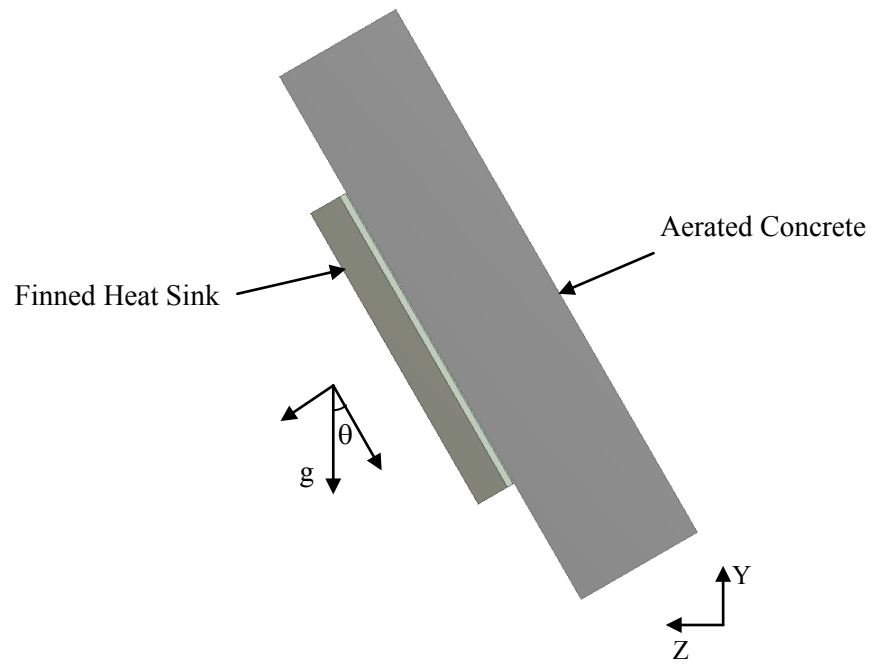
Figure 4.1 Schematic view of inclined assembly in downward direction
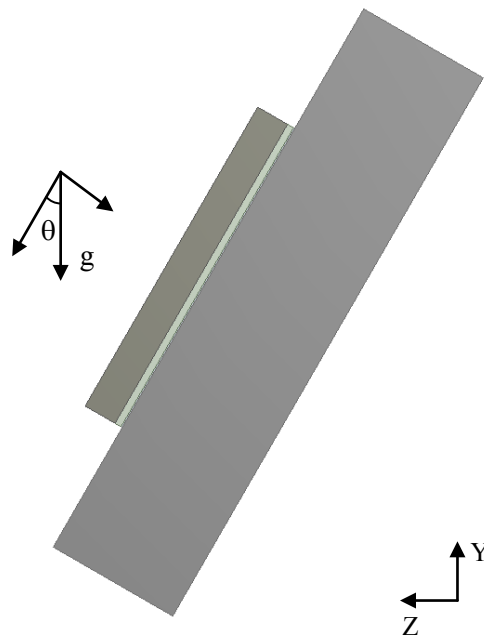
Figure 4.2 Schematic view of inclined assembly in upward direction

Corresponding to the vertically oriented heat sink results, optimum fin spacing was obtained around 12 mm. Due to this fact it is not reasonable to optimize the fin spacing in titled condition, optimum fin spacing which was obtained for vertical configuration is used for investigating tilted configurations. The only geometric parameter which is varied is the fin height. The dimensions of the fin array configurations are shown in Table 4.1.

Table 4.1 Dimensions of fin array configuration for inclined heat sink case

Fin Length L (mm)	Fin Width W (mm)	Fin Thickness t (mm)	Base Thickness d (mm)
250	180	3	5
Set No.	Fin Height H (mm)	Fin Spacing S (mm)	Number of Fins (N)
e1	5	11.7	13
e2	15	11.7	13
e3	25	11.7	13

Four different power input values 25 W, 75 W, 100 W, 125 W were supplied to the heater plate in order to observe the heat transfer from fins for different heat fluxes. The present simulations are conducted at 18 different angles with respect to vertical position which are as follows: ±4°, ±10°, ±20°, ±30°, ±45°, ±60°, ±75°, ±85°, ±90°. Minus signs show the angles in upward direction and plus signs show the angles in downward direction. In section 4.2 only some of the obtained data will be presented to show the individual effects of each of the parameters. The rest of the data is given in Appendix D.

4.2 Results and Discussions

4.2.1 Convection Heat Transfer from Flat Plate

According to the scale analysis in the vertical case, in order to obtain the magnitude of steady state maximum heat trasnfer from a rectangular fin, a correlation was suggested which has a component for convection heat transfer from a bare plate named as $(Q_0)_c$. In this case, similar to vertical configuration, in order to calculate $(Q_0)_c$, for each angle a correlation should be obtained depending on the base-to-ambient temperature difference. For this purpose at each angle, different power inputs ranging from 20 W to 140 W are generated inside the plate. The average temperature of the plate and the convection heat transfer rate are obtained for each power input to the plate. Then a correlation which depends on base-to-ambient temperature is derived for each angle of inclination for bare plate without any fin array on it. As an example, for showing the results obtained for $(Q_0)_c$ Figure 4.3 presents the variation of convection heat transfer from flat plate for different input powers in $\theta = 10^{\circ}$ and the relation attributed to it. Subsequently Figure 4.4 shows the trend of convection heat transfer from flat plate in the course of inclining it in downward direction for $Q_{in} = 100$ W. It can be seen that by tilting the flat plate in downward direction convection heat transfer increases up to a certain angle (around 20° for $Q_{in} = 100$W) which is due to the boundary layer thinning effect and then decreases for the following angles of inclination.
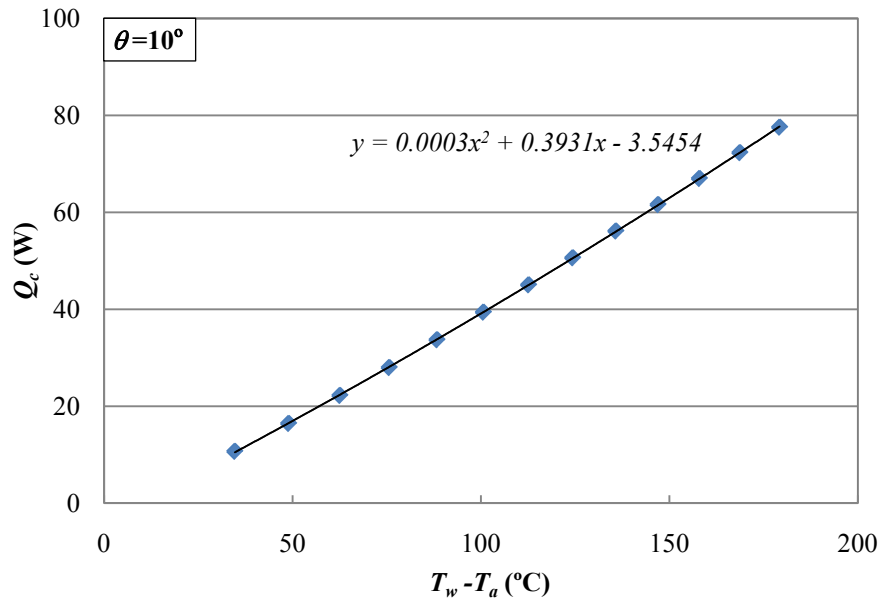
Figure 4.3 Variation of convection heat transfer from flat plate with various base-to-ambient temperature differences at $\theta=10^o$
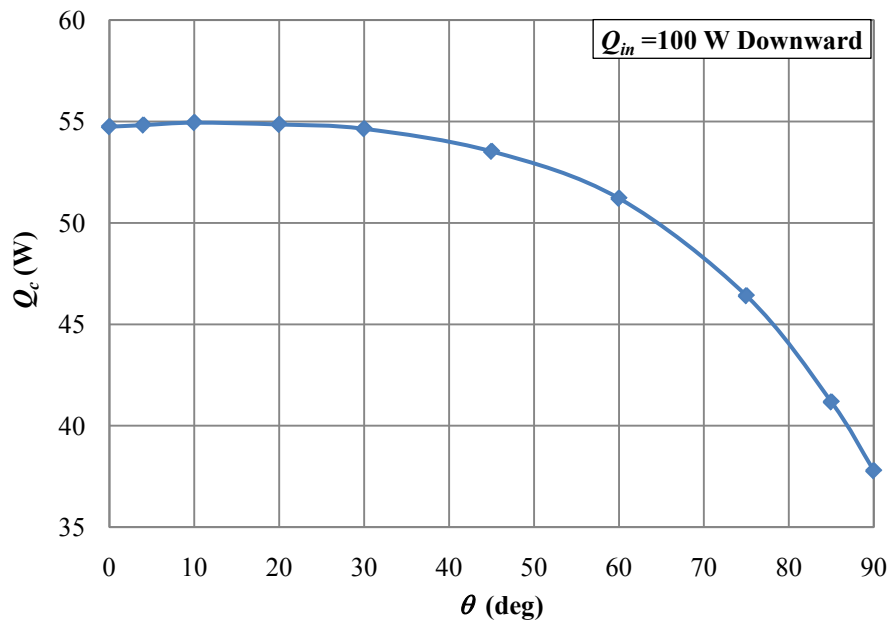
Figure 4.4 Variation of convection heat transfer from flat plate in various angles of downward inclination for $Q_{in}=100$ W

67

4.2.2 Changes in Downward Inclination

After obtaining convection heat trasnfer values for a bare plate, the heat sink setup assembly is investigated in different conditions and results are gathered. Variation of temperature, convection heat transfer and radiation heat transfer are demonstrated in Figure 4.5 to Figure 4.7 respectively for H=25 mm, Q_{in} =125W and 0° - 90° angles of inclination in downward direction.

According to Figure 4.5 in the course of inclination surface average temperature decreases up to θ =4° angle of inclination. After that it increases toward inclination angle θ=90°. In Figure 4.6 convection heat transfer plot also indicates growth between θ =0° to θ =4° angle of inclination resulted from boundary layer thinning effect and then declines toward θ=90°. In Figure 4.7 Radiation heat transfer similar to the surface average temperature trend, decreases upto θ =4° and then increases toward the angle which the heat sink facing down. This confirms the relation between radiation heat transfer and surface temperature. In the course of inclination all parameters related to fin configuration stays the same which brings about the same view factor between heat sink and all other objects. Thus the change in radiation heat transfer is only due to the change in surface temperature.
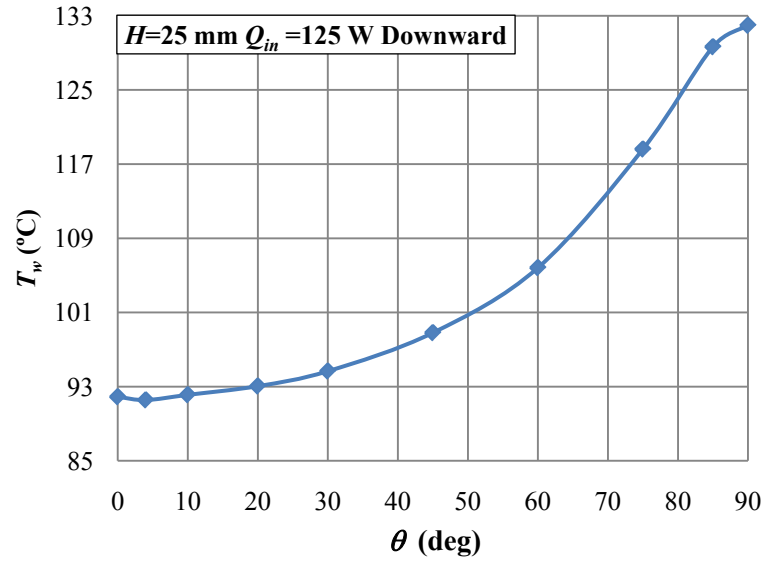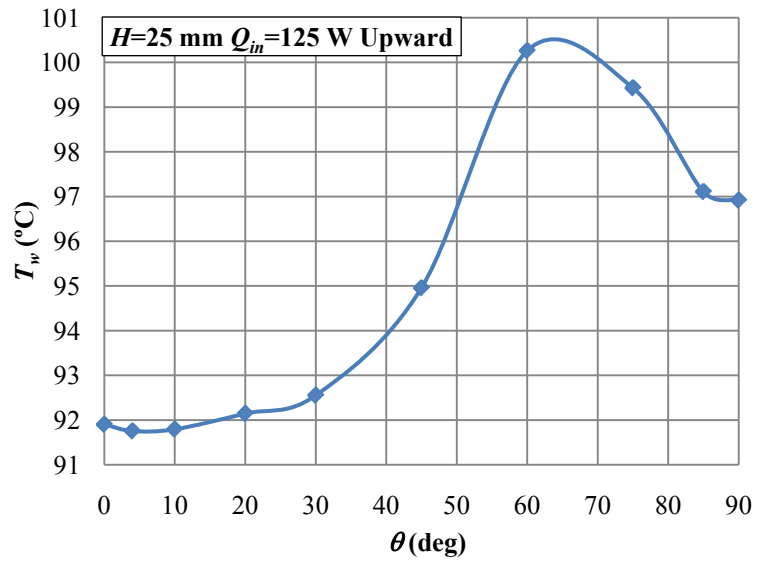
Figure 4.5 Variation of surface average temperature with angle of inclination in downward direction for H=25 mm and Q_{in} =125 W
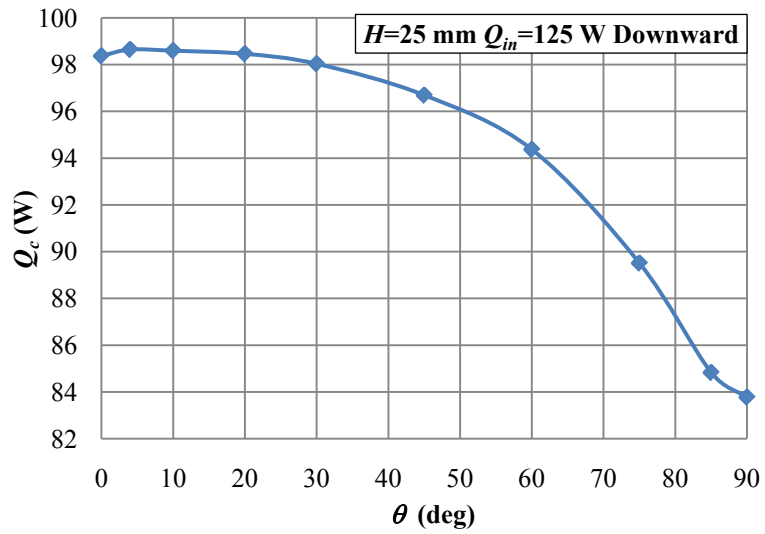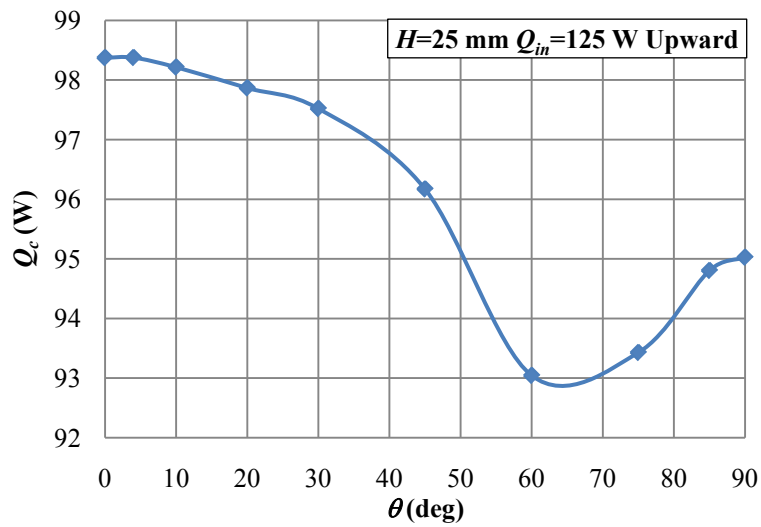

Figure 4.6 Variation of convection heat transfer with angle of inclination in downward direction for H=25 mm and Q_{in}=125 W
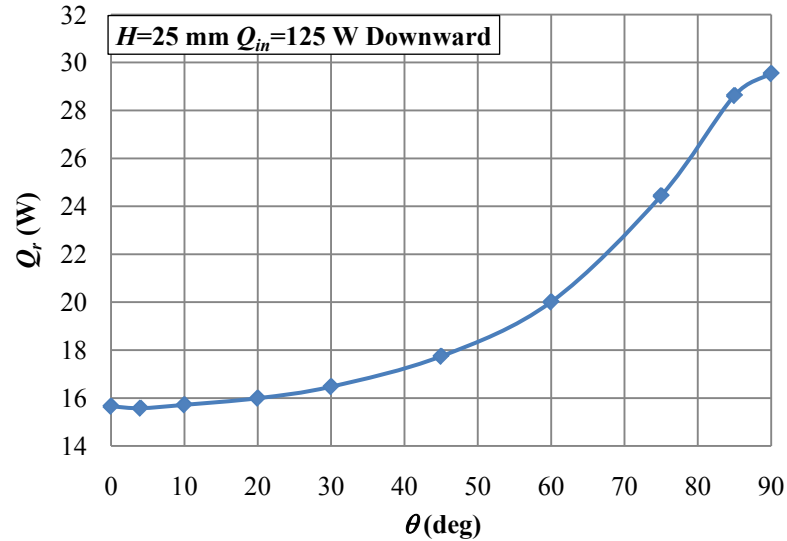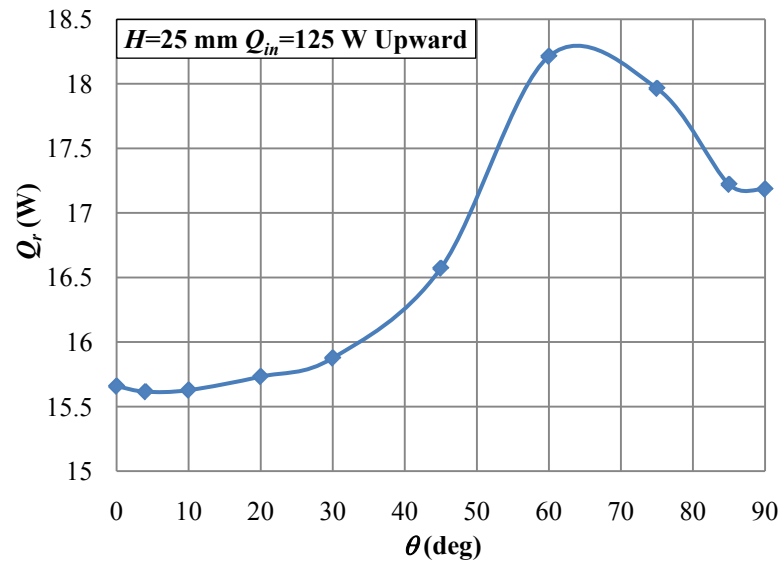
Figure 4.7 Variation of radiation heat transfer with angle of inclination in downward direction for H=25 mm and Q_{in}=125 W

4.2.3 Changes in Upward Inclination

Figure 4.8 to Figure 4.10 demonstrates variation of temperature, convection and radiation heat transfer respectively for H=25 mm, Q_{in} =125 W for 0° - 90° angles of inclination in upward direction.

For the upward direction of inclination as in the downward direction, the surface average temperature and the radiation heat transfer follow the same trend which is a reduction up to θ =-10° and increases upto around θ =-60°. After that point we can see a reduction again in the magnitude of the temperature and the radiation heat transfer. Opposite to these, convection heat transfer increases upto around θ =-4°, decreases up to θ =-60° around the angle which separation takes place, and increases toward θ =-90°. In other words we have a minima and a maxima for these trends in upward direction. Location of maxima and minima can change by the changing power input and geometry parameters of the heat sink.

70

Figure 4.8 Variation of surface average temperature with angle of inclination in upward direction for H=25 mm and Q_{in} =125 W

Figure 4.9 Variation of convection heat transfer with angle of inclination in upward direction for H=25 mm and Q_{in} =125 W

Figure 4.10 Variation of radiation heat transfer with angle of inclination in upward direction for *H*=25 mm and Q_{in}=125 W

4.2.4   Effect of Fin Height

In order to clarify the influence of fin height on the rate of convection heat transfer Figure 4.11 and Figure 4.12 are presented to show the variation of convection heat transfer with respect to angle of inclination in downward and upward directions respectively.
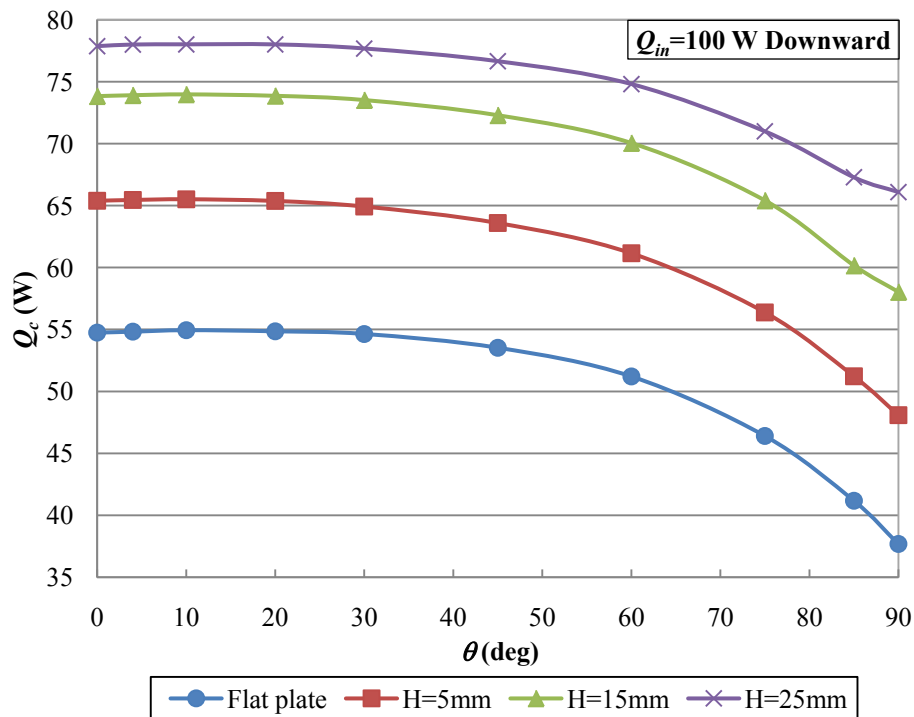
Figure 4.11 Variation of convection heat transfer rate for different fin heights in downward inclination

The effect of increasing the fin height, as in the vertical case, results in higher total cooling surface area and consequently higher steady state convective heat dissipation from the fin arrays. It can be concluded that the taller the fin height the higher the amount of heat that can be dissipated from the fin array surfaces facing downward. And also it is observed that with decreasing fin height, the convection heat transfer rates from fin arrays approach to the values measured from vertical flat plate.

It can be seen in Figure 4.11 that all data follow the same trend similar to flat plate starting from $\theta = 0^{\circ}$ toward $\theta = 90^{\circ}$. But in a certain angle near $\theta = 90^{\circ}$ this trend changes its slope due to occurrence of separation along the surface. This deviation shows itself significantly in taller fin heights.
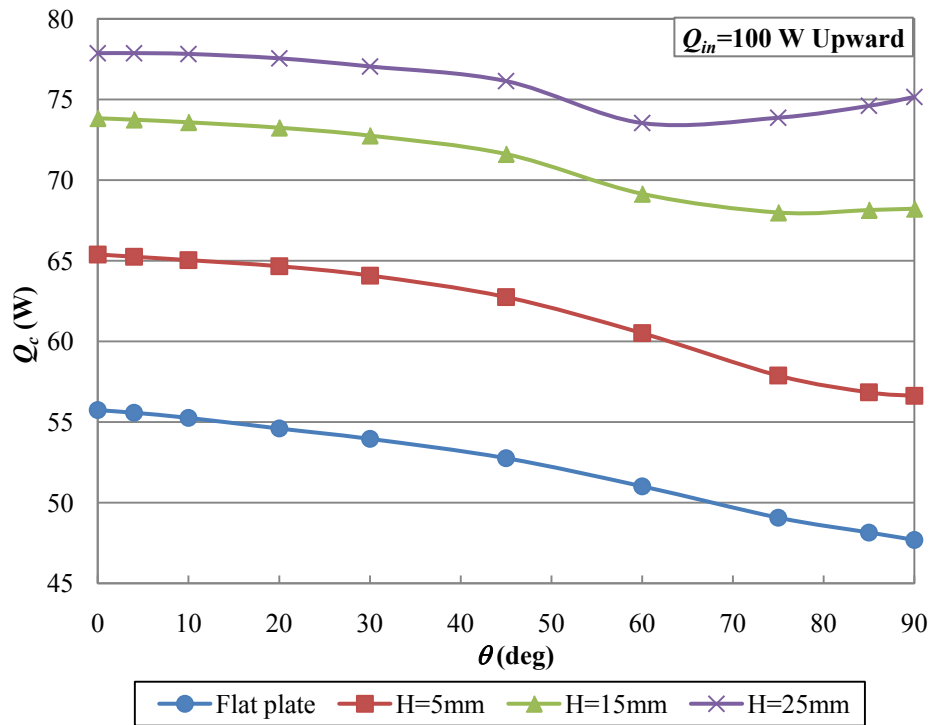
Figure 4.12 Variation of convection heat transfer rate for different fin heights in upward inclination

Similar to the downward direction in Figure 4.12 for the upward direction of inclination, all data corresponding to the convection heat transfer from fin arrays with fin heights H=5 mm, H=15 mm and H=25 mm follow the same trend as the flat plate up to a certain angle of inclination. After this angle which corresponds to an angle where separation takes place on the surface of the fin array, variation of convection heat transfer does not follow the same trend as the flat plate. This deviation is higher in taller fin heights. It can be seen that the separation happens earlier in taller fin heights compared to the shorter ones in the course of heat sink inclination.

4.2.5 Variation of Convection Heat Transfer Rate with Rayleigh Number in Downward Inclination

In order to clearly examine the effect of inclination angle on the amount of heat transfer, change of $Q_c - (Q_0)_c / kH\Delta T (W/L)$ with respect to *Ra Cosθ* is presented in Figure 4.13 for Q_{in} =125 W. It shows results for separate fin heights in inclination angles between 0° and 90° in downward direction. For the vertical orientation and for a small inclination in downward direction ($\theta \leq 4^{\circ}$) the boundary layer thinning effect is more pronounced due to a relatively shorter boundary layer region. The increased gradient of pressure thins the thermal boundary layer and increases heat transfer. Higher angles of inclination reduces the amount of heat transfer dissipated from the surface up to an angle which a separation takes place on the bottom edge. The separation line moves towards the middle of the heat sink with further inclination. According to the figure, due to the separation on the surface of the heat sink, this declined trend changes its direction a little toward higher rate of heat transfer. It can be seen that separation occurs earlier in heat sinks with taller fin heights in the course of inclination. The rest of the plots related to other input powers are given in Appendix D.
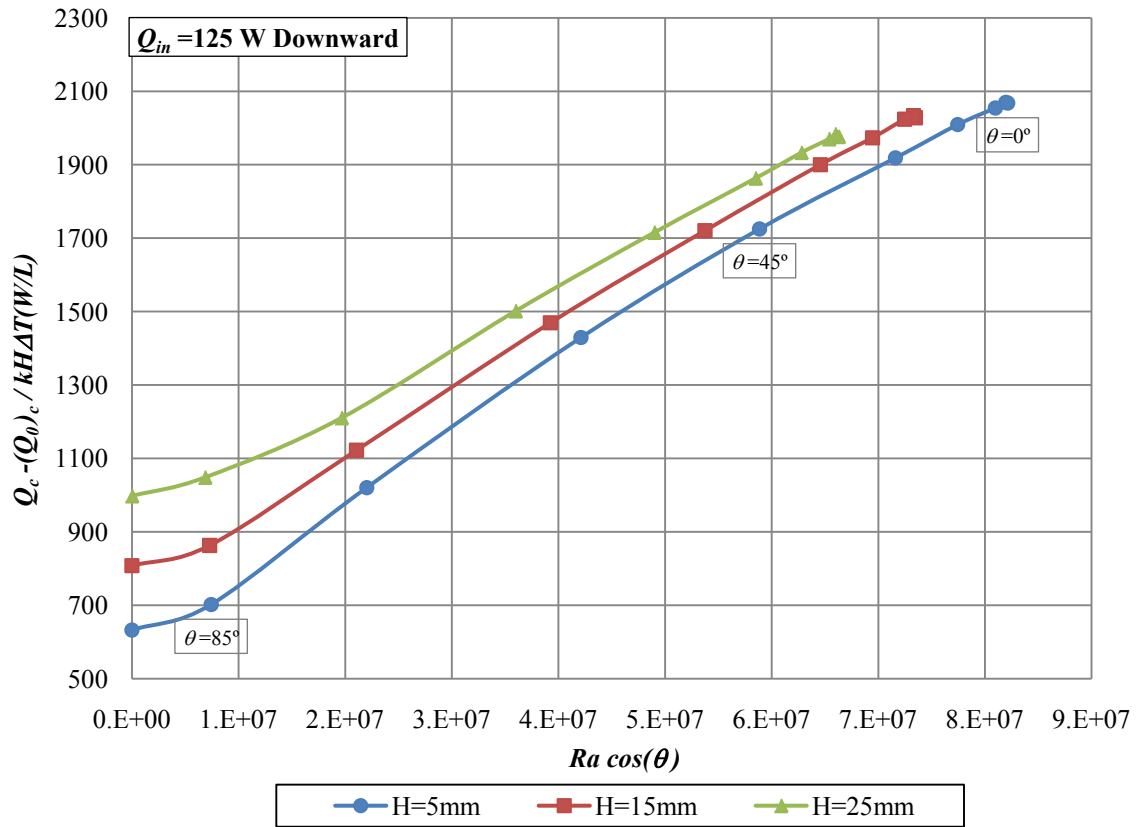
Figure 4.13 Variation of heat transfer rate with Rayleigh number for different fin heights in downward inclination with Q_{in}=125 W

4.2.6 Variation of Convection Heat Transfer Rate with Rayleigh Number in Upward Inclination

Figure 4.14 shows the results for separate fin heights for angles between 0° and 90° in downward direction. As can be seen from this figure, compared to Figure 4.13 related to downward direction, in upward direction separation is more effective in increasing the heat transfer from the surface. One more time, it was observed that separation occurs earlier in taller fin heights in the course of heat sink inclination. As can be seen from Figure 4.14 that the highest values are belong to the inclination angles near to vertical.

This results from simultaneous changes in both Q_c and $(Q_0)_c$. The convection heat transfer from the heat sink surface increases while convection heat transfer decreases from flat plate and as a consequence $Q_c - (Q_0)_c / kH\Delta T (W/L)$ increases.
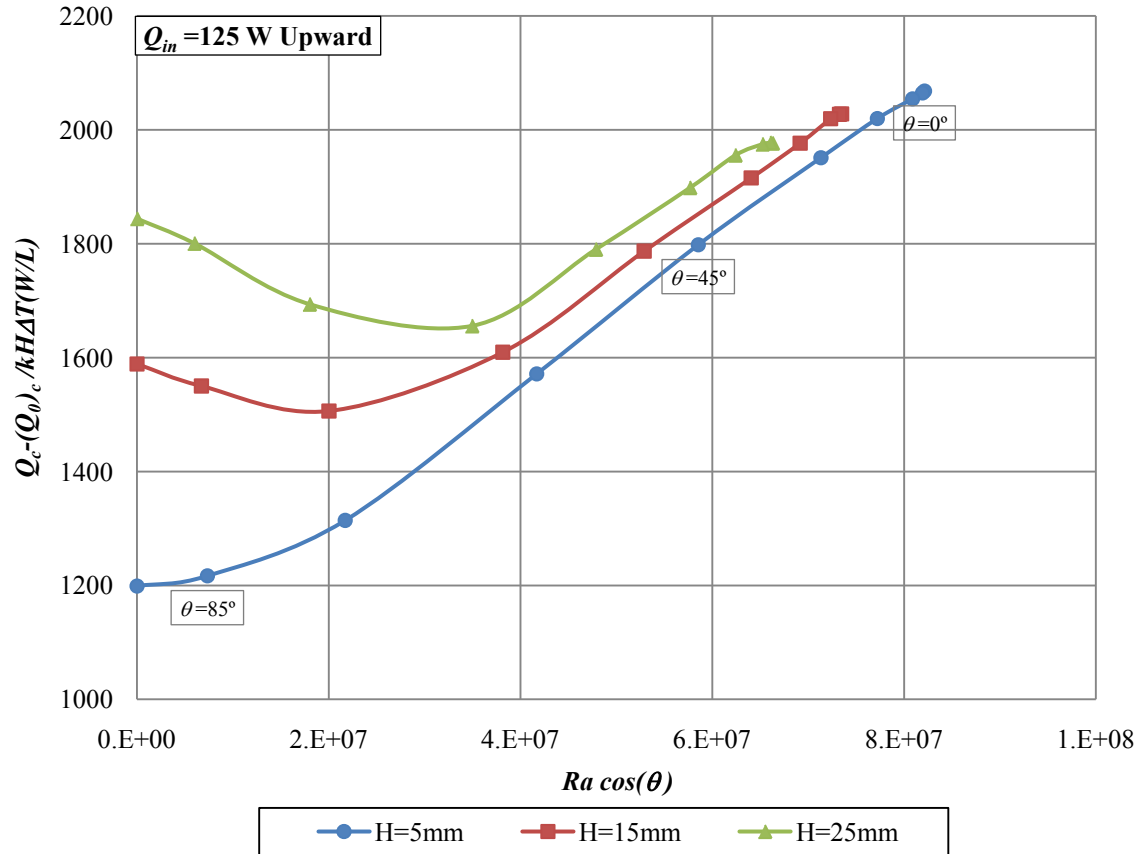
Figure 4.14 Variation of heat transfer rate with Rayleigh number for different fin heights in upward inclination with Q_{in}=125 W

4.2.7 Variation of Surface Temperature along the Heat Sink

Flow and temperature fields occurring over the heat sink surface vary continuously from the lower edge to the upper edge when the plate is inclined from vertical toward horizontal orientation. Some examples of distribution of wall temperature on the cut plane positioned exactly at the middle of the heat sink (width-wise) surface are shown in Figure 4.15 and Figure 4.16. Figure 4.15 illustrates temperature trend from the bottom edge to the upper edge along the heat sink surface in both conditions: facing downwards and facing upwards ($\theta = \pm 90^{\circ}$). According to this figure the temperature patterns in the horizontal heat sink show symmetry with respect to the centerline of the heat sink. In leading edge and trailing edge, the temperature value is approximately the same and it is lower than temperature value in the middle part of the heat sink. It can be seen that the maximum temperature is related to the point where the separation takes place along the heat sink surface. In addition, Figure 4.15 implies the maximum heat flux near the leading edge which decreases along the plate and it increases again at the other end. Temperature drops near these areas caused by the thinning of the boundary layer due to the edge effect. This layer is thickest at the surface center and thinnest at the edges.
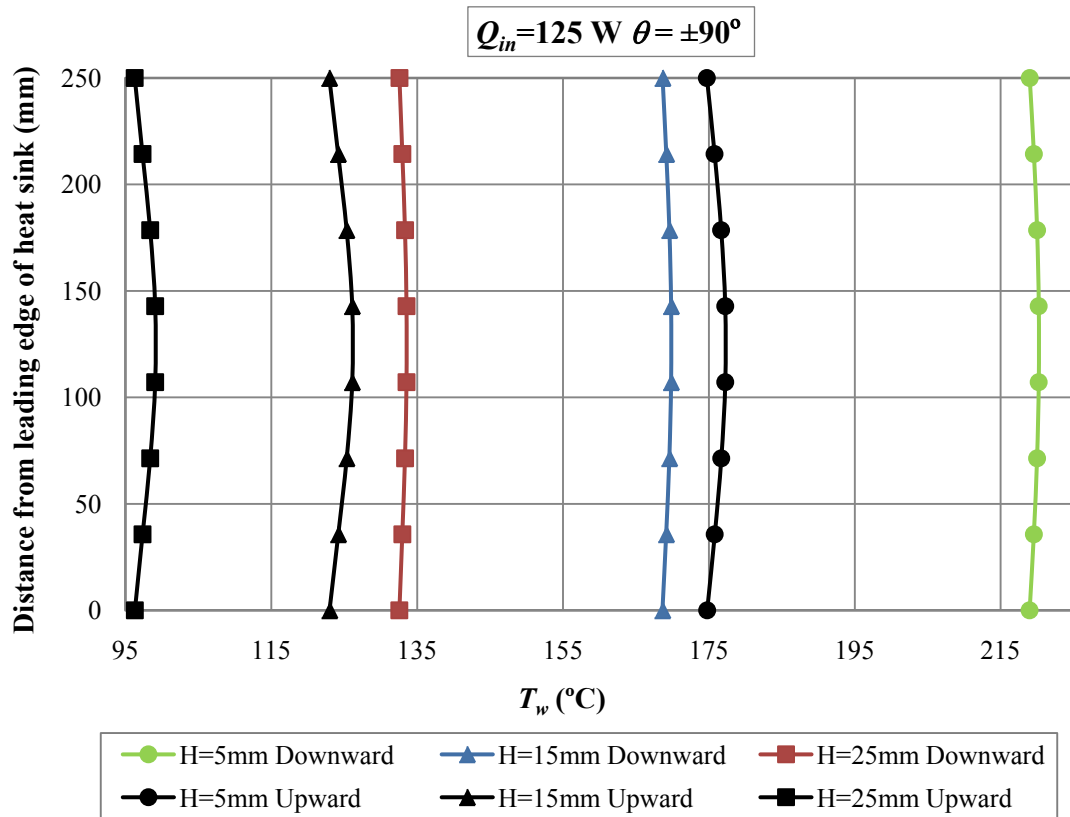
Figure 4.15 Temperature distribution along the surface of heat sink for $\theta = \pm 90°$

Figure 4.16 shows the temperature values along the heat sink from leading edge toward trailing edge for 75 degree of inclination in both directions. According to this figure, leading edge has lower temperature in compare with the other points on the surface of the heat sink which is due to higher amount of air flow in this area than the other points on the surface of the heat sink which itself results from thinner boundary layer. Each temperature trend starts from the lowest value then increases to the maximum (separation point) and finally decreases at the trailing edge.
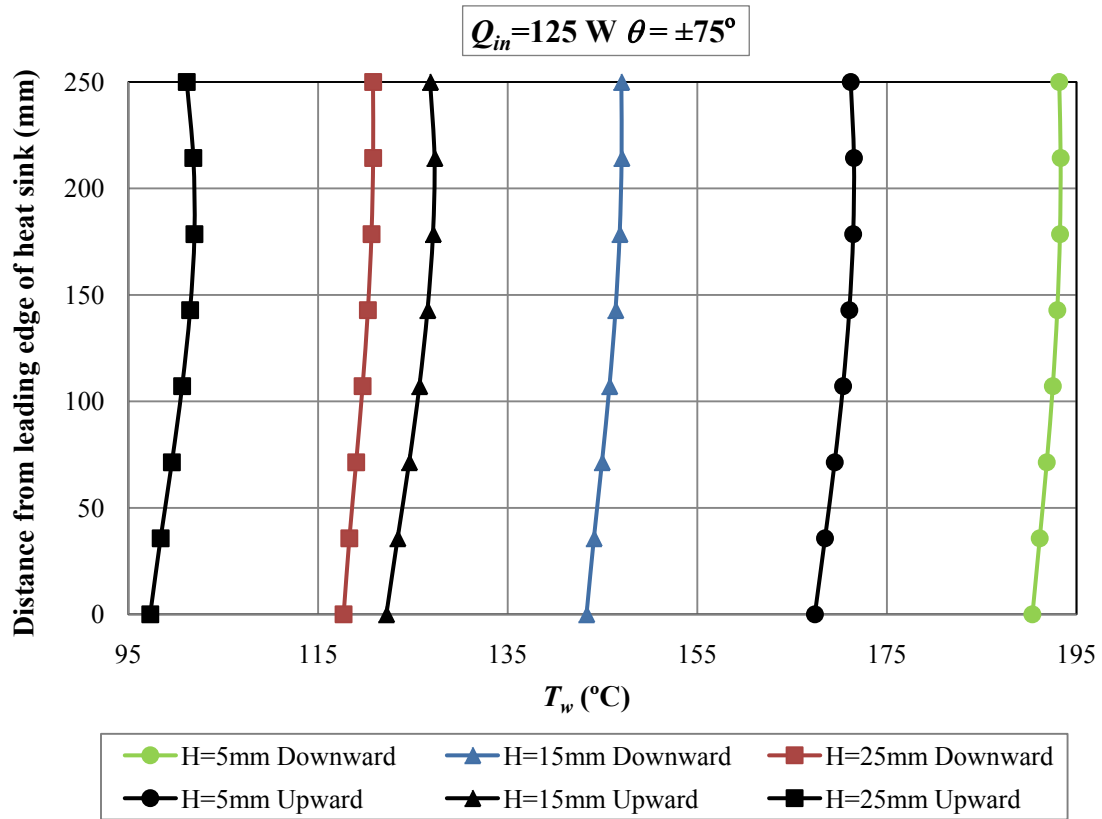
Figure 4.16 Temperature distribution along the surface of heat sink for $\theta = \pm 75^{\circ}$

4.3 Flow Visualization

4.3.1 Variation of Fluid Temperature with Inclination Angle

Different types of flows appear over inclined heat sinks when the inclination angles are large. The ambient fluid first enters from the lower edge of the heat sink, then ascends along the surface, and finally detached from the upper edge, as illustrated in Figure 4.17. The results show that both the descending and ascending flows appear over the heat sink when the inclination angle is high. The ambient fluid enters from the upper edge and descends along the surface. The two flows collide with each other at a certain distance from the plate edge, and then detach from the plate to form a thermal plume as shown in

Figure 4.18. The descending flow occurs over a small range of inclination angles and alters the flow field and heat transfer characteristics substantially from those over the heat sinks of small inclination angles. The collision point shifts further downstream by increasing the angle of inclination. Finally in horizontal condition, separation occurs in the middle and the flow detaches, forming the plume. Figure 4.19 shows the symmetric plume on a heat sink in horizontal orientation.
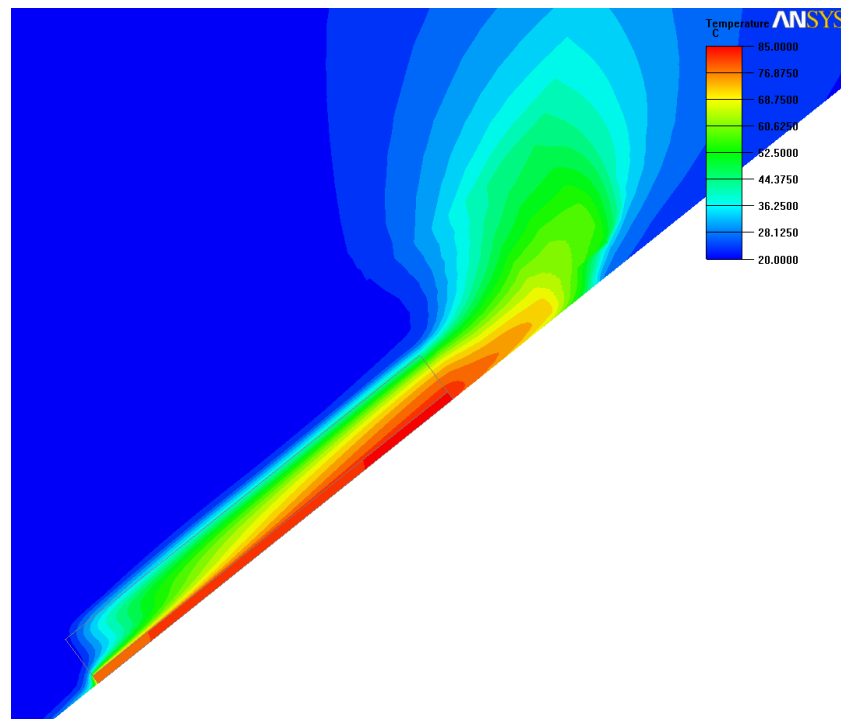
Figure 4.17 Temperature contours at $\theta = -45^\circ$
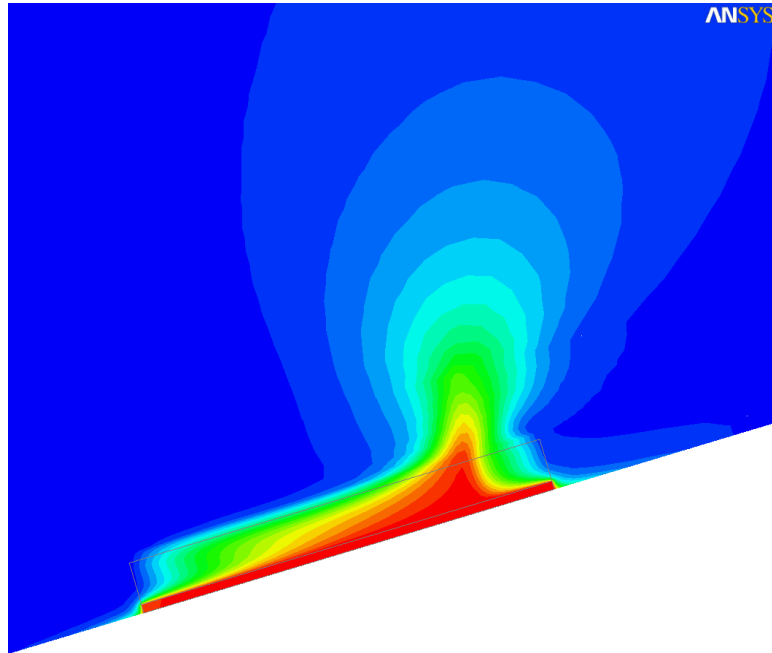
Figure 4.18 Temperature contours at θ =-75$^{\mathrm{o}}$
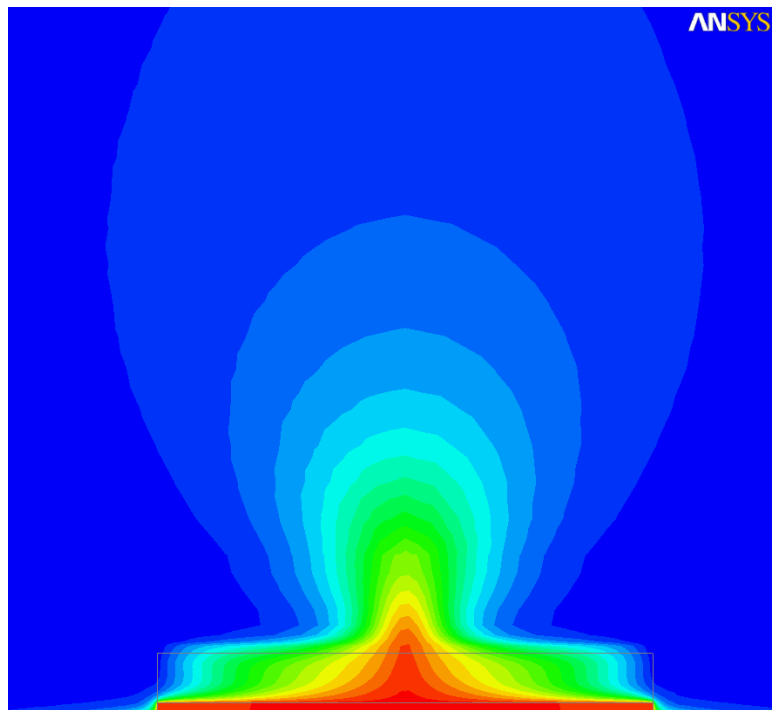
Figure 4.19 Temperature contours at θ =-90$^{\mathrm{o}}$

82

4.3.2   Variation of Flow Speed with Inclination Angle

Since the effect of surface inclination is reflected more strongly in the velocity rather than in the temperature distribution, it would be better to examine velocity distributions with particle traces in the boundary region. Streamlines near to heat sink with different angles of inclination are illustrated on a *y-z* cross section in Figures 4.20 to Figures 4.26. The speed scale is kept the same for all of the figures.

The visualization confirms the occurrence of boundary layer separation and shows that the location of the separation is a function of the angle of inclination. For the unstable case, length between the bottom edge and the point in which separation takes place decreases as the plate fin angle increases from the vertical while for the stable case this length increases as the angle increases from the vertical.

In the course of the visualization experiments, several interesting flows were appeared over the horizontal heat sink. First, the ambient fluid enters from both edges of the heat sink and flows along the surface. Then, the fluids coming from both sides collide with each other at the center of the plate and detach from the plate. Then, they rise from the heat sink as a plume.

As seen in Figure 4.20, the calculated stream lines indicate that far from the heat sink the flow moves upwards towards the heat sink center and as it approaches it, changes direction and moves towards its edges. In the literature, the flow confined between this virtual boundary and the heat sink surface is defined as a boundary layer flow. The boundary layer thickness, at any location, is the distance between the heat sink and the point where the flow lacks any lateral velocity. Boundary layer thickness extends along most of the channel length and shrinks as it approaches to the channel edge.
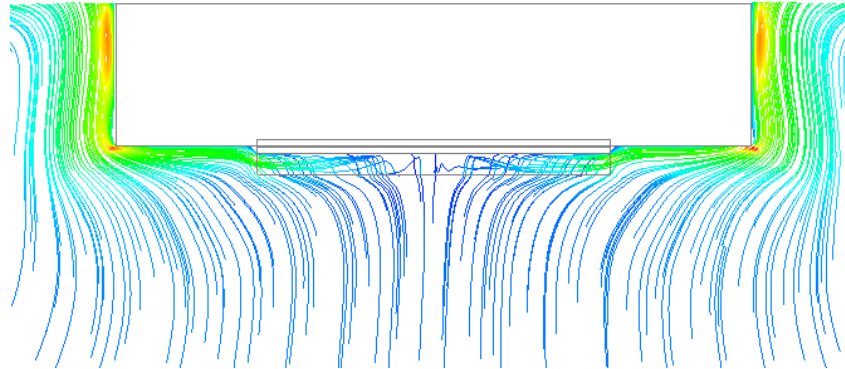
Figure 4.20 Streamlines at $\theta = 90^\circ$

Increasing the inclination angles moves the separation line towards the bottom edge. Figure 4.21 presents the flow over a heat sink when it is inclined 85 degrees with respect to vertical orientation. Separation point still can be seen over the heat sink surface.
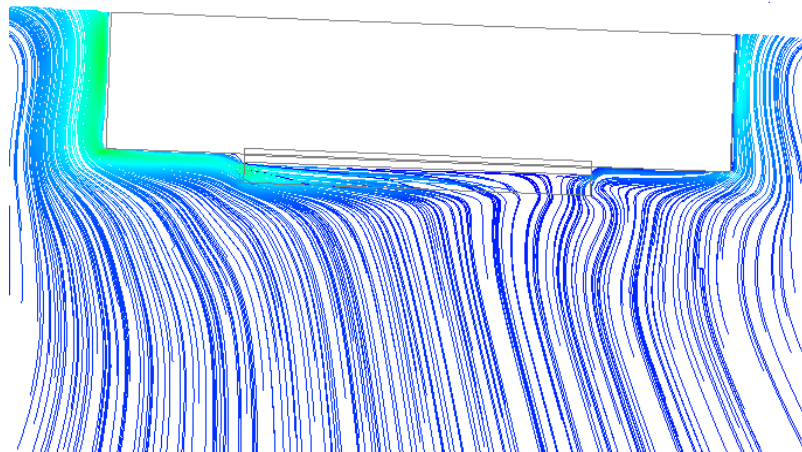
Figure 4.21 Streamlines at $\theta = 85^\circ$

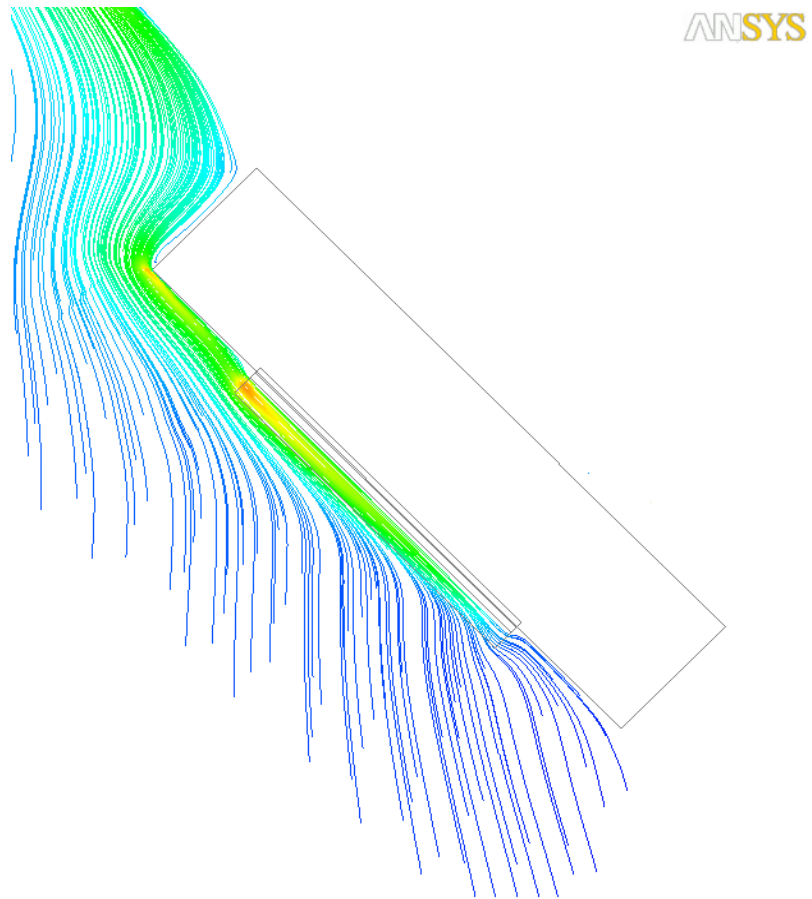By increasing the angle of inclination with respect to horizontal orientation separation disappears over the heat sink. (Figure 4.22)

Figure 4.22 Streamlines at $\theta=45^{\circ}$
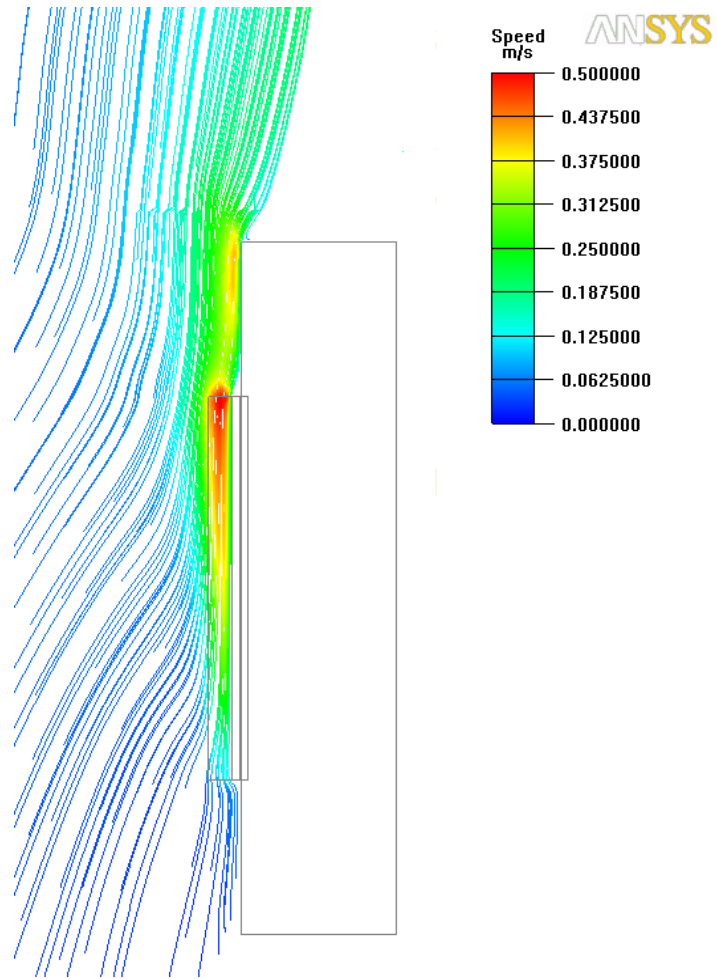
Figure 4.23 Streamlines at $\theta = 0^\circ$
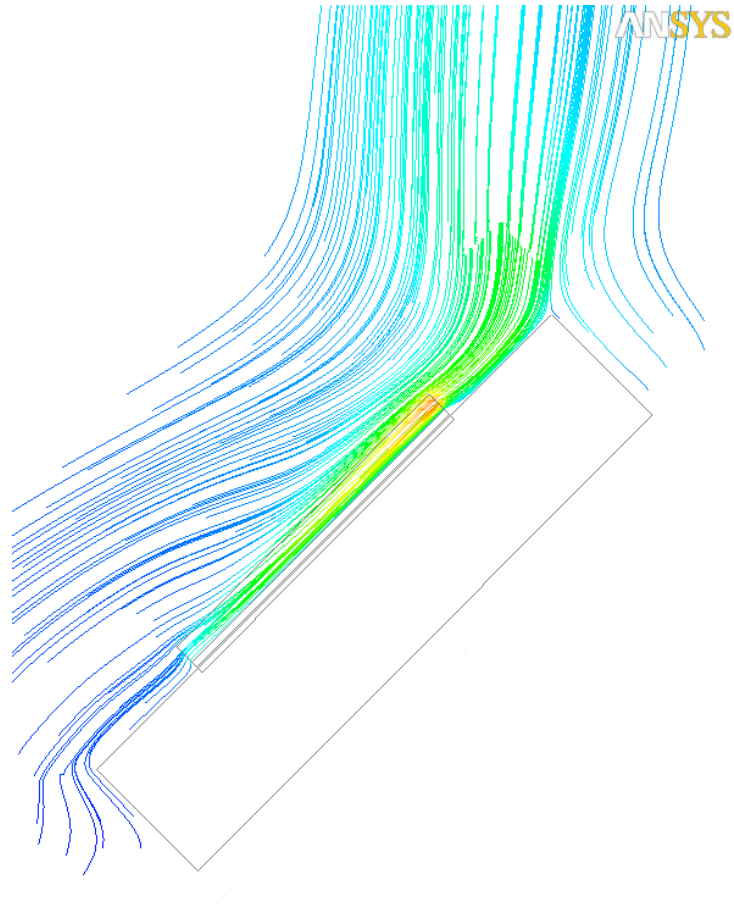
Figure 4.24 Streamlines at θ =-45°

Figure 4.25 shows the streamlines over the heat sink at θ =-75° where separation is started to be seen on the heat sink surface in the course of inclination. Separation is conceivably due to the effect of the velocity component normal to the surface.

In Figure 4.26 for the horizontal surface, the flux distribution near the edge and its similarity to the cases of inclined surfaces indicates the predominance of the velocity component tangential to the surface at its edges.
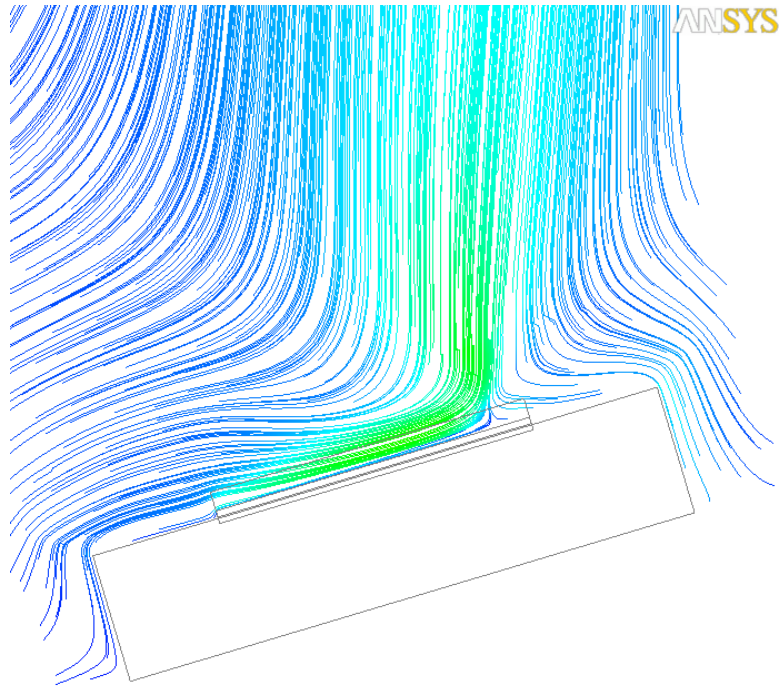
Figure 4.25 Streamlines at $\theta = -75^\circ$
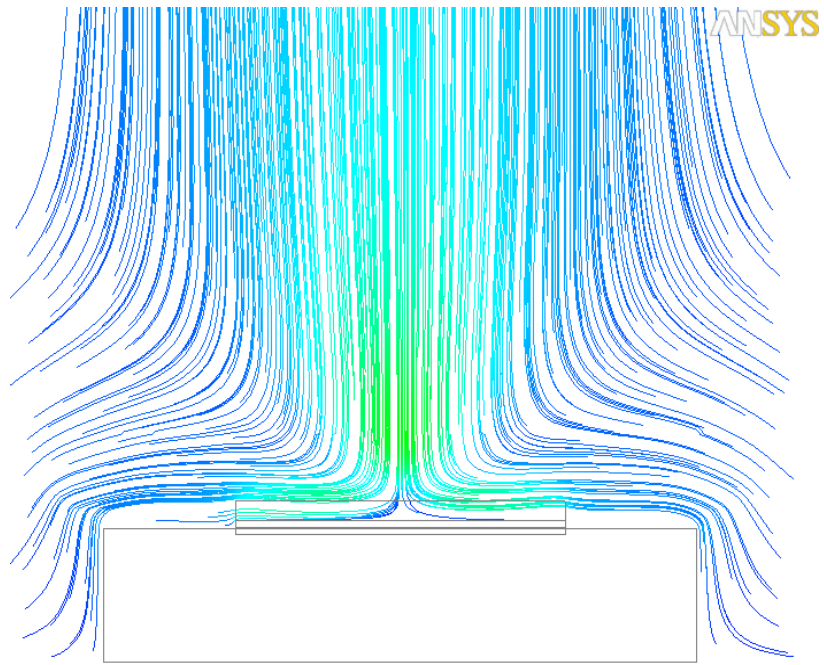
Figure 4.26 Streamlines at $\theta = -90^\circ$

4.3.3 Velocity Vectors in Horizontal Orientation

Figure 4.27 shows the velocity vectors on an *x-z* cross section positioned at the middle of the heat sink (length-wise) that are formed by the downward facing heat sink. In order to make it clear a larger figure from one of the heat sink channels is demonstrated. Boundary layers which are formed between two fins can be easily seen in this figure.
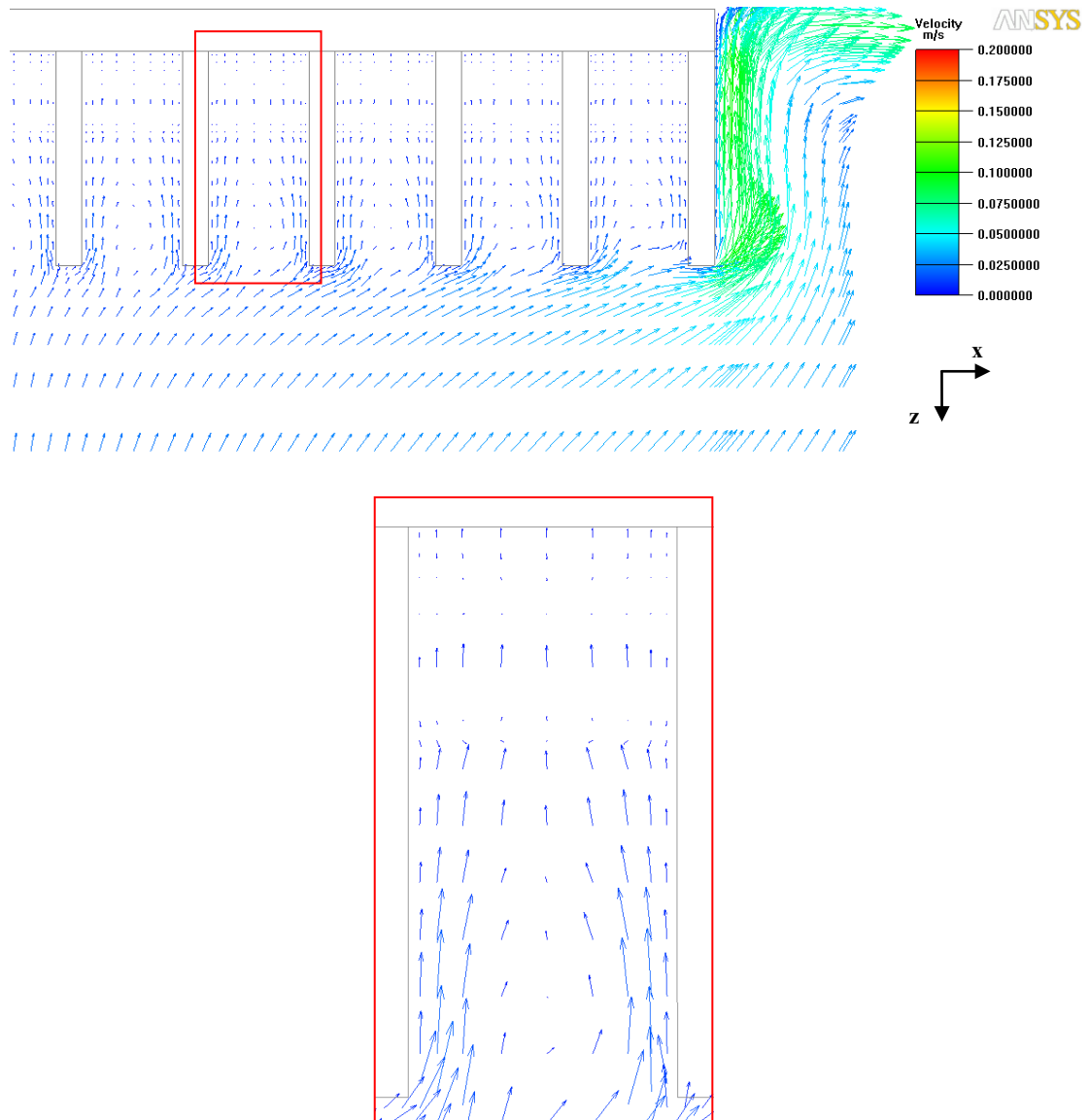
Figure 4.27 Velocity vectors inside a channel at $\theta = 90^\circ$

Similar to the downward direction Figure 4.28 shows the heat sink in an inclination angle $\theta = -90°$ where the heat sink faces upward. Also a larger picture of velocity vectors from inter-fin spacing is displayed to show the boundary layer formation at this angle of inclination.
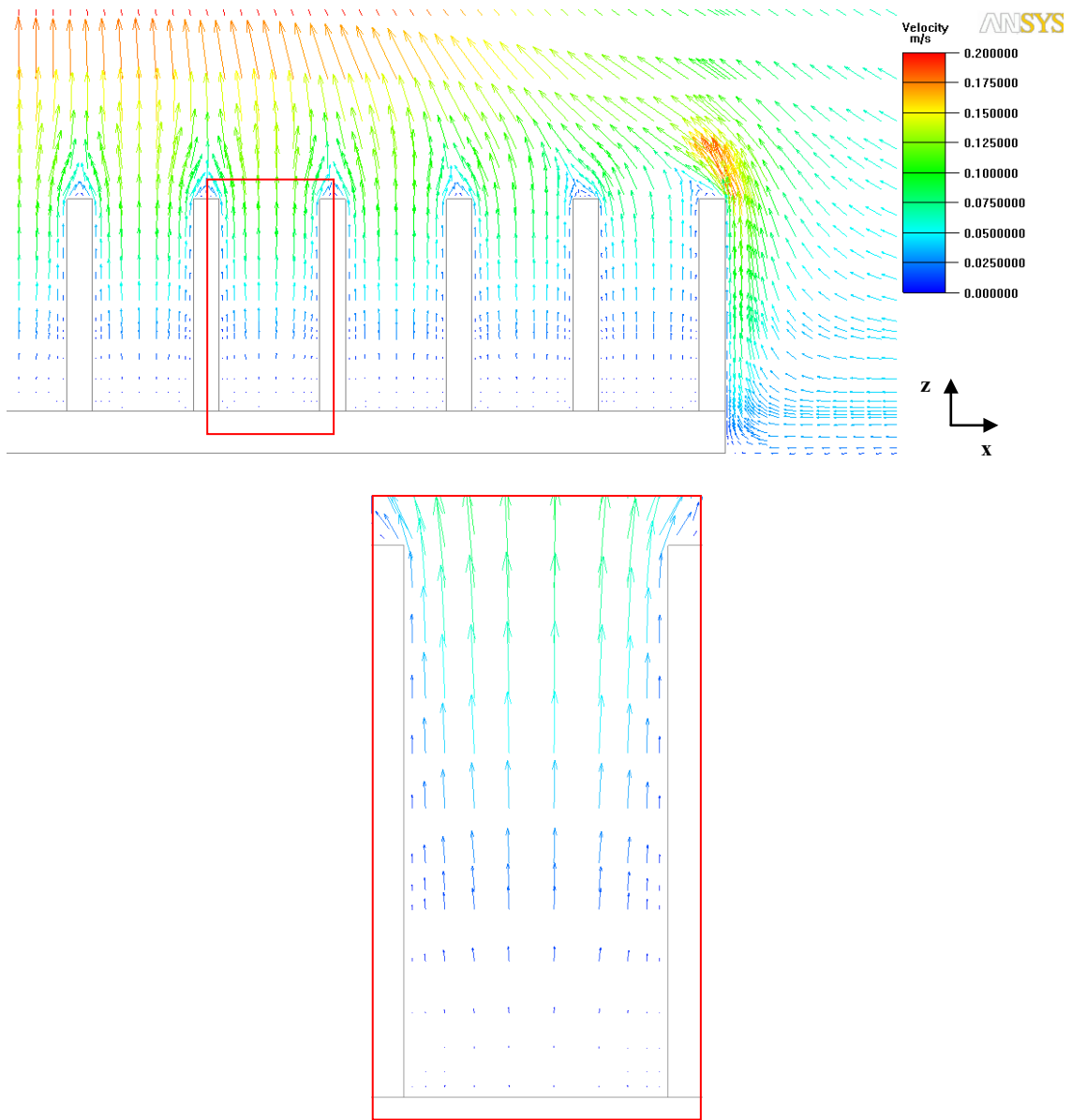
Figure 4.28 Velocity vectors inside a channel at θ =-90$^{\text{o}}$

The flows over horizontal or slightly inclined heat sinks are inherently unstable because of top-heavy and bottom-light arrangements and complicated boundary layer interactions. Thus, an exchange of the fluids occurs over the heat sink, resulting in a very complex flow and heat transfer behavior

4.3.4   Variation of Flow Speed with Fin Height in Downward Inclination

In order to show the variation of flow speed with fin height in downward direction of inclination, the following fin configuration is used:

- Input power, Q_{in} =100 W
- Angle of inclination, θ =85º

Speed contours of the flow for different fin heights, H=25 mm, H=15 mm, H=5 mm are shown on an *x-y* cross section in Figure 4.29 to Figure 4.31 respectively. The speed scale is the same for all the figures.
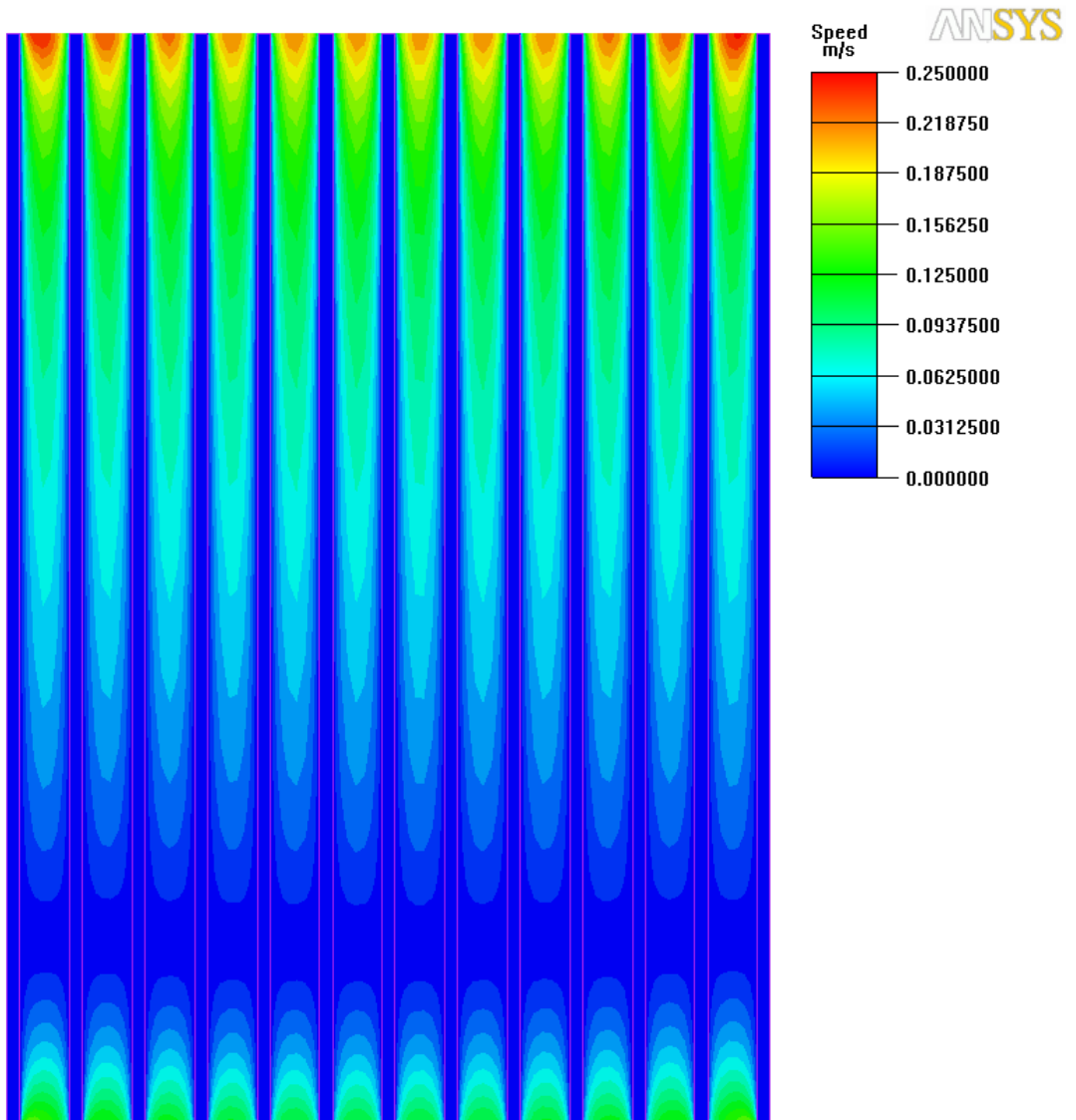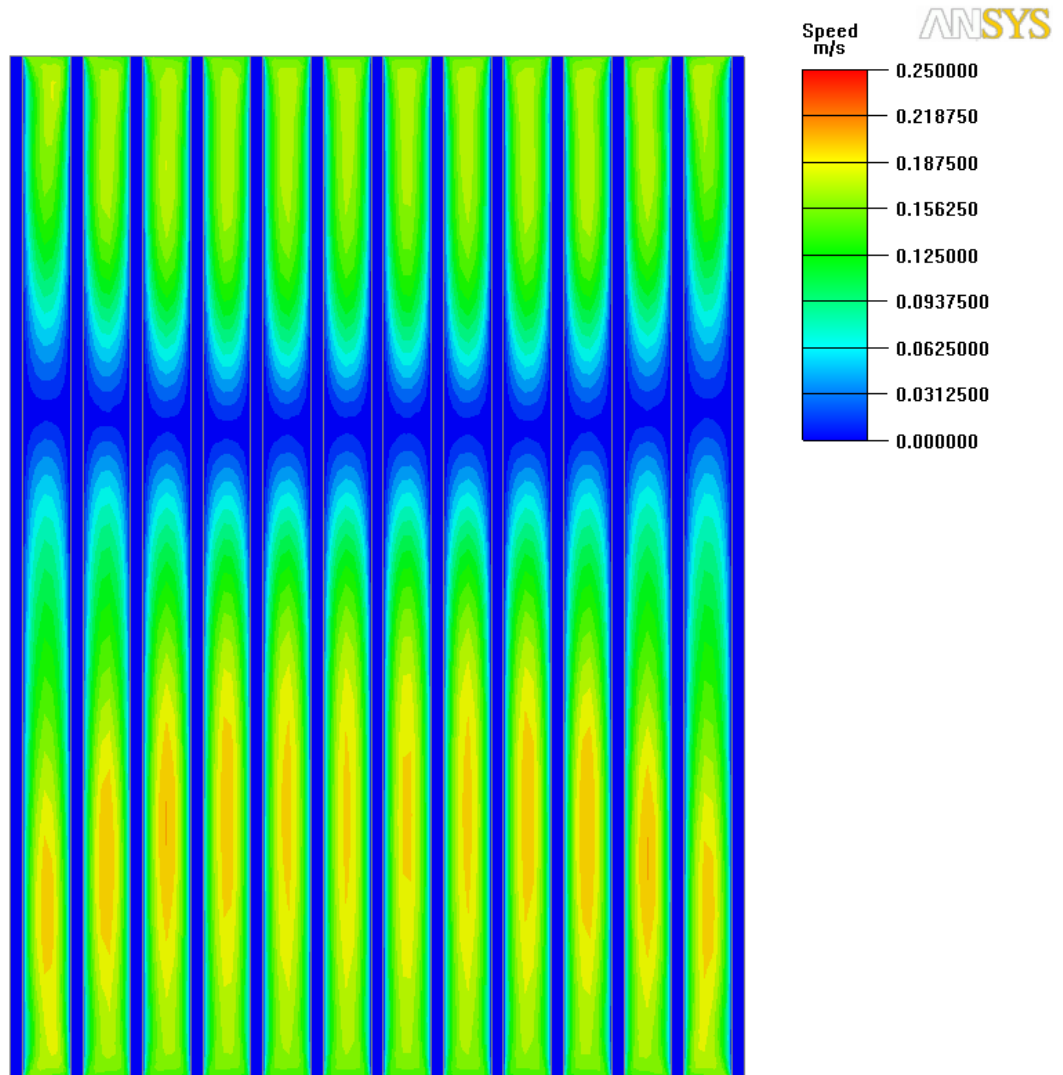
Figure 4.29 Speed contours for H=25 mm, θ =85$^\text{o}$
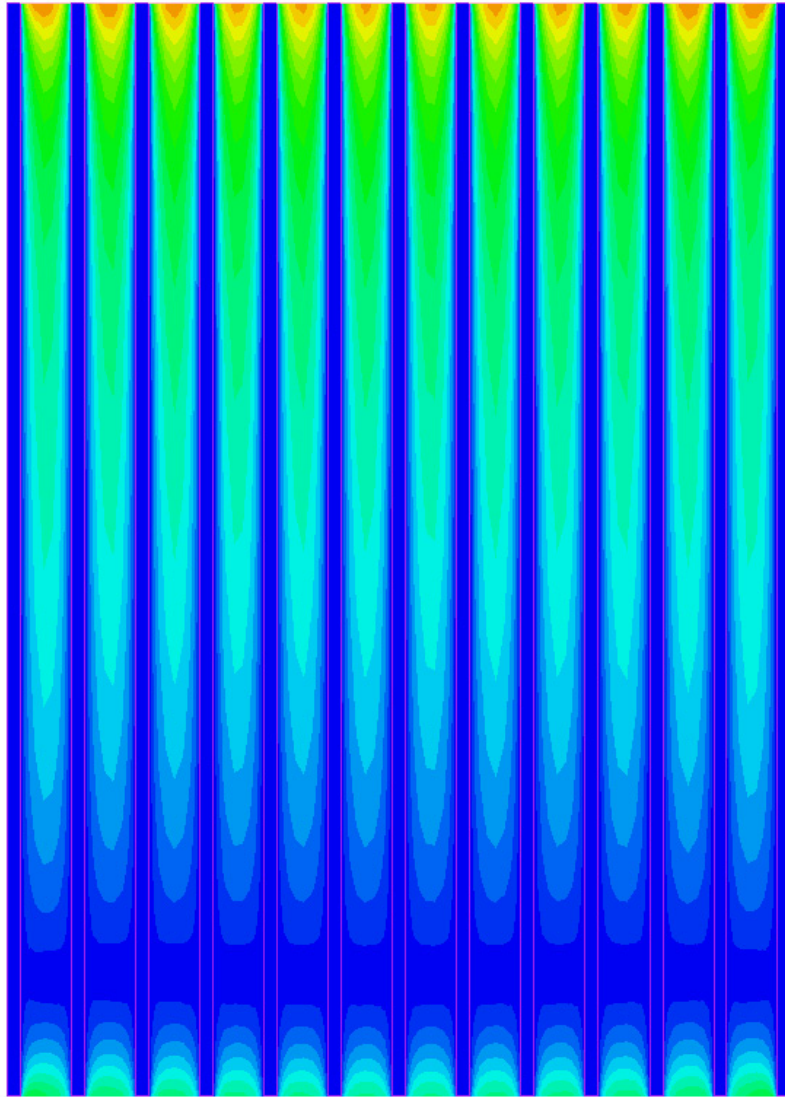
Figure 4.30 Speed contours for *H*=15 mm, θ=85°
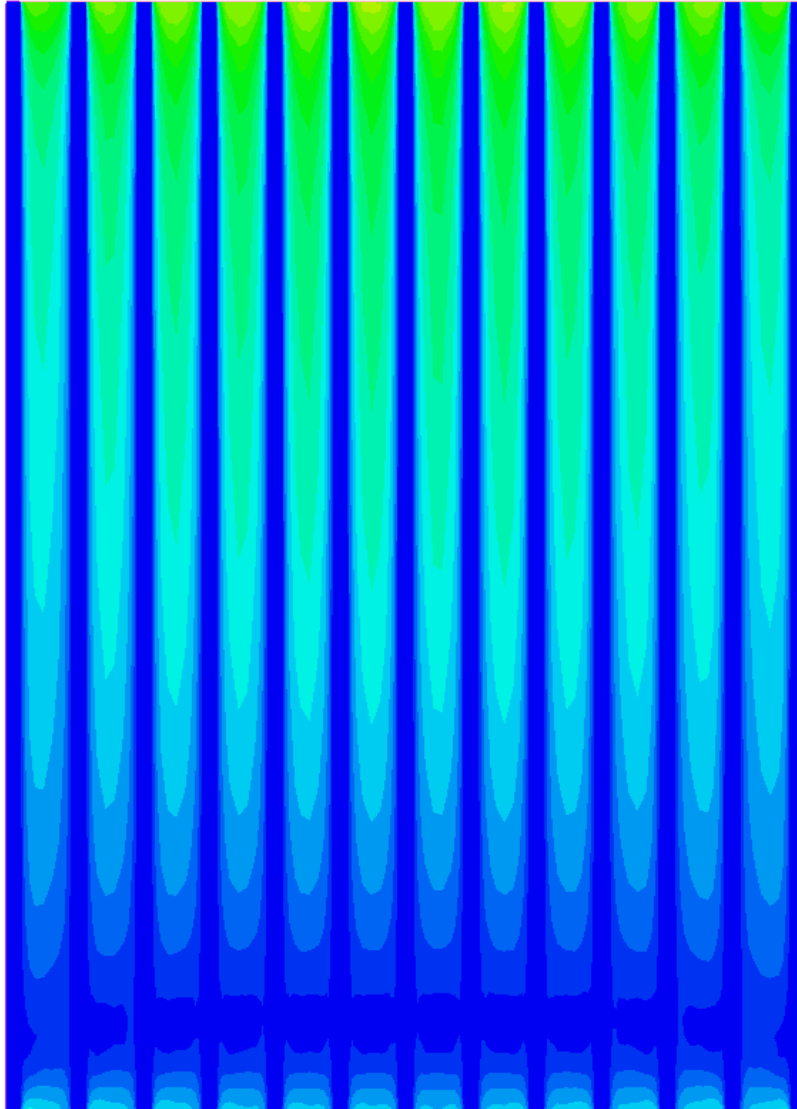
Figure 4.31 Speed contours for *H*=5 mm, θ =85°

It can be seen from the figures that using taller fin heights leads to higher speeds at the edges of the heat sink. A larger fin height simultaneously increases the driving force and increases friction thus enhancing the movement of the flow separation line toward the center of the heat sink. The taller the fin height the closer the separation point to the

94

middle of each channel. According to these figures separation takes place in all channels and approximately in the same location along each one.

4.3.5   Variation of Flow Speed with Fin Height in Upward Inclination

In order to show the variation of flow speed with fin height in upward direction of inclination, the following fin configuration is used:

- Power input, Q_{in}=100 W
- Angle of inclination, θ =-85º

Speed contours of the flow for different fin heights, H=25 mm, H=15 mm, H=5 mm are shown on an x-y cross section in Figure 4.32 to Figure 4.34 respectively. The speed scale is the same for all the figures.

Figure 4.32 Speed contours for H=25 mm, θ =-85°

The places which are shown with blue color in speed contours (near 0 m/s) demonstrate the separation point along each channel.
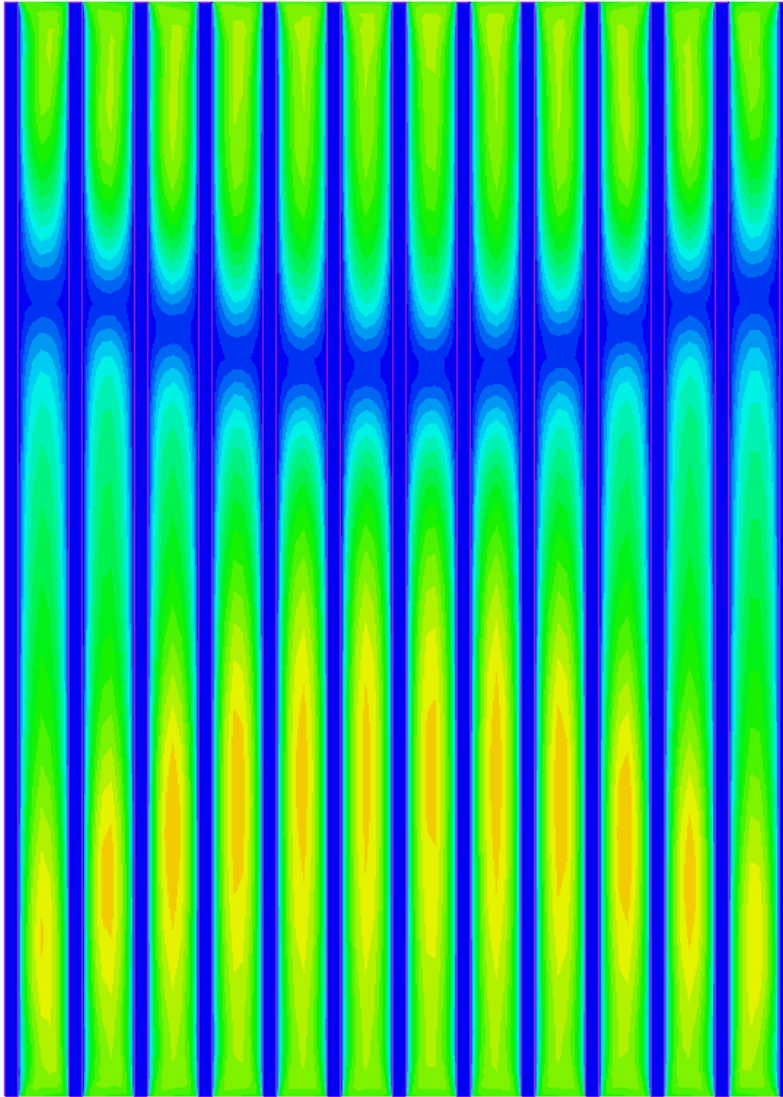
Figure 4.33 Speed contours for *H*=15 mm, θ =-85$^\text{o}$
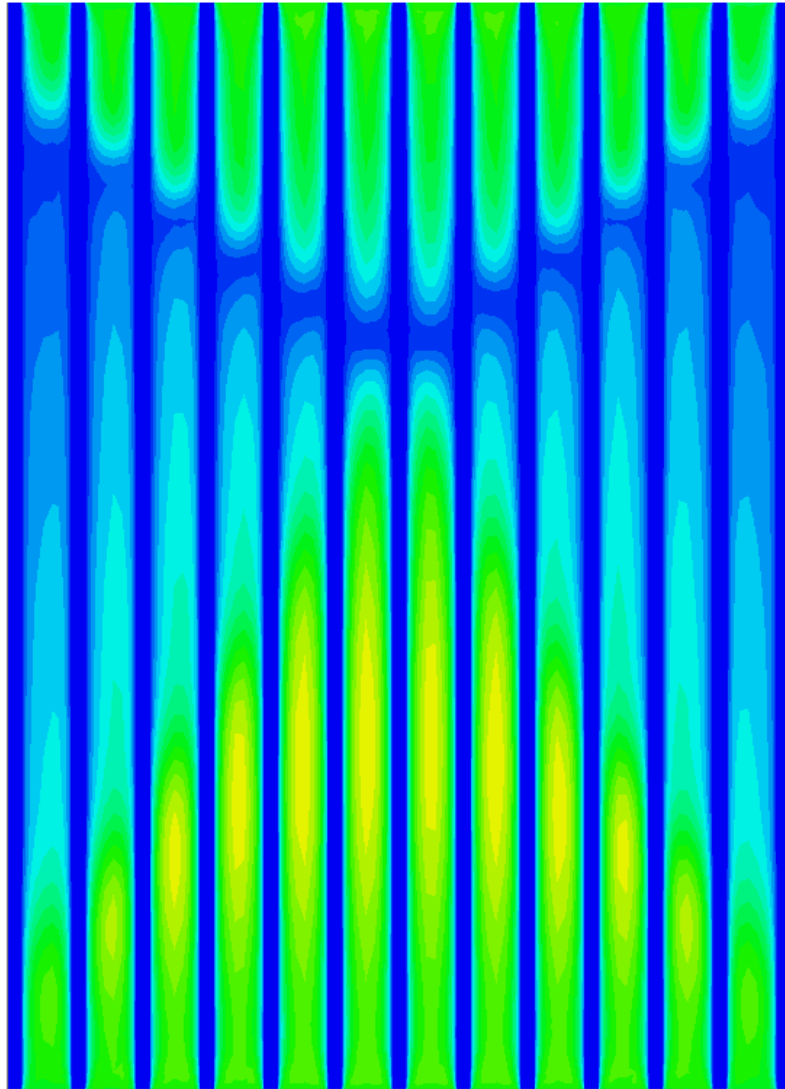
Figure 4.34 Speed contours for H=5 mm, θ =-85°

The two flows collided with each other at a certain distance from the heat sink bottom edge in each channel. These distances are almost the same for H=25 mm. But in smaller fin heights, H=15 mm and H=5 mm, this symmetric condition cannot be seen. From middle channels toward side channels the distance between bottom edge and the point of separation increases. A heat sink which has a component in the upward vertical direction is more susceptible to instability. In a heat sink with smaller fin height this instability increases due to reduction in friction and driving force. This tendency to instability can be easily seen in Figure 4.34 for H=5 mm.

4.4   Comparison and Verification

4.4.1   Comparison of Results for Downward Inclination

In order to validate the results, all data obtained for different array gemoetries, inclination angles and temperture differences in current numerical study are collected in the same plot which shows the variation of $Q_c - (Q_0)_c / kH\Delta T(W/L)$ according to Rayleigh number. The study which was done by Mittelman et al [32] is somewhat similar for making a comparison between the results. Figure 4.35 displays all the results for downward direction besides the results obtained in Ref. [32] which are performed for angles 60°-90°. As seen, the numerical results and experimental data are in good agreement.
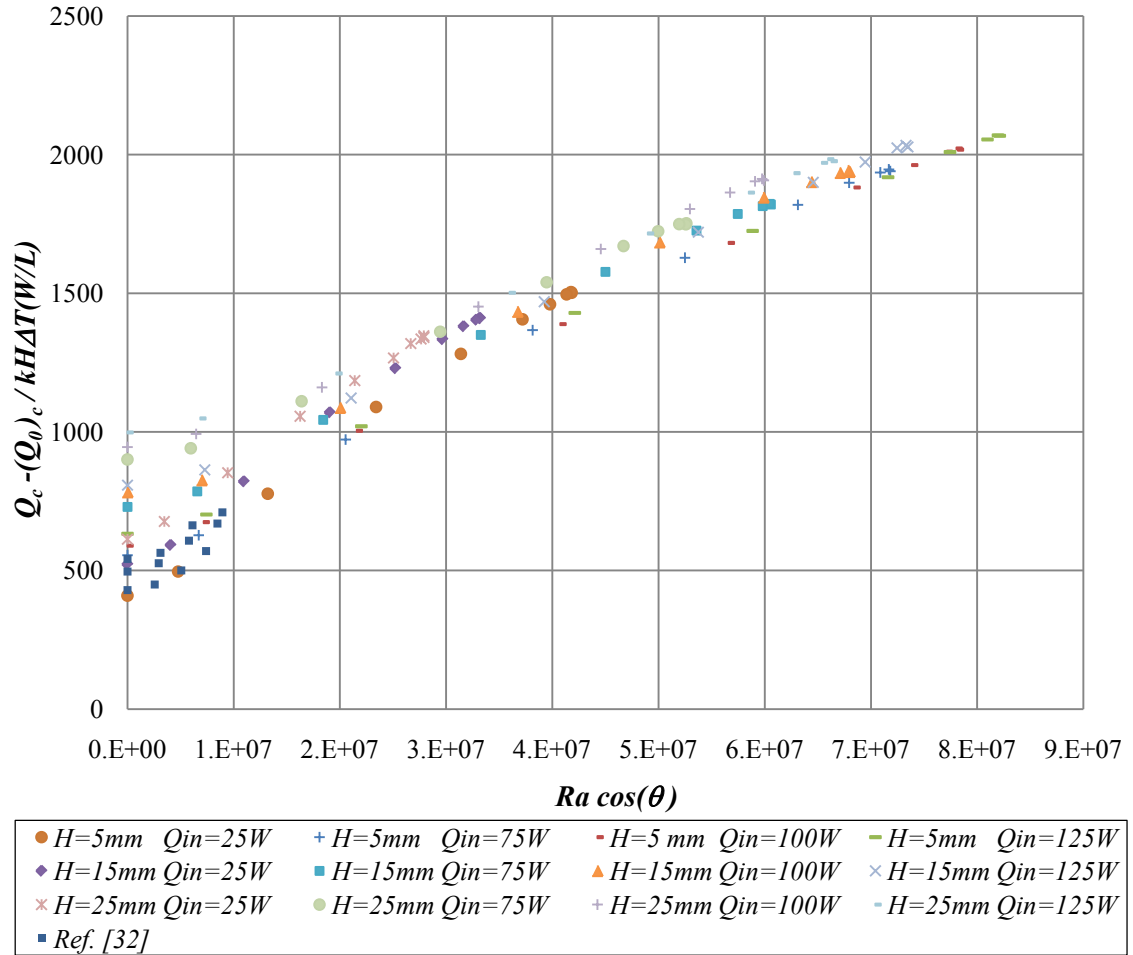
Figure 4.35 Comparison between numerical and experiment results

4.4.2 Comparison of Results for Upward Inclination

Similar to the downward direction, on the other side for upward direction as noted before only experimental study exists in the literature is the one performed by Starner and McManus [18] for the angle of inclination θ =-45°. Keeping in mind that current study is an idealized experiment, we do not have any room wall temperature variations, no room wall roghness and also the geometric parameters are not exactly the same,

Figure 4.36 presents a comparison between current study and the study done by Starner and McManus in $\theta=-45^\circ$. The similar trend can be easily seen in both studies.
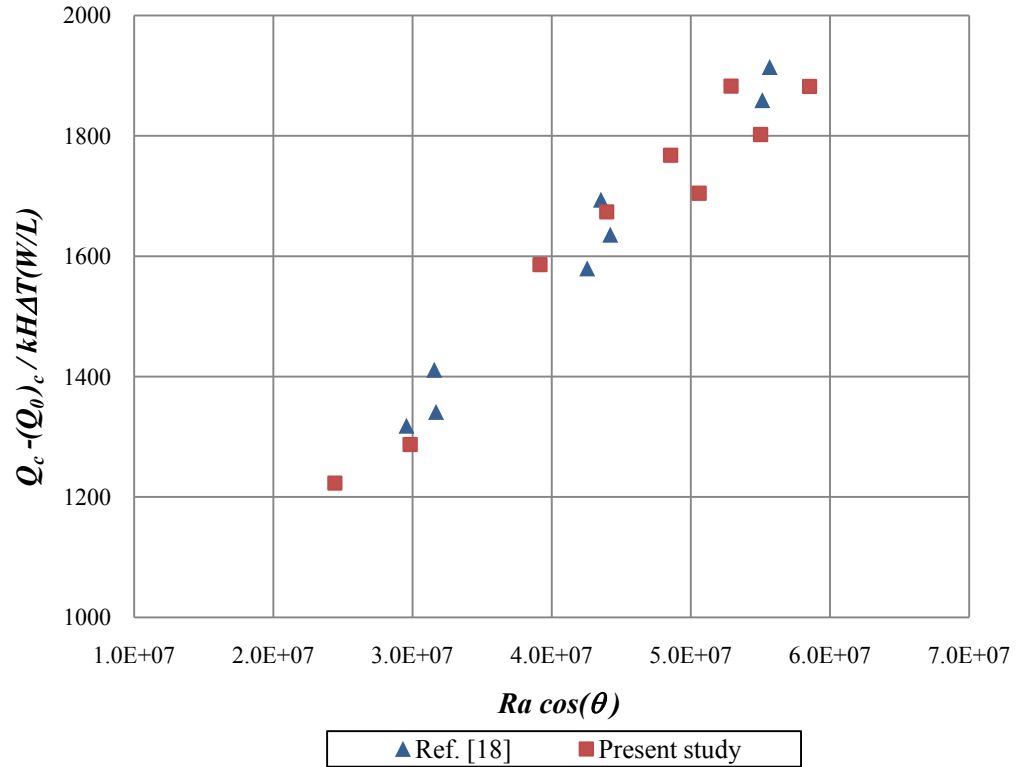
Figure 4.36 Comparison between present study and Ref. [18] at $\theta=-45^\circ$

In addition, similar to the Figure 4.35 for downward direction of inclination, Figure 4.37 presents variation of $Q_c - (Q_0)_c / kH\Delta T \, (W/L)$ with respect to Rayleigh number for all data obtained for upward direction of inclination.
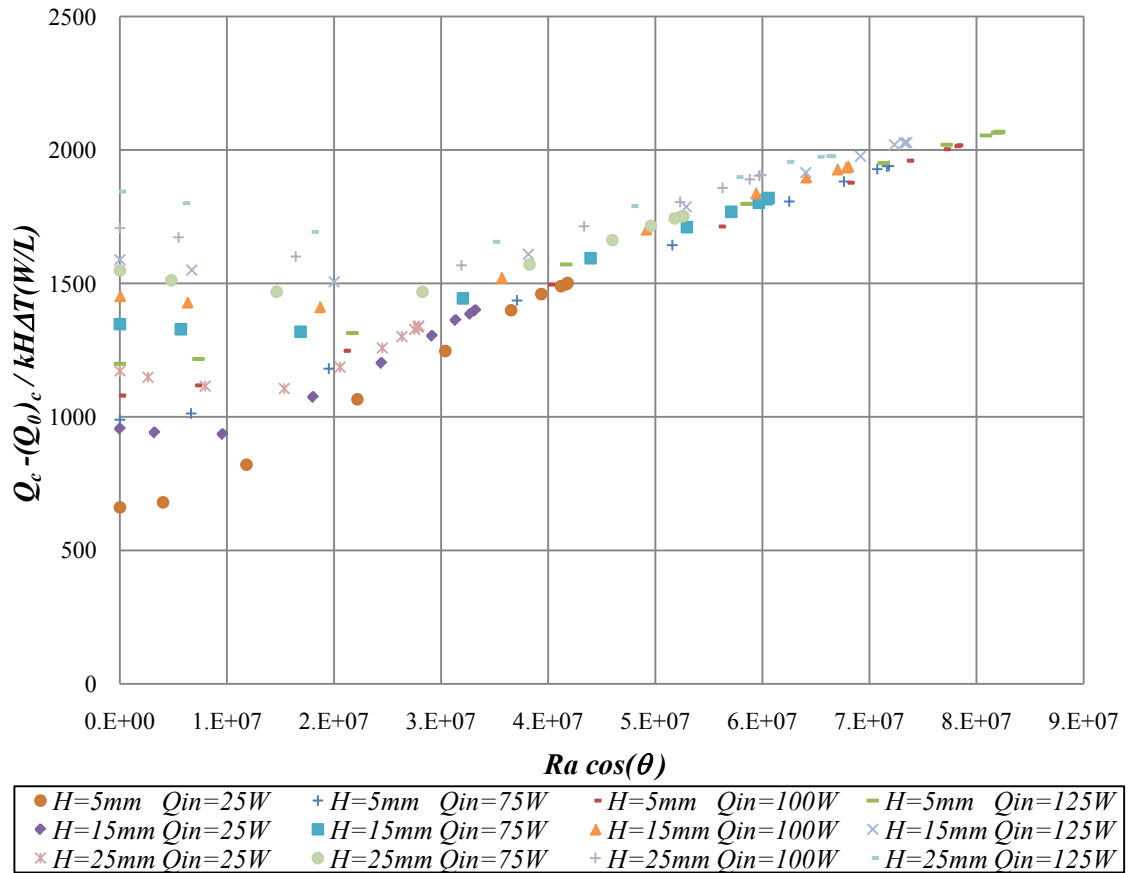
Figure 4.37 Variation of heat transfer in upward direction for different
fin heights and input powers

4.4.3 Comparison of Vertical Case Correlation and Inclined Case Results

In order to examine whether the correlation derived in the vertical case can be used in the current case for inclined orientation, all the data obtained are gathered in a plot as shown in Figure 4.38 and Figure 4.39 for downward and upward direction respectively. The trendline which is formed in each plot illustrates the results which are achieved by using the vertical case correlation except by multiplying Rayleigh number by the cosine of the angle of inclination. Equation (4.1) shows the correlation used to form this trendline.

$$\frac{Q_c - (Q_0)_c}{kH\Delta T(W/L)} = 0.2363 \ (\text{Ra} \cos \theta)^{0.5} \tag{4.1}$$
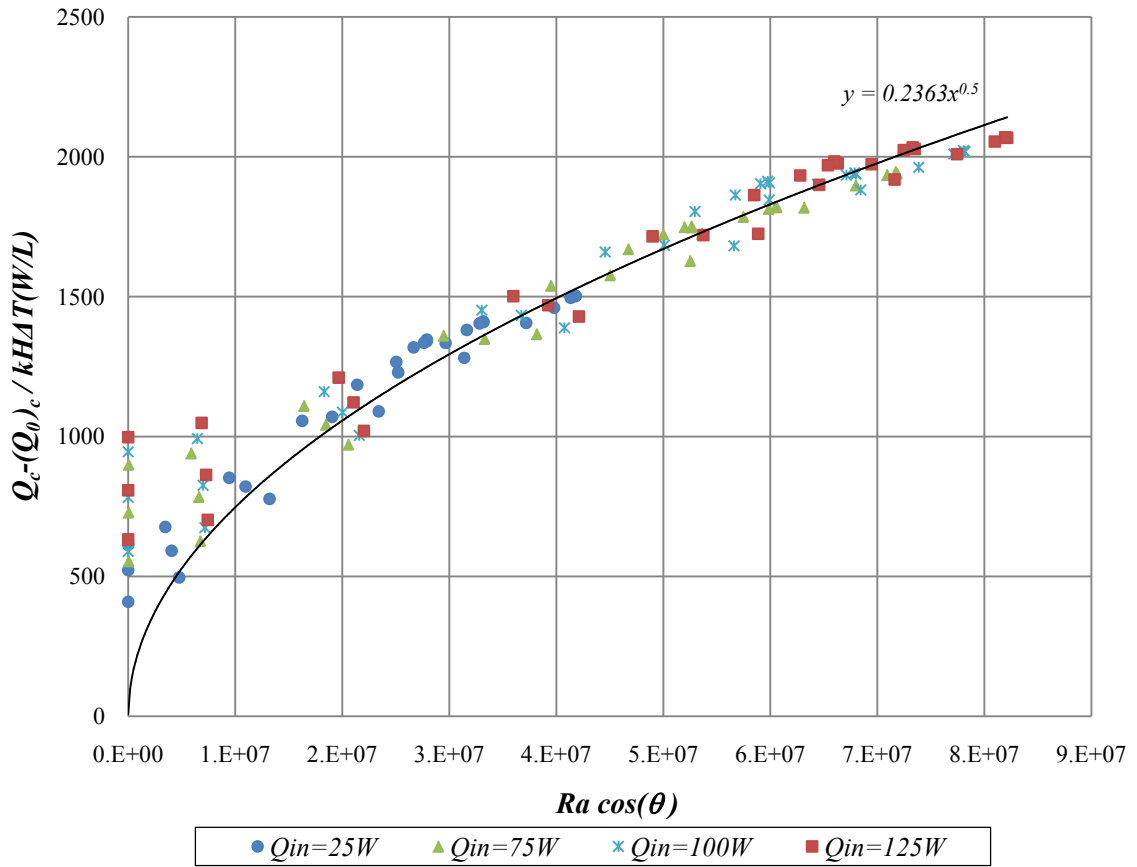
Figure 4.38 Comparsion between Equation (4.1) and data obtained for downward inclination

103
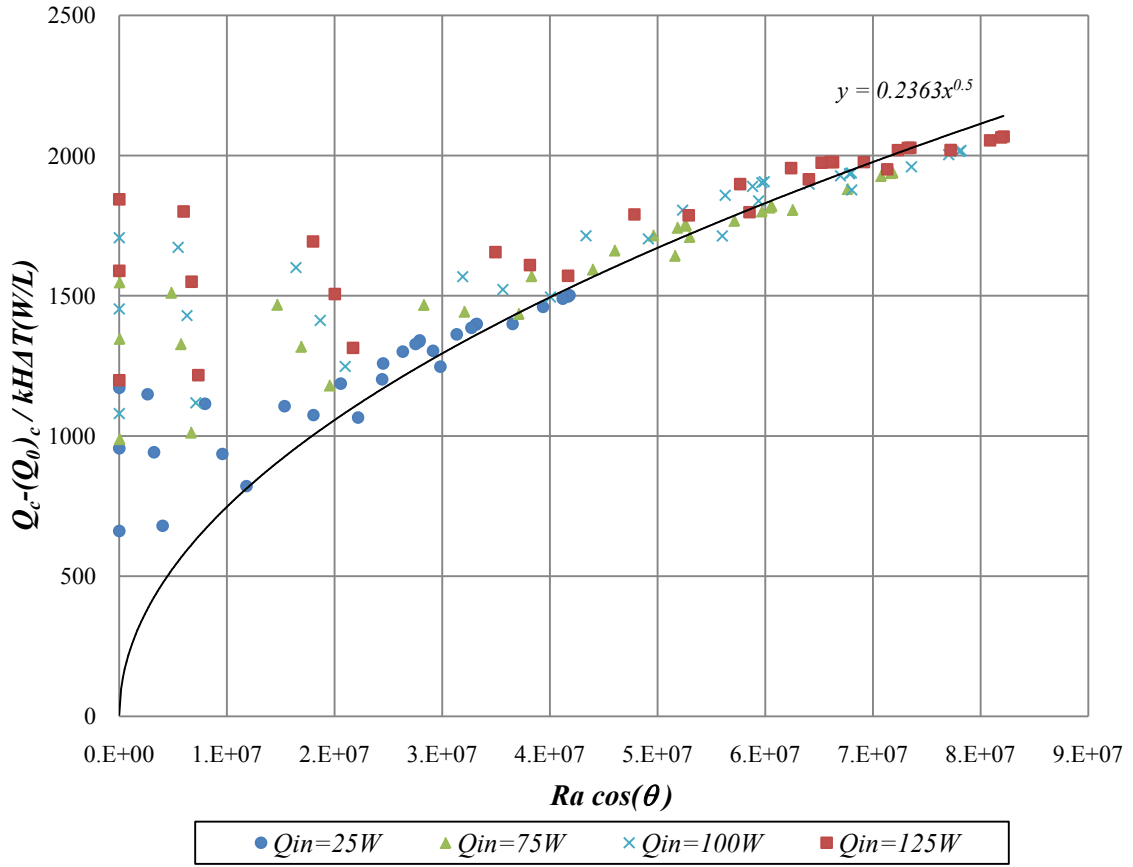
Figure 4.39 Comparsion between Equation (4.1) and data obtained for upward inclination

As shown in these figures besides some cases, the Equation (4.1) generally is not applicable for finding the amount of heat transfer from the heat sink surface in inclined orientations especially in the higher inclination angles. Obviously, the modified formula through the replacement of g by $g\ cos\theta$ cannot track the actual effect of heat sink inclination on the heat transfer rate due to changes in boundary layer thickness especially in each channel corners between plate and fins. Also in the course of heat sink inclination the amount of air that enters into each channel changes which influences the dissipation of heat considerably. Moreover, this formula does not account for the separation line location. These facts probably explain the large disagreement of the

results at higher inclination angles. For better examining the differences between the results which have been obtained by simulation and the results that can be achieved by the correlation suggested in the vertical case, the pure convection heat transfer values with respect to the angle of inclination are demonstrated in two separate plots. Figure 4.40 and Figure 4.41 show this comparison for specific fin array configuration with H=25 mm and Q_{in}=75 W for downward and upward directions of inclination respectively.
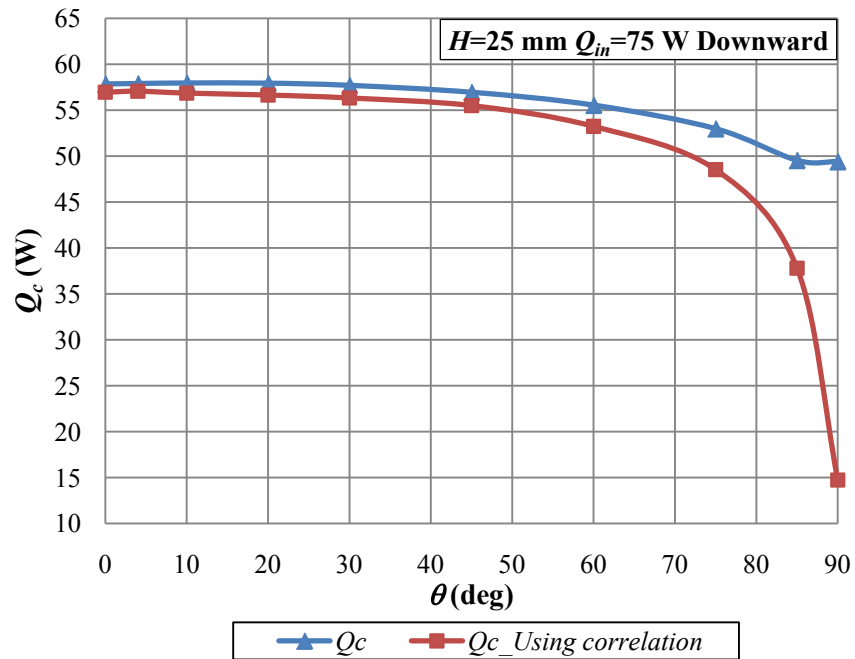
Figure 4.40 Comparison between convection heat transfer obtained by simulation and Equation (4.1) in downward inclination for H=25 mm, Q_{in}=75 W
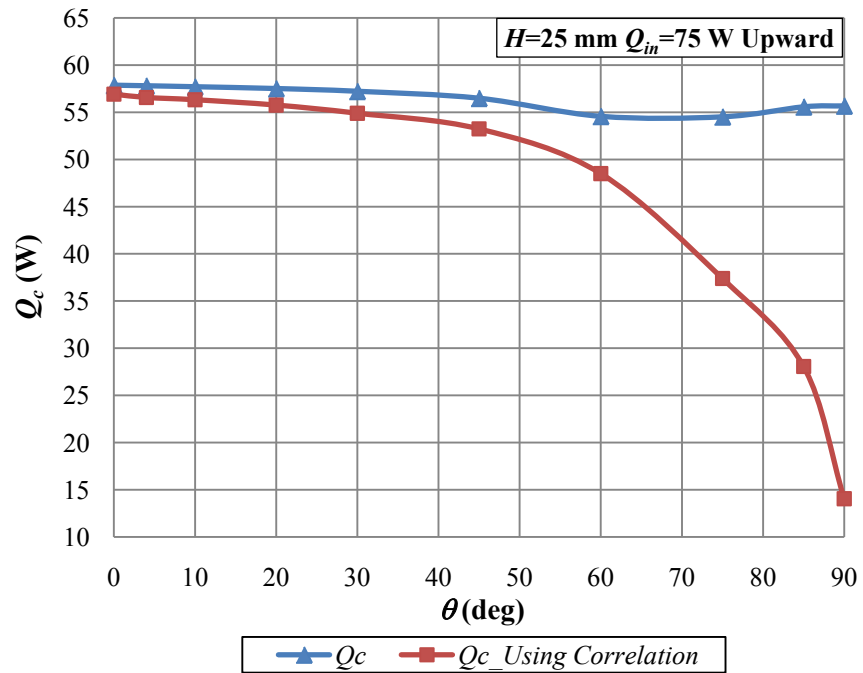
Figure 4.41 Comparison between convection heat transfer obtained by simulation and Equation (4.1) in upward inclination for H=25 mm, Q_{in}=75 W

For both direction using the vertical case correlation may be acceptable up to 45º. At higher angles, especially very close to horizontal, errors from using vertical correlation become very large.

CHAPTER 5

CONCLUSION

In this study steady state natural convection heat transfer from plate finned heat sinks at different angles of inclinations are investigated with the help of a commercial CFD code ANSYS Fluent. The main objectives of this study were to show the advantage of CFD solutions for natural convection from finned heat sinks by simulating experimental cases from literature and also fill the gap in the literature by presenting a comprehensive study on the effect of heat sink inclination on the flow properties.

For this purposes one of the recent experimental works in this area was chosen for making a similar numerical model inside Fluent. Before the analysis the constructed model was verified. For verification, two separate methods were performed for natural convection from vertical flat plate. Results were compared with theoritical and experimental results.

After model verification, simulations for the vertical orientation of the heat sink were performed to investigate the effects of geometric parameters on the heat dissipation from the heat sink. It was found that convection heat transfer rate depends on fin length, fin height and fin spacing as predicted. The results and their comparison with the literature were given in Chapter 3. It was found that for a given fin spacing, the convection heat transfer rate from fins increases with increasing fin height. Besides, for the lower fin height, as the fin spacing increases, convection heat transfer rate decreases and approaches that of a vertical plate. Additionally, as the power input increases, buoyancy

induced flow is more effective and as a result of this, the convective heat transfer increases. Also because of thermal layer thickness reduction along the plate fin, surface temperature decreases. At a given fin height and fin length, the convection heat transfer rate from fin arrays increases fin spacing, and it reaches to a maximum value and then it begins to decrease with further increase in fin spacing.

A scale anaylysis is applied similar to the experimental reference to produce order-of-magnitude estimate for the optimum fin spacing value. As a result of scale analysis, for the optimum fin spacing, a correlation was suggested as given below:

$$\frac{S_{opt}}{L} = 4.032 \times Ra_L^{-0.25} \tag{5.1}$$

Equation (5.1) is a relation between Rayleigh number based on fin length and optimum spacing ratio for maximum heat transfer rate from fin arrays. As a result of the present numerical study, optimum fin spacing minimizing the surface temperature was found as 11.75 mm.

The second correlation was suggested to find an order-of-magnitude for the maximum convection heat transfer rate from the fin arrays as presented in Equation (5.2).

$$Q_{c\max} - (Q_0)_c \leq 0.2363(Ra_L)^{0.5} kH\Delta T \frac{W}{L} \tag{5.2}$$

After verifying the vertical case results and thus the model itself by comparing with experimental study, the simulations were performed for the situations where the heat sink inclined from the vertical position. For this purpose, the same vertical model was used by just changing the direction of gravity acceleration in ANSYS Fluent. Optimum fin spacing which was suggested in vertical case was used for investigating the inclined case. Large number of angles was examined in both direction of inclination. Effects of various parameters on the heat transfer rate were demonstrated.

It was observed that Rayleigh number varies markedly with the angle of inclination. The effect of inclining the heat sink so that it has a component in the upward vertical direction (negative inclination angles) is to make the flow more susceptible to instability. On the other hand, a heat sink whose normal has a downward directed component is less susceptible to instability.

In this study the location of separation line is tracked by numerical simulations. It was confirmed that the position of separation line on the heat sink surface mostly depends on the inclination angle. Separation starts at a certain angle along the surface and in upward inclinations it is nearer to the leading edge the larger the inclination angle of the surface. Separation changes the heat transfer coefficients considerably. It was observed that the effect of power input is not significant on the location of separation point on the heat sink surface. Also Fin height was found as the most important parameter which influences the heat dissipation magnitude significantly. A larger fin height not only increases the total surface area which leads to higher rate of convection heat transfer but also increases the driving force and enhances the movement of the flow separation line toward the center of the heat sink.

The results of analyses and their comparison with literature were given in Chapter 4. Results showed that Equation (5.2) which was obtained for vertical case is not applicable for the inclined case by using $Ra\,cos\theta$ instead of Ra through this correlation. Changes in boundary layer thicknesses, especially in each channel corner, and changes in amount of air enters into the channels with respect to inclination angle are the reasons behind this behavior.

REFERENCES

[1] Yazıcıoğlu B., "Performance of Rectangular Fins on a Vertical Base in Free Convection Heat Transfer", M.S. Thesis in Mechanical Engineering, Middle East Technical University, Ankara, (2005).

[2] Yazıcıoğlu B., Yüncü H., "Optimum Fin Spacing of Rectangular Fins on a Vertical Base in Free Convection Heat Transfer", Heat and Mass Transfer 44, 11-21, (2007).

[3] Yazıcıoğlu B., Yüncü H., "A Correlation for Optimum Fin Spacing of Vertically-Based Rectangular Fin Arrays Subjected to Natural Convection Heat Transfer", Journal of Thermal Science and Technology 29, 99-105, (2009).

[4] Güvenç A., Yüncü H., "An Experimental Investigation on Performance of Rectangular Fins on a Vertical Base in Free Convection Heat Transfer", Heat and Mass Transfer 37, 409-416, (2001).

[5] Leung C. W., Probert S. D., "Heat–Exchanger Design: Optimal Uniform Thickness of Vertical Rectangular Fins Protruding Perpendicularly Outwards, at Uniform Separations, from a Vertical Rectangular Base", Applied Energy, 26, 111-118, (1987).

[6] Leung C. W., Probert S. D., Shilston M. J., "Heat Exchanger Design: Thermal Performances of Rectangular Fins Protruding from Vertical or Horizontal Rectangular Bases", Applied Energy 20, 123-140, (1985).

[7] Leung C. W., Probert S. D., "Thermal Effectiveness of Short Protrusion Rectangular, Heat Exchanger Fins", Applied Energy 34, 1-8, (1989).

[8] Ko Y. M., Leung C. W., Probert S. D., "Steady-State Free-Convective Cooling of Heat Exchangers with Vertical Rectangular Fins: Effect of Fin Material", Applied Energy, 34, 181-191, (1989).

[9] Leung C. W., Probert S. D., Shilston M.J., "Heat Exchanger: Optimal Separation for Vertical Rectangular Fins Protruding from a Vertical Rectangular Base", Applied Energy 19, 77-85, (1985).

[10] Leung C. W., Probert S. D., Shilston M. J., "Heat Transfer Performances of Vertical Rectangular fins protruding from Rectangular Bases: Effect of Fin Length", Applied Energy 22, 313-318, (1986).

[11] Leung C. W., Probert S.D., "Natural-convective heat exchanger with vertical rectangular fins and base: design criteria", IMechE Proceedings 201, 365-372, (1987).

[12] Leung C. W., Probert S.D., "Heat-Exchanger Performance: Influence of Gap Width between Consecutive Vertical Rectangular Fin Arrays", Applied Energy 56, 1-8, (1997).

[13] Yüncü H., Anbar G., "An Experimental Investigation on Performance of Rectangular Fins on a Horizontal Base in Free Convection Heat Transfer", Heat and Mass Transfer 33, 507-514, (1998).

[14] Yüncü H., Mobedi M., "A Three Dimensional Numerical Study on Natural Convection Heat Transfer from Short Horizontal Rectangular Fin Array", Heat and Mass Transfer 39, 267-275, (2003).

[15] Yildiz Ş., Yüncü H., "An Experimental Investigation on Performance of Annular Fins on a Horizontal Cylinder in Free Convection Heat Transfer", Heat and Mass Transfer 40, 239-251, (2004).

[16] Mobedi M., Sunden B., "Natural Convection Heat Transfer from a Thermal Heat Source Located in a vertical Plate Fin", International Communications in Heat and Mass Transfer 33, 943-950, (2006).

[17] Elenbaas W., "Heat Dissipation of Parallel Plates by Free Convection", Physica 9, 1-28, (1942).

[18] Starner K. E., McManus H. N., "An Experimental Investigation of Free Convection Heat Transfer from Rectangular Fin Arrays", Journal of Heat Transfer 85, 273-278, (1963).

[19] Welling J. R., Wooldridge C.V., "Free Convection Heat Transfer Coefficient From Rectangular Fin Arrays", ASME Journal of Heat Transfer 87, 439-444, (1965).

[20] Jones C. D., Smith L. F., "Optimum Arrangement of Rectangular Fins on Horizontal Surfaces for Free Convection Heat Transfer", Journal of Heat Transfer 92, 6-10, (1970).

[21] Fitzroy N. D., "Optimum Spacing of Fins Cooled by Free Convection", Journal of Heat Transfer 93, 462-463, (1971).

[22] Bilitzky, A., "The Effect of Geometry on Heat Transfer by Free Convection from a Fin Array", M. S. thesis, Department of Mechanical Engineering, Ben-Gurion University of the Negev, Beer Sheva, Israel. (1986).

[23] Baskaya S., Sivrioglu M., Ozek M., "Parametric Study of Natural Convection Heat Transfer from Horizontal Rectangular Fin Arrays", International Journal of Thermal Science 39, 797-805, (2000).

[24] Harahap F., Lesmana H., "Measurements of heat dissipation from miniaturized vertical rectangular fin arrays under dominant natural convection conditions", Heat Mass Transfer 42, 1025-1036, (2006).

[25] Nada S. A., "Natural Convection Heat Transfer in Horizontal and Vertical Closed Narrow Enclosures with Heated Rectangular Finned Base Plate", International Journal of Heat and Mass Transfer 50, 667-679, (2007).

[26] Kundu B., Das P.K., "Performance and Optimum Design Analysis of Convective Fin Arrays Attached to Flat and Curved Primary Surfaces", International Journal of Refrigeration 32, 1-14, (2008).

[27] Yalcin H. G., Baskaya S., Siviroglu M., "Numerical Analysis of Natural Convection Heat Transfer from Rectangular Shrouded Fin Arrays on a Horizontal Surface", International Communications in Heat and Mass Transfer 35, 299-311, (2008).

[28] Dialameh L., Yaghoubi M., Abouali O., "Natural Convection from an Array of Horizontal Rectangular Thick Fins with Short Length", Applied Thermal Engineering 28, 2371-2379, (2008).

[29] Çakar K. M., "Numerical Investigation of Natural Convection from Vertical Plate Finned Heat Sinks", Middle East Technical University (METU) M.S. Thesis, Ankara, Turkey, (2009).

[30] Fujii T., Imura H., Natural-convection heat transfer from a plate with arbitrary inclination, International Journal of Heat and Mass Transfer 15, 755-767, (1972).

[31] Dayan A., Kushnir R., Mittelman G., Ullmann A., Laminar free convection underneath a downward facing hot fin array, International Journal of Heat and Mass Transfer 47, 2849-2860, (2004).

[32] Mittelman G., Dayan A., Dado-Turjeman A., Ullmann A., Laminar free convection underneath a downward facing inclined hot fin array, International Journal of Heat and Mass Transfer 50, 2582-2589, (2007).

[33] Dayan A., Kushnir R., Ullmann A., Laminar free convection underneath a hot horizontal infinite flat strip, International Journal of Heat and Mass Transfer 45, 4021-4031, (2002).

[34] Komori K., Kito S., Nakamura T., Inaguma Y., Inagaki T., Fluid flow and heat transfer in the transition process of natural convection over an inclined plate, Heat Transfer Asian Research 30, 648-659, (2001).

[35] Kimura F., Yoshioka T., Kitamura K., Yamaguchi M., Sami T., Fluid flow and heat Transfer of natural convection at a slightly inclined, upward-Facing, heated plate, Heat Transfer Asian Research 31, 362-275, (2002).

[36] Kimura F., Kitamura K., Yamaguchi M., Asami T., Fluid flow and heat trassnfer of natural convection adjacent to upward facing inclined heated plates, Heat Transfer Asian Research 32, 278-291, (2003).

[37] Biertümpfel R., Beer H., Natural convection heat transfer increase at the laminar-turbulent transition in the presence of instationary longitudinal vortices, International Jounral of Heat and Mass Transfer 46, 3109-3117, (2003).

[38] Lloyd J. R., Sparrow E. M., On the instability of natural convection flow on inclined plates, Journal of Fluid Mechanics 42, 465-470, (1970).

[39] Kakaç S., Yüncü H., Hijikata K., Cooling of electronic systems, NATO ASI Series. Kluwer Academic Publishers, Dordrecht, (1994).

[40] Kraus A., Bar-Cohen A., Wative A., Cooling Electronic Equipment, Mechanical Engineers Handbook, John Wiley & Sons, New York, (2006).

[41] Bejan A., Convective Heat transfer, John Wiley & Sons, New York, (1984).

[42] Incropera F. P., Dewitt D. P., Fundamentals of Heat and Mass Transfer, John Wiley & Sons, New York, (1990).

[43] Mcadams W.H., Heat Transmission, McGraw-Hill, New York, (1954).

[44] ANSYS 12.1 User's Guide, Fluent Inc.

APPENDIX A

MESH SIZE CONTROL

In order to find the necessary mesh size and amount, three different mesh sizes are used to analyze a sample fin configuration. The results obtained from three different mesh amounts are compared with each other.

Sample fin configuration is as follows:

- Fin length, L=250 mm
- Fin height, H=25 mm
- Number of fins, N=16
- Power input, Q_{in} = 100 W

A.1   Mesh Size A

The following mesh control properties are used for this mesh size:

- Max X size = 27 mm
- Max Y size = 75 mm
- Max Z size = 20 mm
- Min elements is gap = 3
- Min elements on edge = 2
- Max size ratio = 2

- No object parameters are used.

When this mesh control properties are used, the total cell number is 1485832.

Mesh A is displayed on an *x-z* cross section in Figure A.1.
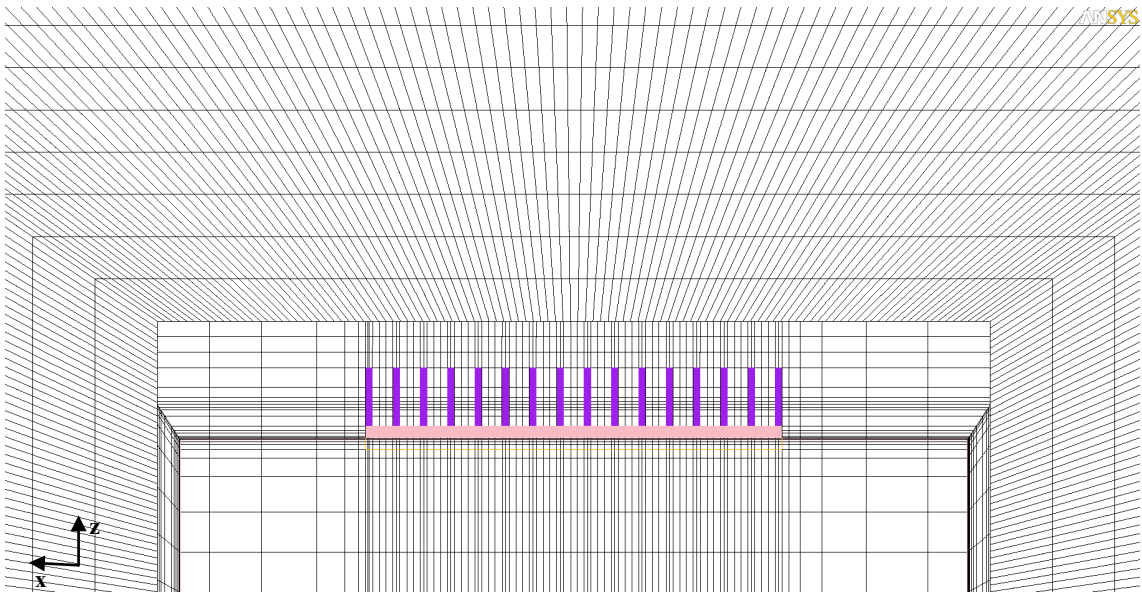
Figure A.1 Mesh structure for mesh size A

A.2   Mesh Size B

The following mesh control properties are used for this mesh size:

- Max X size = 27 mm
- Max Y size = 75 mm
- Max Z size = 20 mm
- Min elements in gap = 3
- Min elements on edge = 3
- Max size ratio = 2
- Object parameters for fin arrays are used as follows:

- o Pins X element count = 2
- o Pins Y element count = 60
- o Pins Z element count = 10
- o Base element height = 0.5 mm
- o Pins element height = 0.5 mm
- o Base element ratio = 1.5
- o Pins element ratio = 1.5

As a result total mesh amount for this mesh size is 2634264. Mesh B is displayed on an *x-z* cross section in Figure A.2.
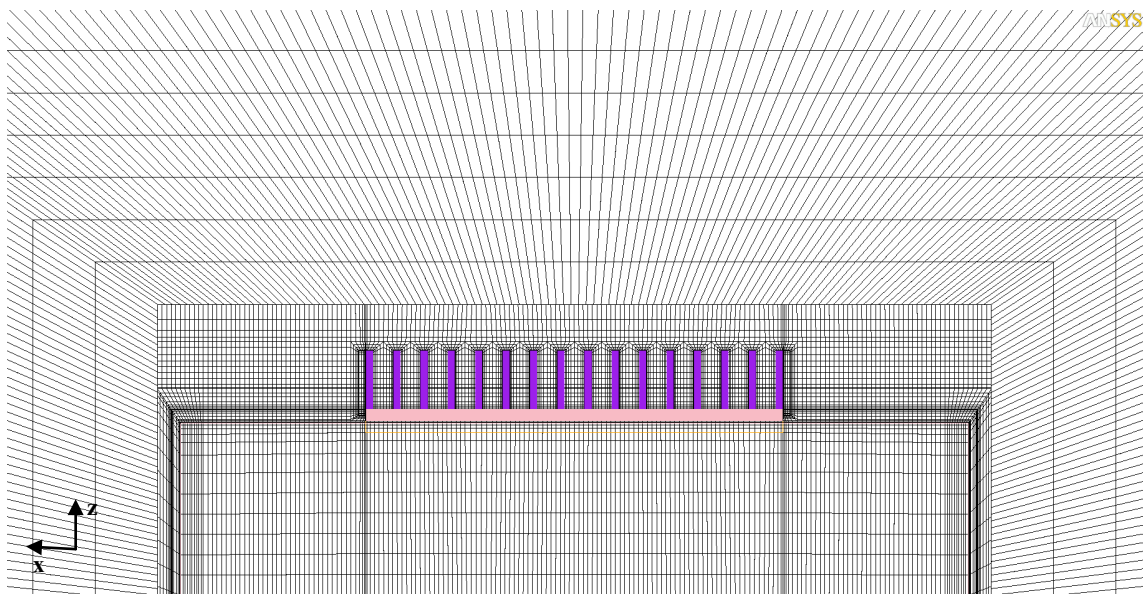
Figure A.2 Mesh structure for mesh size B

A.3 Mesh Size C

The following mesh control properties are used for this mesh size:

- Max X size = 27 mm
- Max Y size = 75 mm

- Max Z size = 20 mm

- Min elements in gap = 3

- Min elements on edge = 2

- Max size ratio = 2

- Object parameters for fin arrays are used as follows:

  o Pins X element count = 4

  o Pins Y element count = 80

  o Pins Z element count = 20

  o Base element height = 0.5 mm

  o Pins element height = 0.5 mm

  o Base element ratio = 1.2

  o Pins element ratio = 1.2

Total number of cells with these mesh control parameters is 3977608. Mesh C is displayed on an *x-z* cross section in Figure A.1.

.
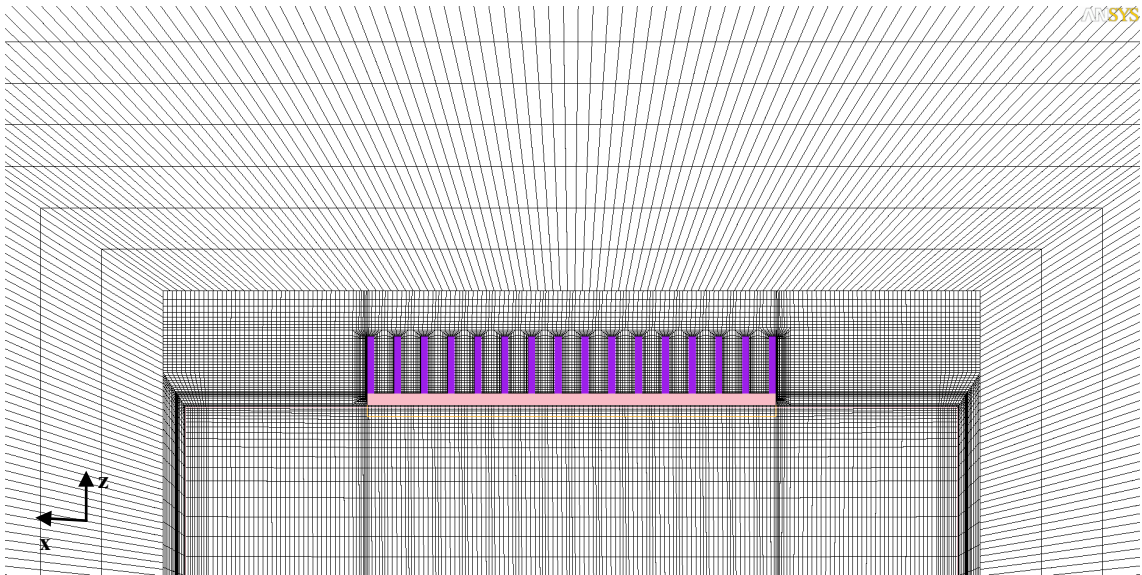
Figure A.3 Mesh structure for mesh size C

A.4 Comparison between different Mesh Sizes

The results obtained from three different mesh size controls are given in Table A.1.

Table A.1 Comparison of three mesh amounts

	Number of Cells	Computational Time	T_w (°C)	Q_c (W)
Mesh Size A	1685832	74 mins	83.7459	73.463
Mesh Size B	2834264	176 mins	80.5957	76.991
Mesh Size C	4077608	352 mins	80.4802	76.924

It can be seen from the Table A.1 that mesh size B and mesh size C give similar results. Since mesh size B gives as accurate results as mesh size C and still has lower computational time, it is taken as optimum mesh size. Therefore parameters for mesh size B is used for all of the fin array configurations investigated in this study.

APPENDIX B

SAMPLE CALCULATION FOR VERIFICATION PROCEDURE

The validity of numerical results was examined by comparing results in the literature and data obtained in present study. Following example shows the procedure for obtaining data for comparison. Sample fin configuration characteristic are as follows:

- $Q_{in} = 80W$
- $T_w = 152.32\,^{\circ}C$
- $Q_c = 38.15\ W$
- $A = 0.045\ m^2$
- $L = 0.25\ m$

For obtaining Nu and Ra numbers the flow properties are needed in the film temperature:

$$T_f = \frac{T_w + T_a}{2} = \frac{152.32 + 20}{2} = 86.16$$

$$\beta = \frac{1}{T_f} = \frac{1}{86.16 + 273.15} = 0.0027831 (1/K) \qquad k = 3.071 \times 10^{-2}\ W/mK$$

$$v = 2.194 \times 10^{-5}\ m^2/s \qquad \alpha = 3.146 \times 10^{-5}\ m^2/s \qquad Pr = 0.698$$

$$Ra = \frac{g\beta L^3 (T_w - T_a)}{\nu\alpha} = 81761171$$

$$h = \frac{Q}{A \times (T_w\text{-}T_a)} = 6.407$$

$$Nu = \frac{h \times L}{k} = 52.16311$$

The correlations exist in the literature are as follows:

- McAdam's correlation:

$$Nu = 0.59 \times Ra^{1/4} = 56.103349$$

- Churchill and Usagi's correlation :

$$Nu = \frac{0.67 \times Ra^{1/4}}{\left[1 + \left(\frac{0.492}{Pr}\right)^{9/16}\right]^{4/9}} = 48.80723$$

- Churchill and Chu's first correlation:

$$Nu = \left[0.825 + \frac{0.387 \times Ra^{1/6}}{\left[1 + \left(\frac{0.492}{Pr}\right)^{9/16}\right]^{8/27}}\right]^2 = 57.38379$$

- Churchill and Chu's second correlation:

$$Nu = 0.68 + \frac{0.67 \times Ra^{1/4}}{\left[1 + \left(\frac{0.492}{Pr}\right)^{9/16}\right]^{4/9}} = 49.48723$$

APPENDIX C
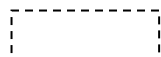
SAMPLE STUDY RESULTS FOR THE ASSEMBLY
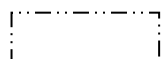
C.1   Sample Fin Configuration

- Input Power, Q_{in}= 125 W
- Fin Length, L = 340 mm
- Height of fins, H = 15 mm
- Fin Spacing, S = 32.4 mm
- Number of fins, N = 6

C.2   Illustration of Heat Flow Values from each Component

:   Total heat transfer (W)

:   Radiative heat transfer (W)

:   Average temperature ($^{\circ}$C)

C.2.1 Heater Plate
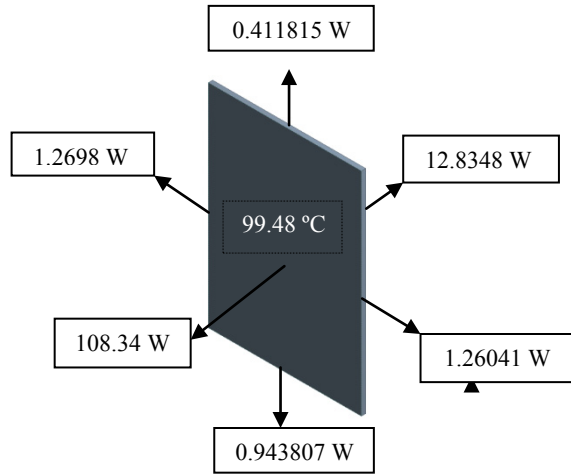
Figure B.1 Illustration of heat flow values for heater plate

Energy Balance Equation:

$$Q_{in} + Q_{out} \approx 0 \rightarrow -125 + 12.8348 + 0.411815 + 1.2698 + 108.34 + 0.943807 + 1.2604 \approx 0$$

C.2.2 Heat Sink
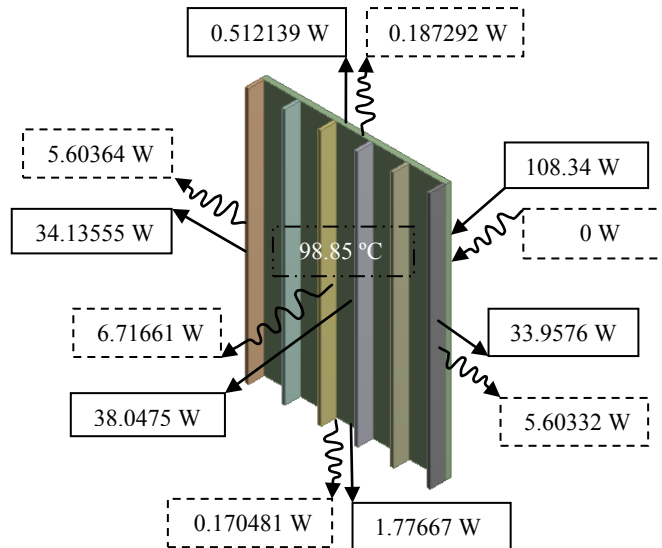
Figure B.2 Illustration of heat flow values for heat sink

Energy Balance Equation:

$$Q_{in} + Q_{out} \approx 0 \quad \rightarrow \quad \text{-}108.34 + 0.512139 + 34.13555 + 38.0475 + 1.77667 + 33.9576 \approx 0$$

Radiative heat transfer from heat sink:

$$Q_{rad} = 0.187292 + 5.60364 + 6.71661 + 0.170481 + 5.60332 + 0 = 18.2813$$

Convection heat transfer from heat sink:

$$Q_c = Q_{in} - Q_{rad} = 108.34 - 18.2813 = 90.05866$$

C.2.3   Concrete Block
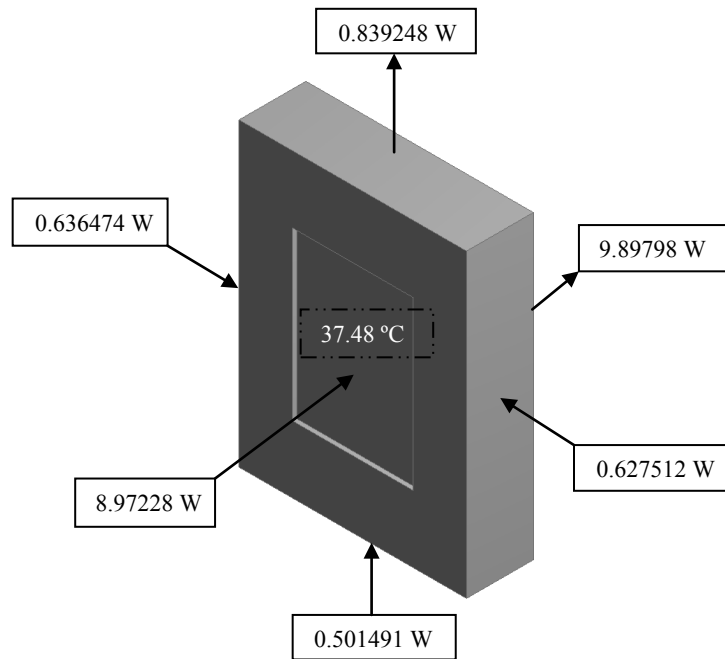
Figure B.3 Illustration of heat flow values for concrete block

Energy Balance Equation:

$$Q_{in} + Q_{out} \approx 0 \quad \rightarrow \quad 9.89798 + 0.839248 - 0.636474 - 8.97228 - 0.501491 - 0.627512 \approx 0$$

APPENDIX D

RESULTS

D.1   Vertical Case Results

Figures which are not shown in chapter 3 for vertical case are presented in this section.

D.1.1   Variation of Fin Array Temperature with Fin Spacing
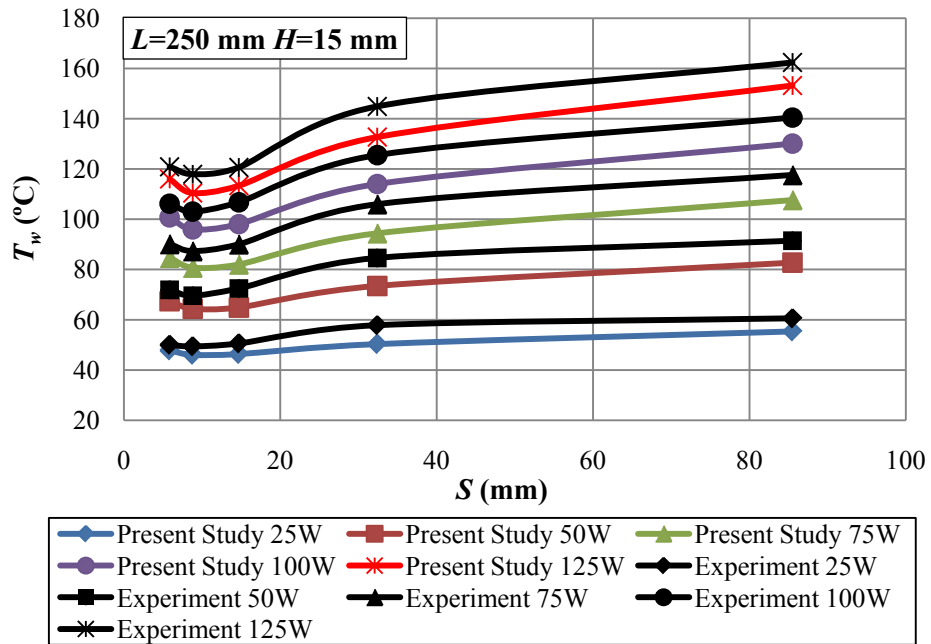
Figure D.1 Variation of fin array average temperature with fin spacing for
L=250 mm, *H*=15 mm
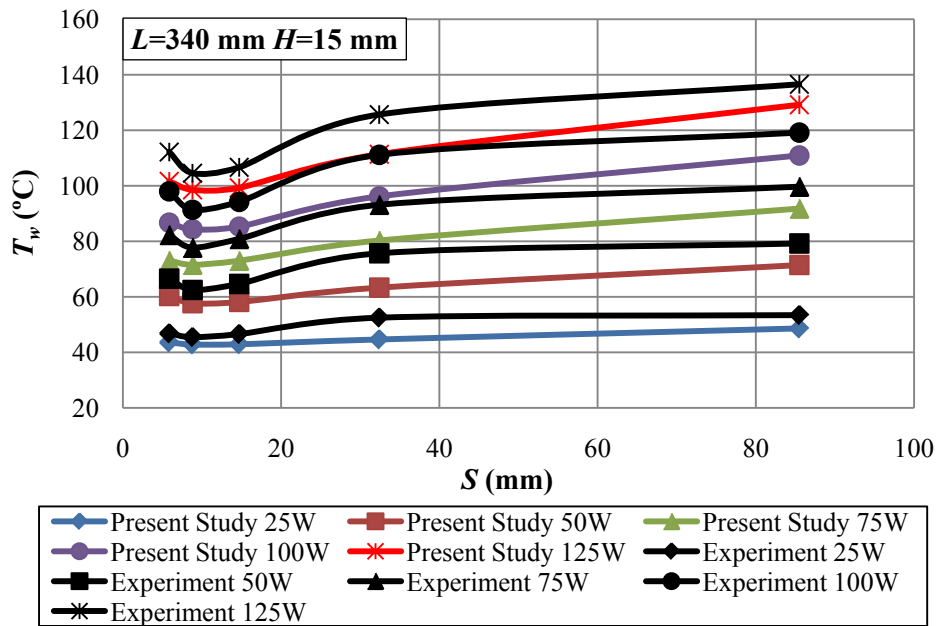
Figure D.2 Variation of fin array average temperature with fin spacing for
L=340 mm, *H*=15 mm
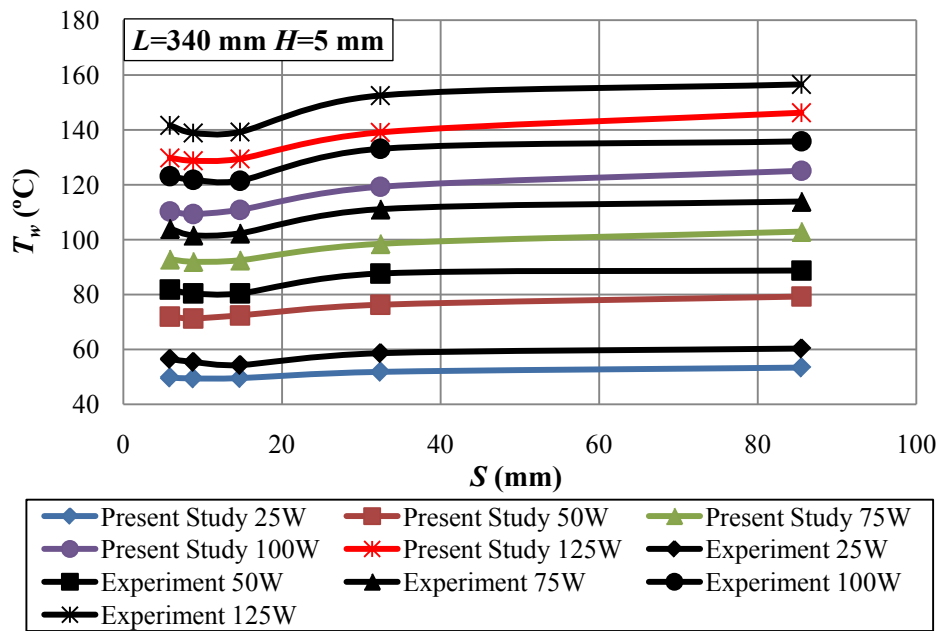
Figure D.3 Variation of fin array average temperature with fin spacing for
L=340 mm, *H*=5 mm

127

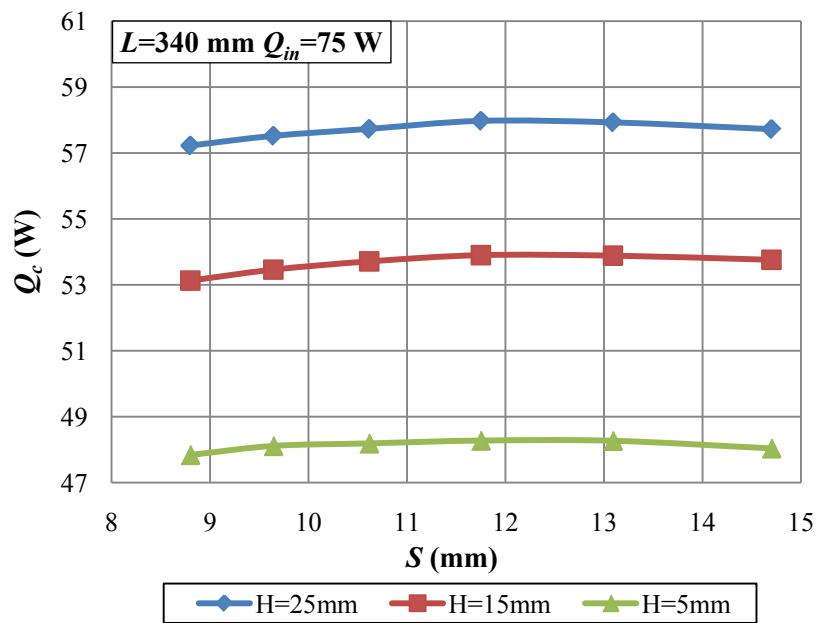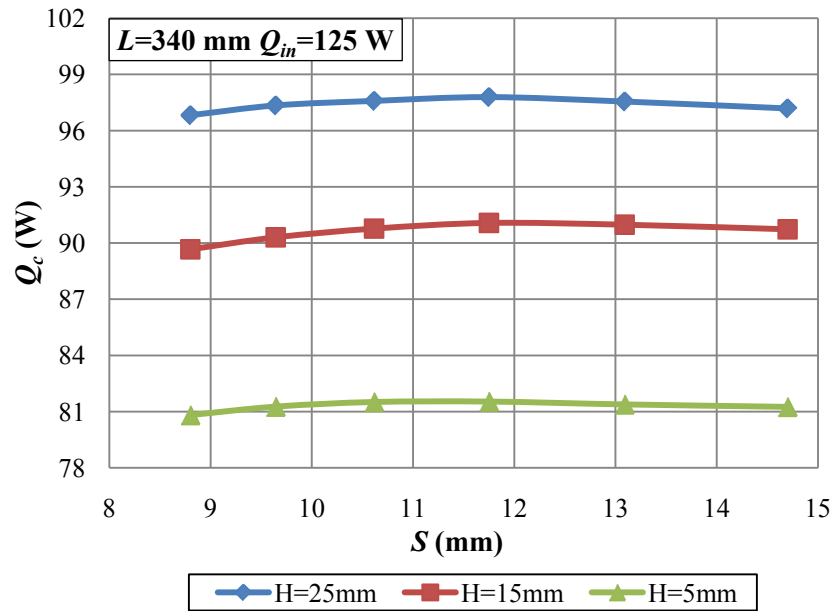**D.1.2 Variation of Convection Heat Transfer Rate with Fin Spacing**
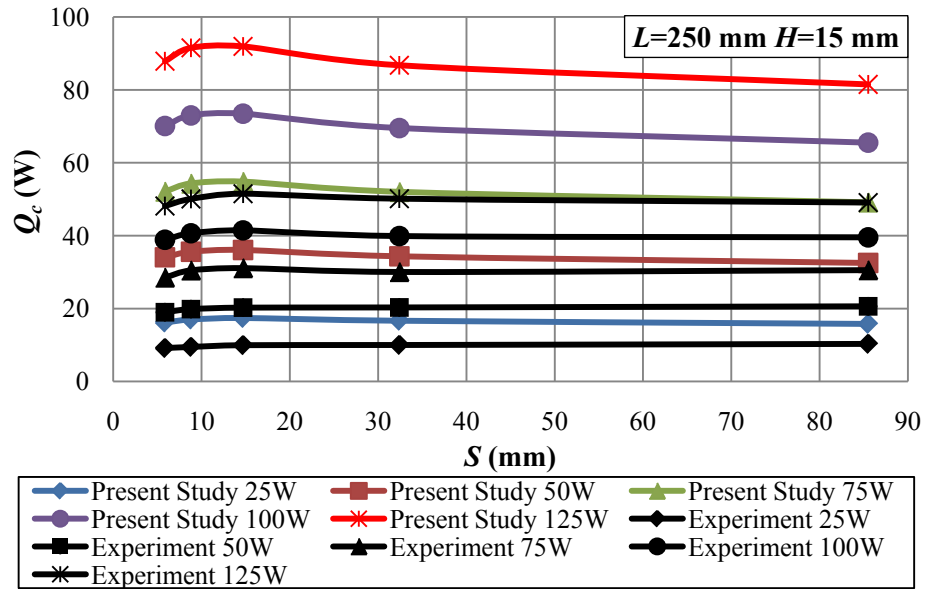
Figure D.4 Variation of convection heat transfer with fin spacing for
L=250 mm, H=15 mm
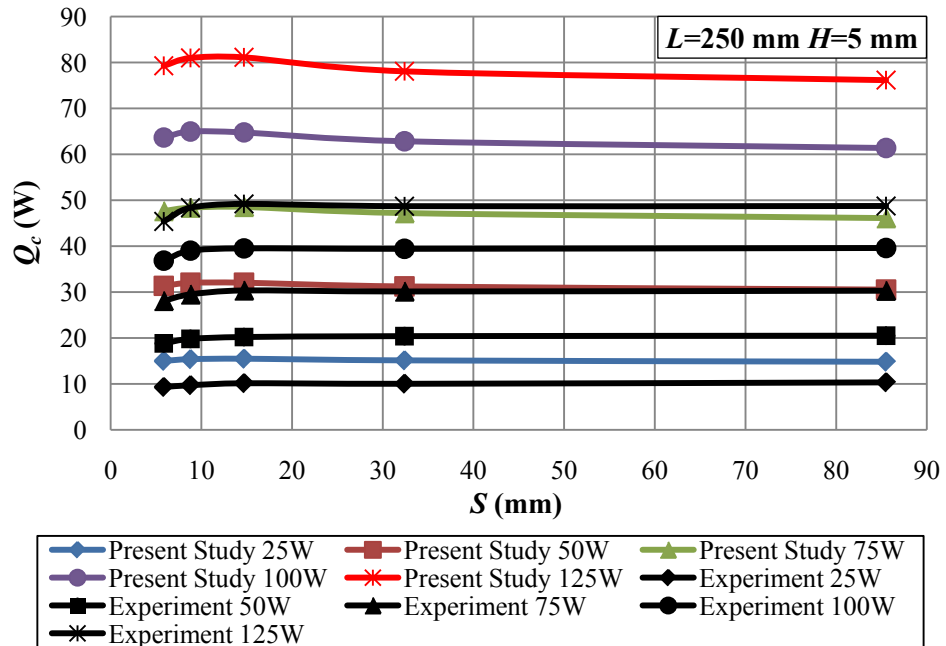
Figure D.5 Variation of convection heat transfer with fin spacing for
L=250 mm, H=5 mm
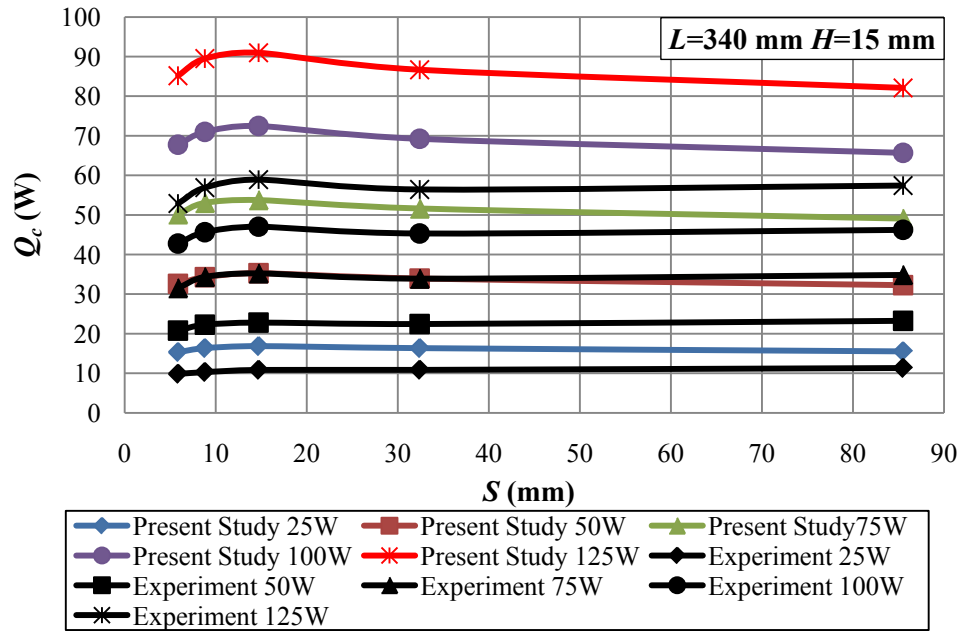
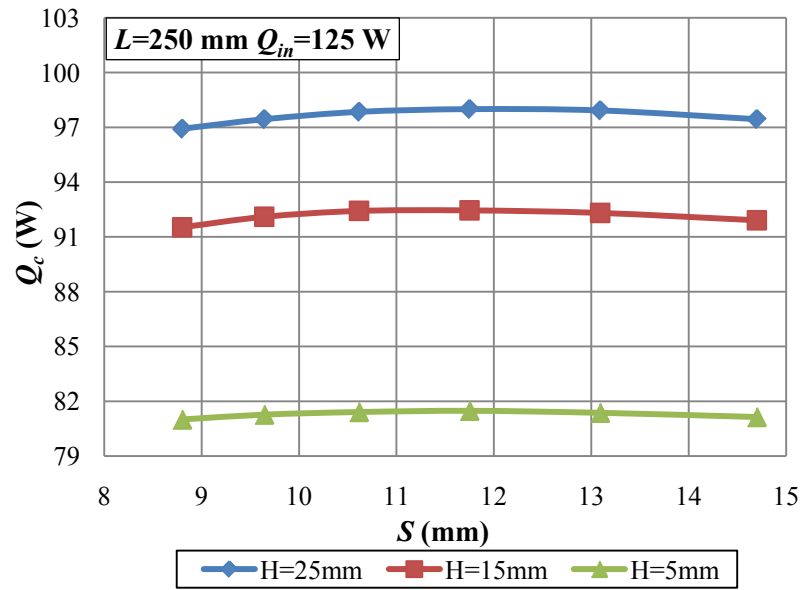Figure D.6 Variation of convection heat transfer with fin spacing for
L=340 mm, *H*=15 mm
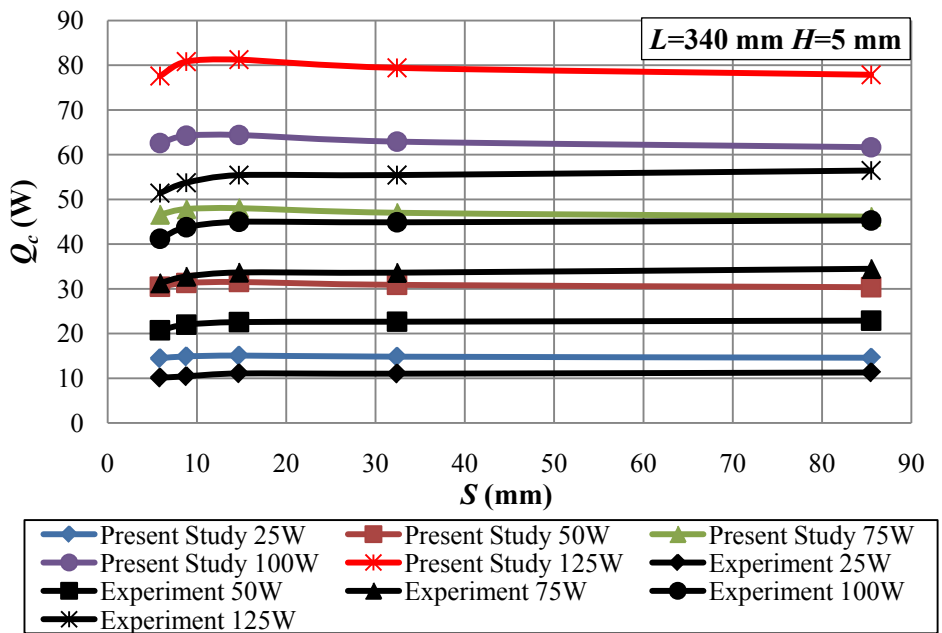
Figure D.7 Variation of convection heat transfer with fin spacing for
L=340 mm, *H*=5 mm

D.1.3 Optimum Fin Spacing for Minimum Fin Temperature
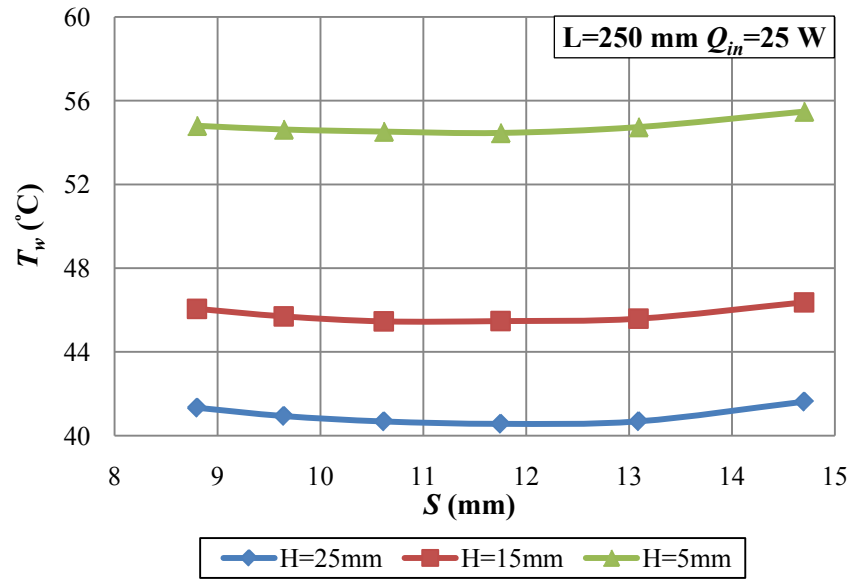
Figure D.8 Variation of fin array average temperature with fin spacing for
L=250 mm, Q_{in}=25 W
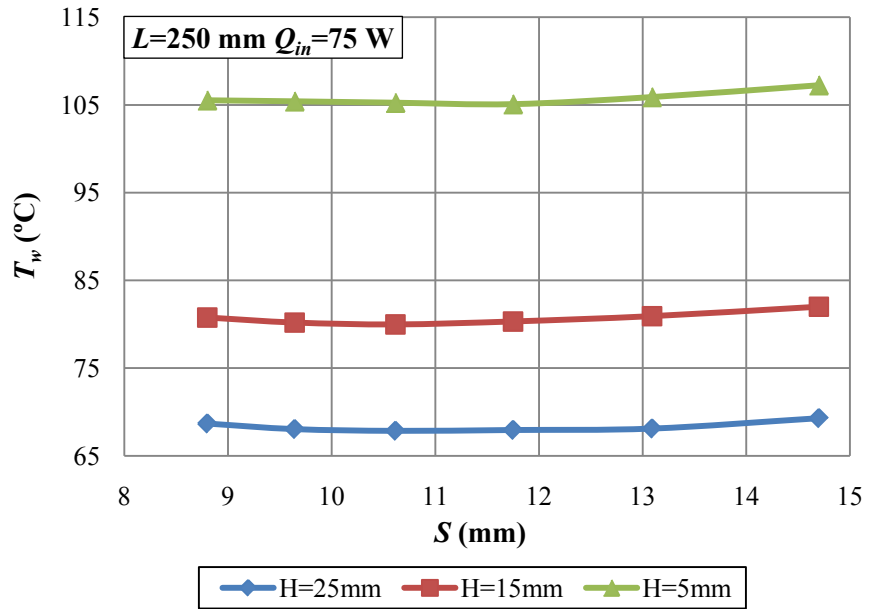
Figure D.9 Variation of fin array average temperature with fin spacing for
L=250 mm, Q_{in}=75 W
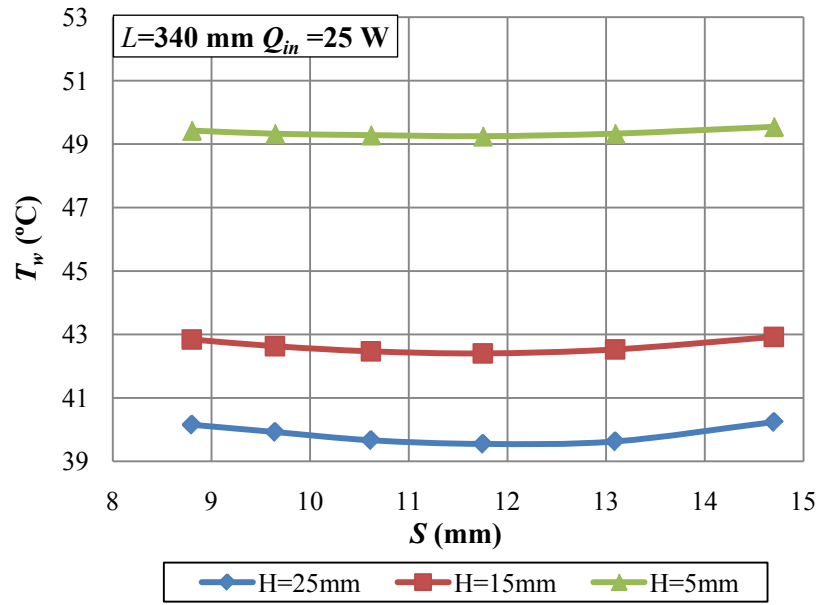
Figure D.10 Variation of fin array average temperature with fin spacing for
L=340 mm, *Q*_{*in*}=25 W
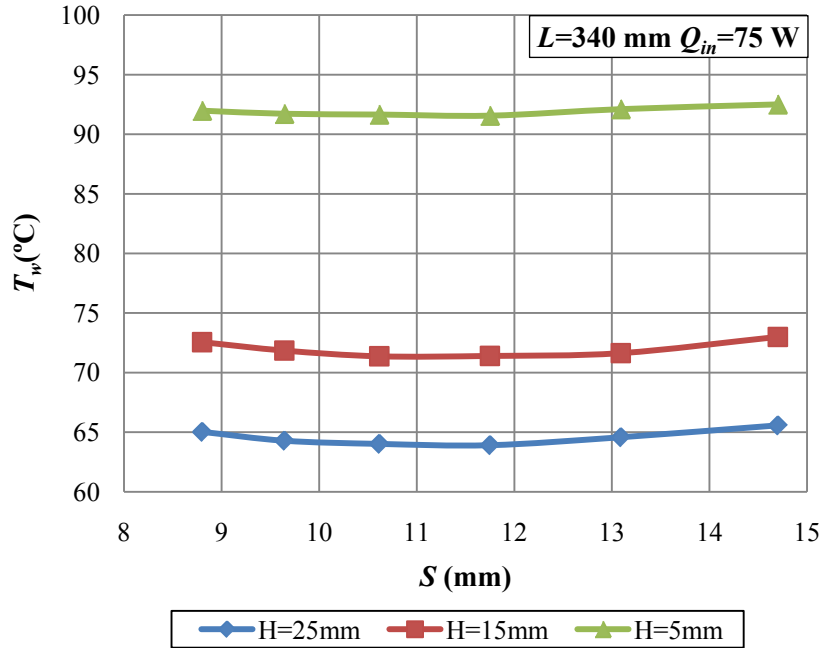
Figure D.11 Variation of fin array average temperature with fin spacing for
L=250 mm, *Q*_{*in*}=75 W

131
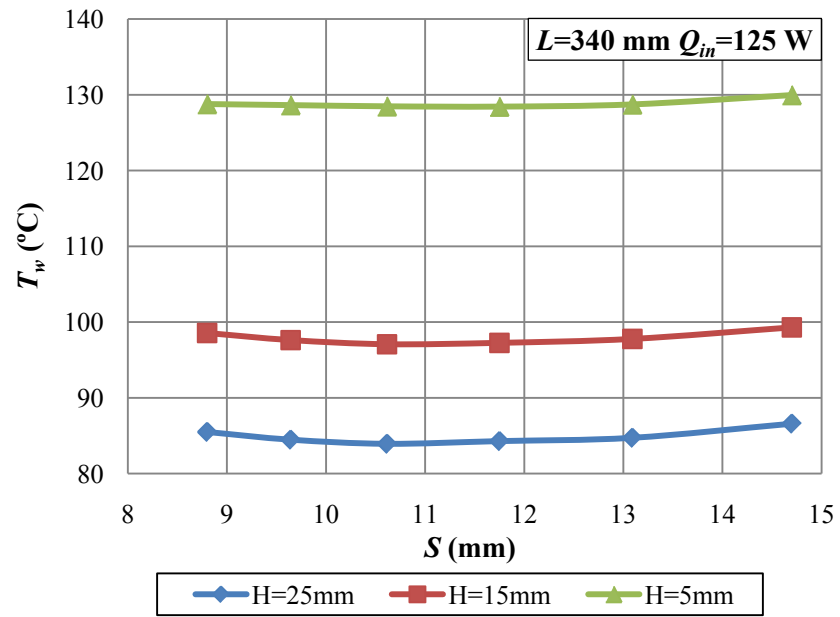
Figure D.12 Variation of fin array average temperature with fin spacing for
L=340 mm, *Q*$_{in}$=125 W

D.1.4   Optimum Fin Spacing for Maximum Convection Heat Transfer Rate
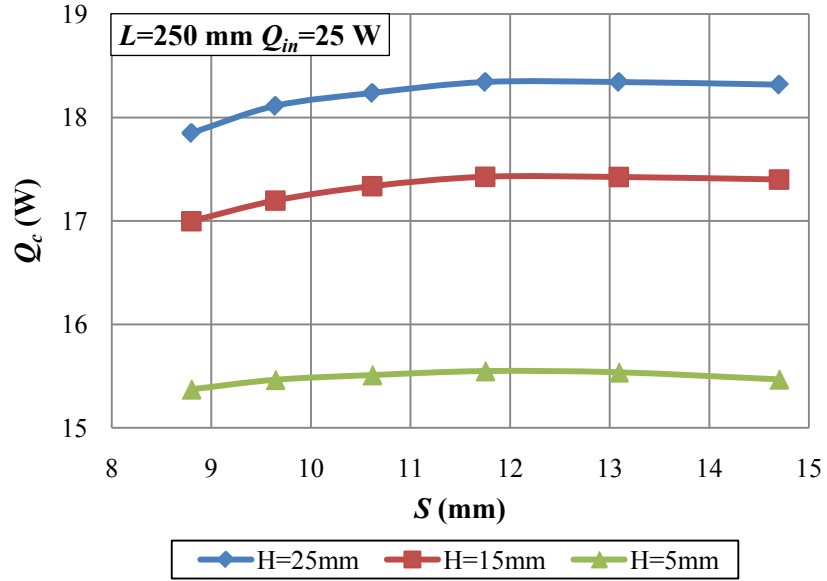
Figure D.13 Variation of convection heat transfer with fin spacing for L=250 mm, Q_{in}=25 W
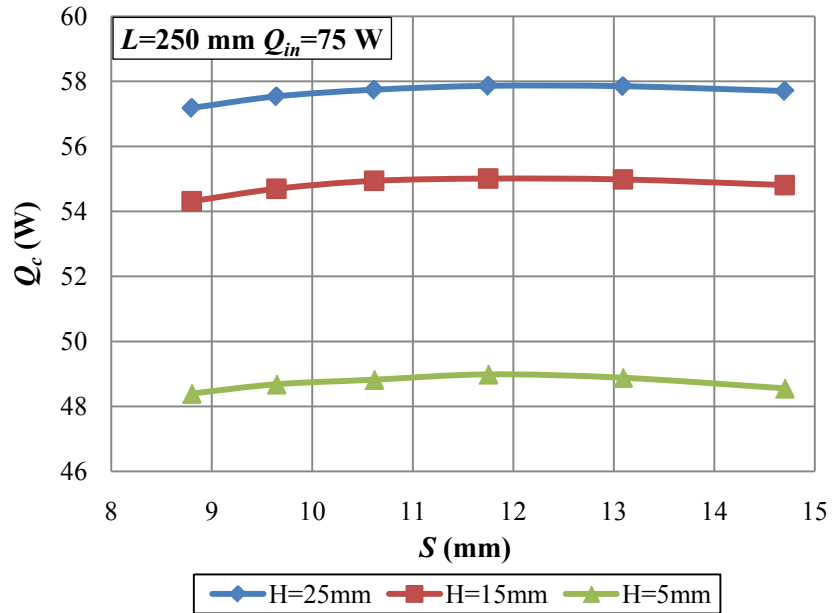
Figure D.14 Variation of convection heat transfer with fin spacing for L=250 mm, Q_{in}=75 W
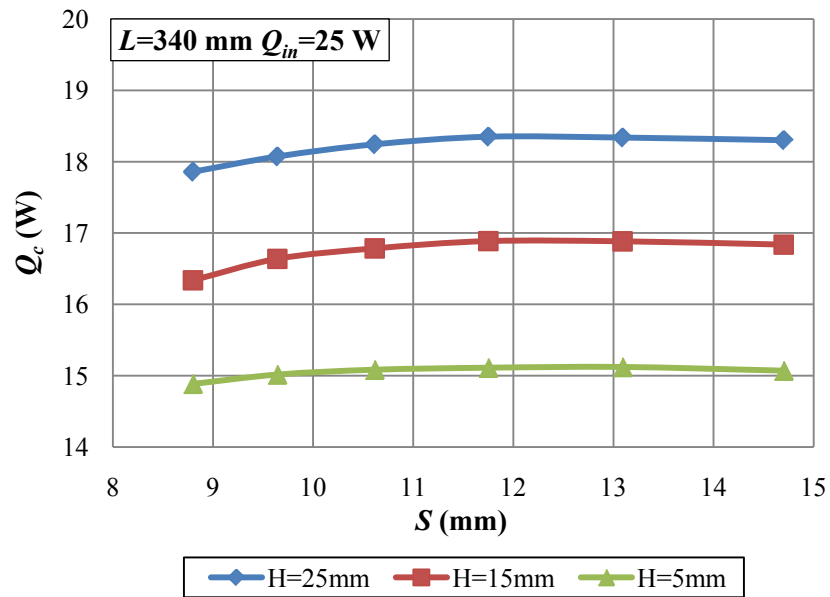
Figure D.15 Variation of convection heat transfer with fin spacing for
L = 340 mm, Q_{in}=25 W

Figure D.16 Variation of convection heat transfer with fin spacing for
L=340 mm, Q_{in}=75 W

Figure D.17 Variation of convection heat transfer with fin spacing for
L=340 mm, Q_{in} =125 W

Figure D.18 Variation of convection heat transfer with fin spacing for
L=250 mm, Q_{in} =125 W

D.2   Inclined Case Results

Figures which are not shown in chapter 4 for inclined case are presented in this section.

D.2.1   Variation of Convection Heat Transfer with Angle in Downward Inclination
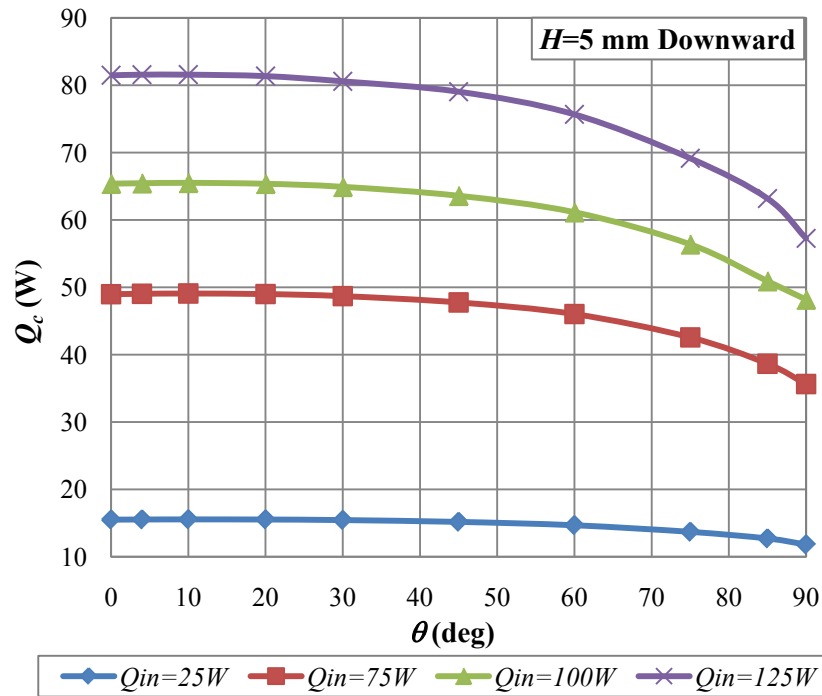
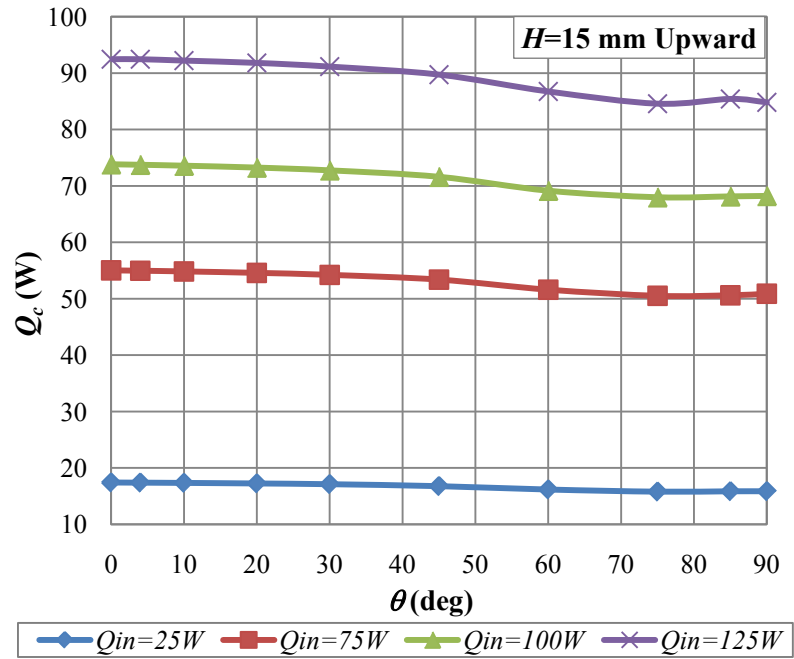Figure D.19 Variation of convection heat transfer for H=5 mm in downward inclination
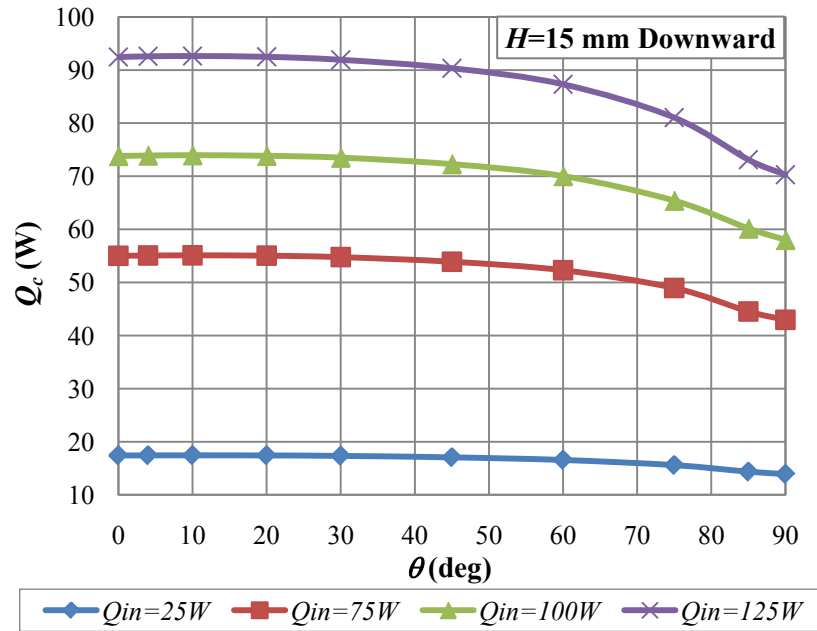
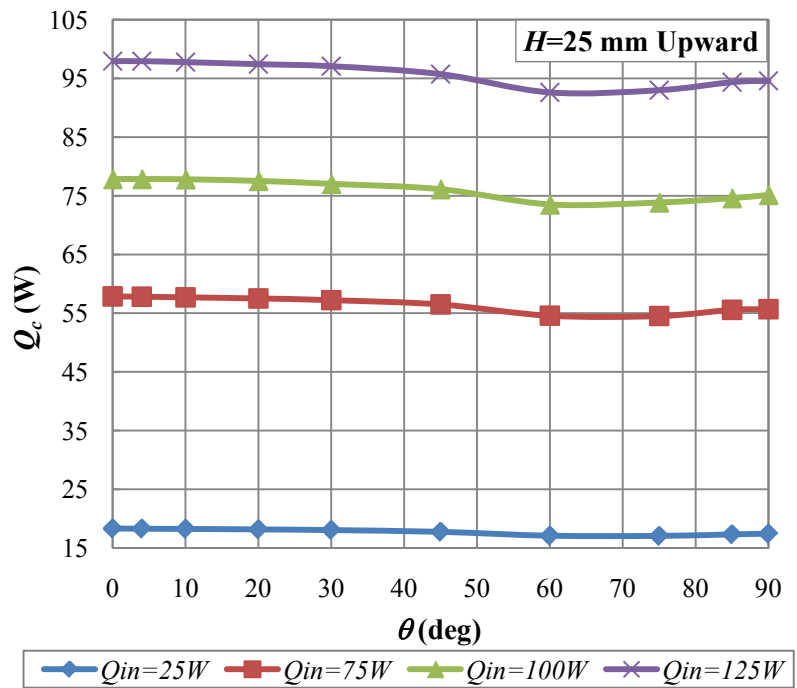Figure D.20 Variation of convection heat transfer for *H*=15 mm in downward inclination
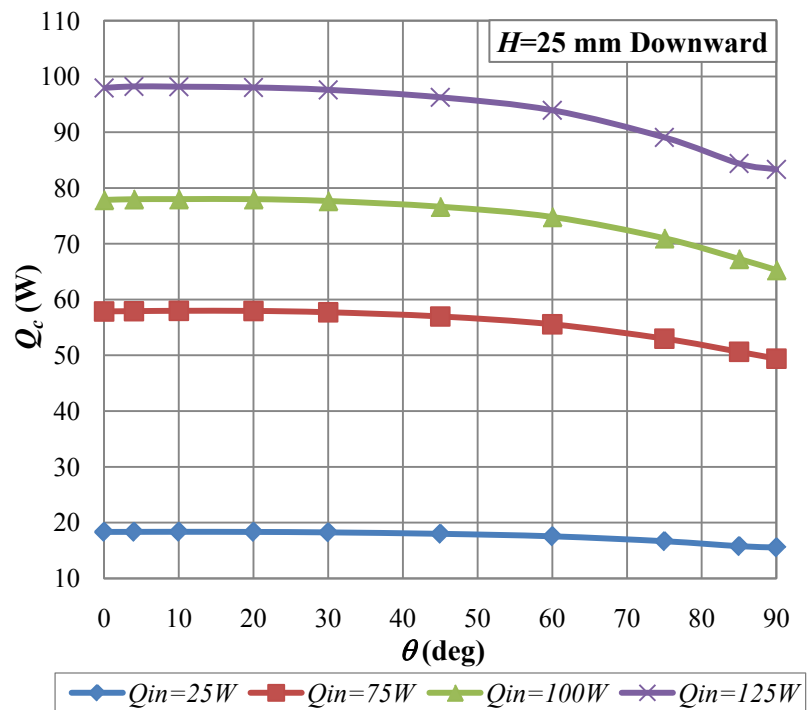
Figure D.21 Variation of convection heat transfer for *H*=25 mm in downward inclination

137

D.2.2 Variation of Convection Heat Transfer with Angle in Upward Inclination
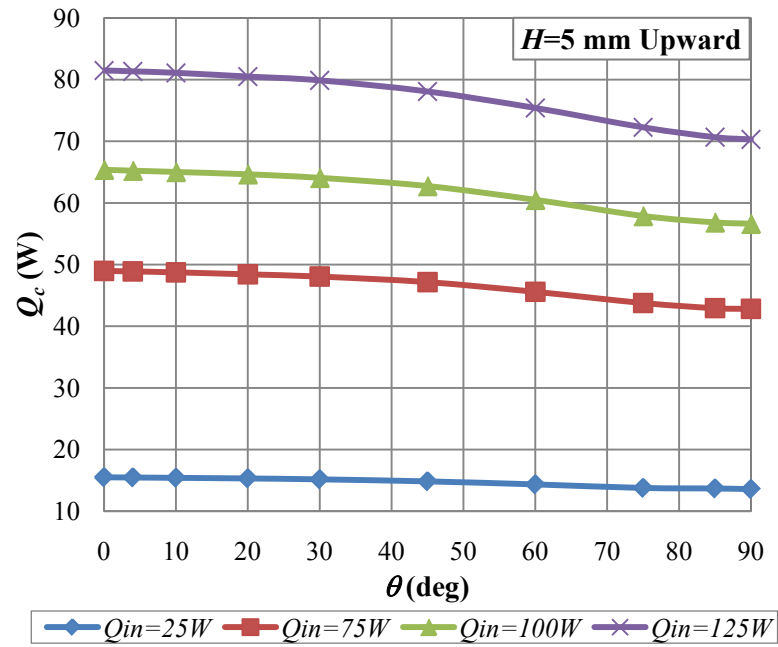
Figure D.22 Variation of convection heat transfer for H=5 mm in upward inclination

Figure D.23 Variation of convection heat transfer for *H*=15 mm in upward inclination

Figure D.24 Variation of convection heat transfer for *H*=25 mm in upward inclination

D.2.3 Variation of Heat Transfer Rate with Rayleigh number in Downward Inclination
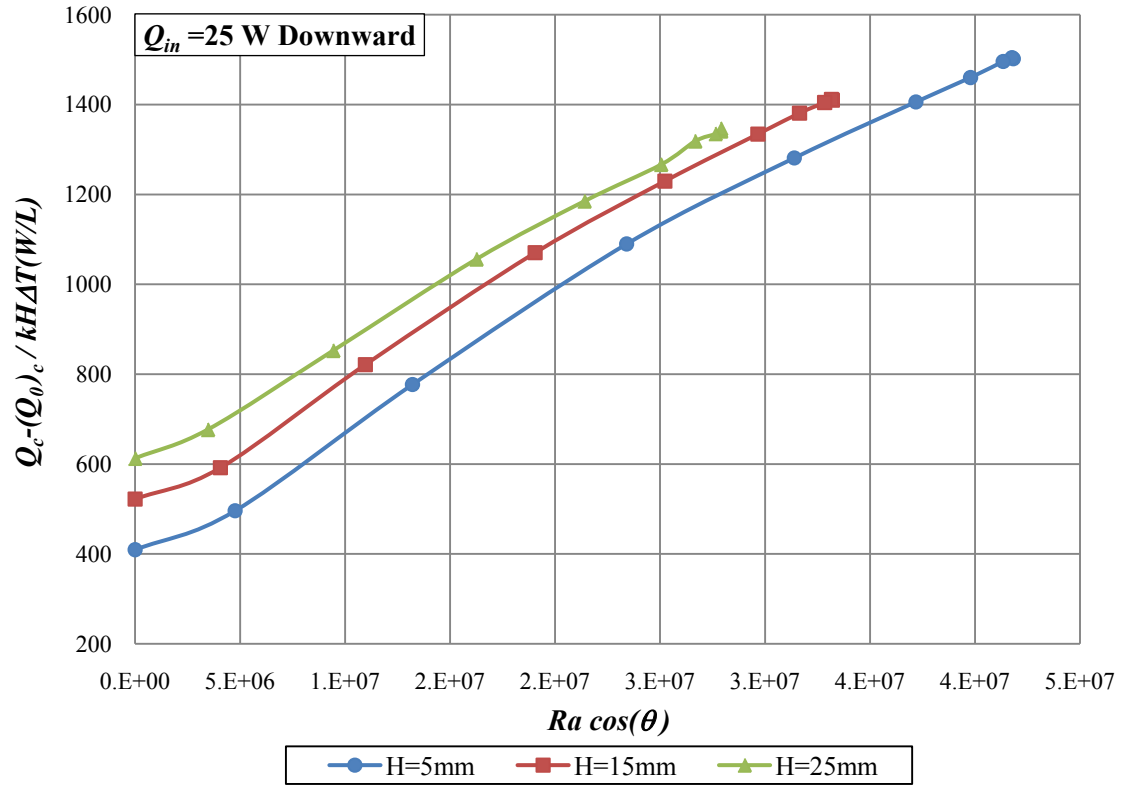
Figure D.25 Variation of heat transfer rate with Rayleigh number for different fin heights through downward inclination with Q_{in}=25 W
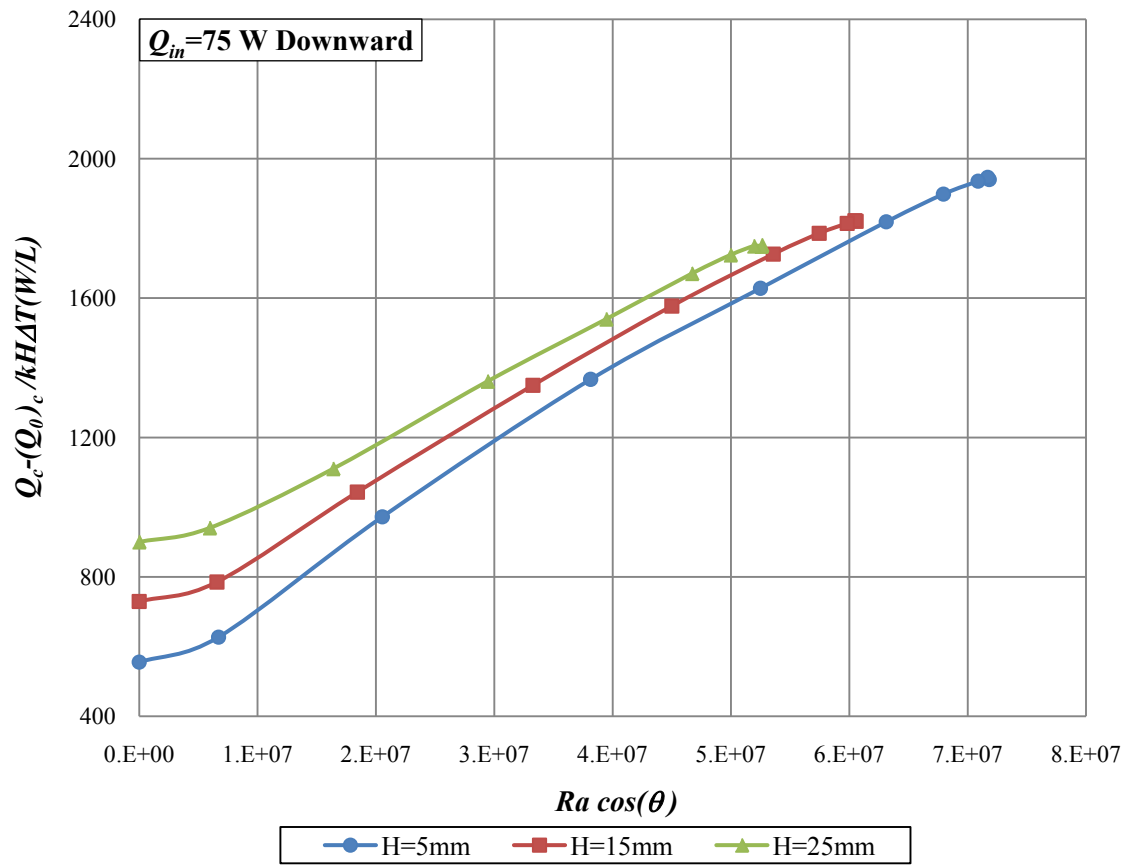
Figure D.26 Variation of heat transfer rate with Rayleigh number for different fin heights through downward inclination with Q_{in}=75 W
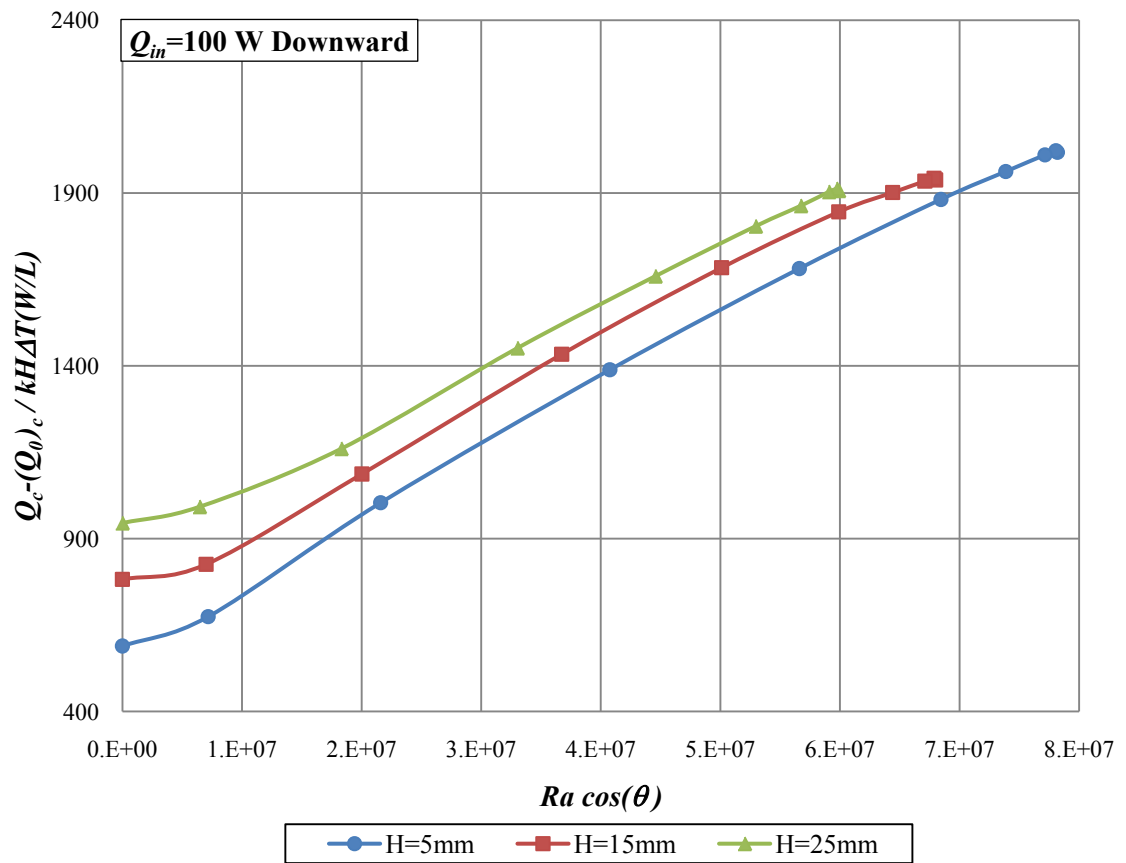
Figure D.27 Variation of heat transfer rate with Rayleigh number for different fin heights through downward inclination with Q_{in}=100 W

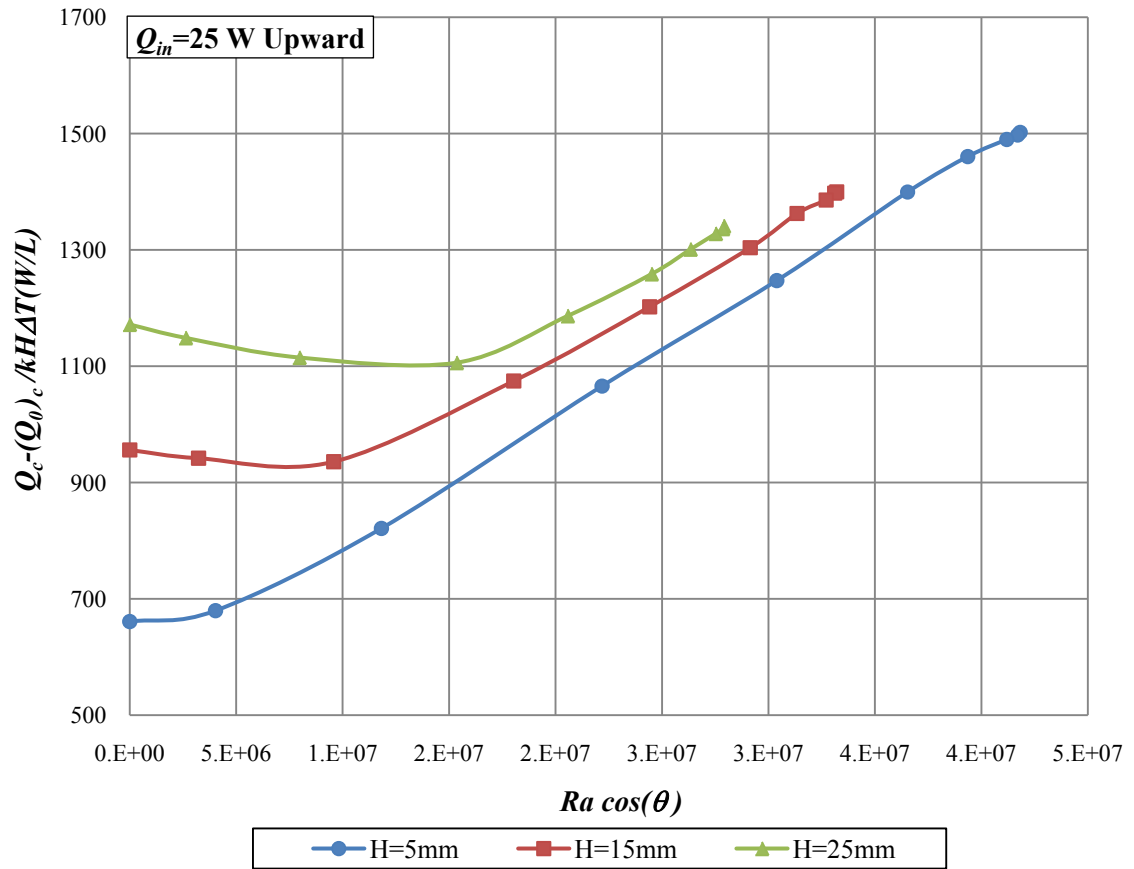## D.2.4 Variation of Heat Transfer Rate with Rayleigh Number in Upward Inclination

Figure D.28 Variation of heat transfer rate with Rayleigh number for different fin heights through upward inclination with Q_{in}=25 W
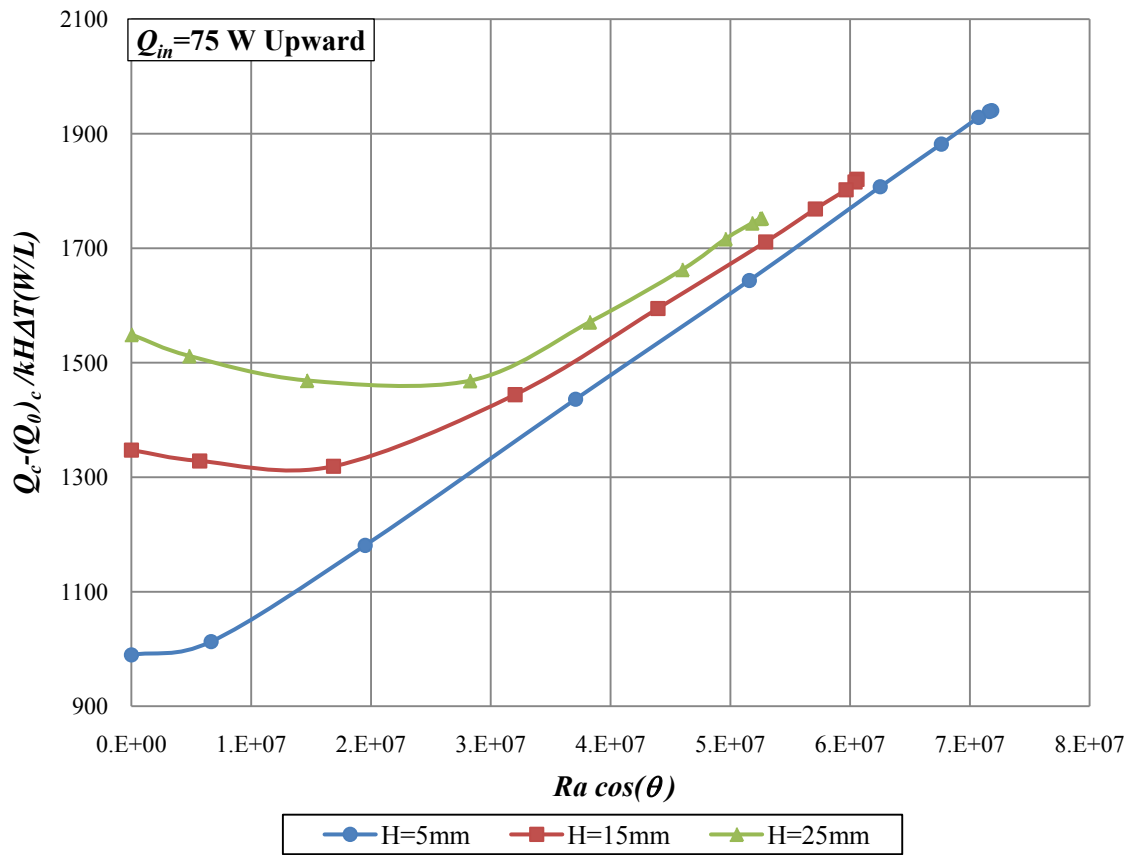
Figure D.29 Variation of heat transfer rate with Rayleigh number for different fin heights through upward inclination with Q_{in}=75 W
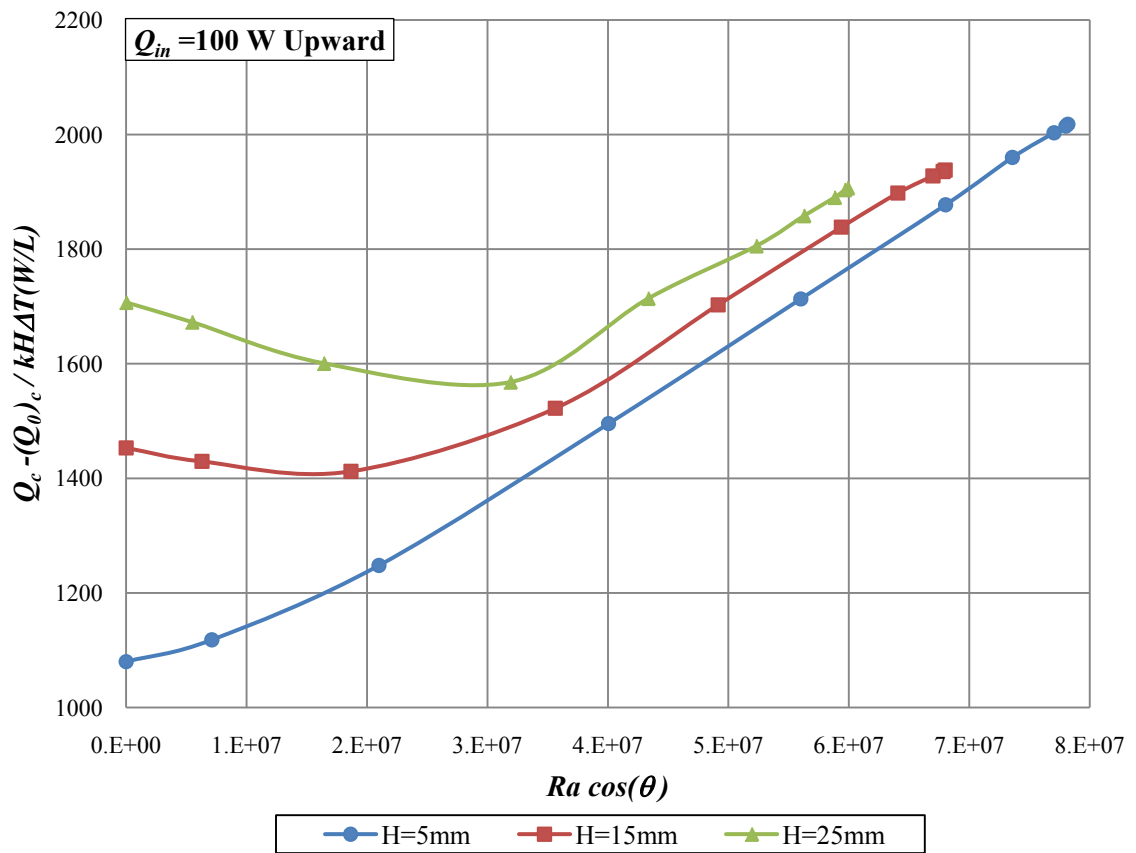
Figure D.30 Variation of heat transfer rate with Rayleigh number for different fin heights through upward inclination with Q_{in}=100 W